ABSTRACT

Title of dissertation: PERSISTENCE AND SURVIVAL ASPECTS OF FLUCTUATION PHENOMENA IN SURFACES

Magdalena Constantin,
Doctor of Philosophy, 2005

Dissertation directed by: Professor Sankar Das Sarma
Department of Physics

Controlling the stability of nanostructures is an important fundamental issue in nanoscience. A key problem in this respect is the random stochastic interface dynamics associated with equilibrium nanometer scale thermal fluctuations, which can be understood by applying first–passage statistical concepts, such as the temporal persistence [survival] probability $P(t)$ [$S(t)$]. $P(t)$ [$S(t)$] measures the probability of the step height *not* returning to the original [average] value within a given time interval. In this study, we measure the persistence exponent θ associated with the power–law decay of $P(t)$ at large time scale and also the survival time scale, τ_s, describing the exponential decay of $S(t)$ for several nonequilibrium surface growth processes and fluctuating steps on solid surfaces. We show that for growth models in the Molecular Beam Epitaxy universality class, the nonlinearity of the underlying equation is clearly reflected in the difference between the measured values of the positive and negative persistence exponents. We also find that the survival time scale

provides useful information about the physical mechanism underlying step fluctuations. An exact relation between long-time behaviors of the survival probability and the autocorrelation function is established and numerically verified. The dependencies of the persistence and survival probabilities on the system size and the sampling time are shown to be described by simple scaling forms. We introduce the generalizations of the persistence and survival probabilities for surface fluctuations. Our measurements of the persistent large deviations probability and associated family of exponents show good agreement with the corresponding quantities measured experimentally using scanning tunneling microscopy dynamical images of step fluctuations. The spatial persistence and survival probabilities are also theoretically analyzed. Finally, we investigate the connection between the generalizations of the spatial and temporal persistence probabilities.

PERSISTENCE AND SURVIVAL ASPECTS OF FLUCTUATION PHENOMENA IN SURFACES

by

Magdalena Constantin

Dissertation submitted to the Faculty of the Graduate School of the
University of Maryland, College Park in partial fulfillment
of the requirements for the degree of
Doctor of Philosophy
2005

Advisory Committee:

Professor Sankar Das Sarma, Chair/Advisor
Professor Ellen D. Williams
Professor Theodore Lee Einstein
Professor John D. Weeks
Professor Victor M. Yakovenko

To my parents, Cristiana and Constantin Găleată

ACKNOWLEDGEMENTS

I would like to start my acknowledgements by thanking my thesis advisor, Professor Sankar Das Sarma, for allowing me to be part of his extraordinary research group. I warmly thank him for his support and excellent advice during my time as a graduate student. I have enjoyed working on interesting surface science problems under his invaluable scientific supervision for the last four years. I have also enjoyed the extraordinary collaboration with Professor Chandan Dasgupta, who was a visiting professor in our Condensed Matter Theory Center, and I thank him for his support, for many discussions on our projects dealing with persistence and survival of step fluctuations, and for always being so helpful and giving wise advices.

Special thanks are due to Professors Ellen Williams, Ted Einstein, John Weeks, and Victor Yakovenko for agreeing to serve on my thesis committee and for sparing their invaluable time reviewing the manuscript.

Our research group has always been a very good environment for doing physics, and I would like to thank all the members of the Condensed Matter Theory Center at the University of Maryland, College Park, for many useful interactions and discussions over the last four years and also the staff members, Ms. Margaret Lukomska

and Ms. Mattie Dowd, for being very helpful with many administrative problems.

I would also like to warmly acknowledge my friendship with Professor Belita Koiller whose interest for my work motivated me to work harder and who also opened my interest for the exciting field of quantum computing.

I would also like to acknowledge my collaborators from the Experimental Surface Science Group: Dan Dougherty, Alexander Bondarchuk, and especially Professor Ellen Williams. I warmly thank Prof. Williams for her invaluable discussions and for offering me the possibility to connect my research project with reality, by using her experimental data on surface step fluctuations. Her tenacity and deep understanding of physics problems have been of great inspiration to me. Also, the Surface Science seminars, directed by Professors Ellen Williams and Ted Einstein, have always been of great interest and have broaden my physics knowledge. Many thanks are due to my colleagues from the Surface Science group, Tim Stasevich, Hailu Gebremariam, Ferenc Szalma, and especially my close friend, Mihaela Breban, for many useful and refreshing discussions.

It was also a great pleasure to work with our (former) diploma student Dr. Patcha Punyindu Chatraphorn, even for a very short time. I would like to acknowledge the contributions to this thesis due to Dr. Satya N. Majumdar. Our discussions about the problem of persistence in stochastic processes helped me to make progress with my thesis projects.

My first two years of graduate studies at Carnegie Mellon University will always be warmly remembered, especially the friendly atmosphere of the physics department. I would like to thank Professors Mike Widom, Robert Swendsen, Ling-

Fong Li, Sara Majetich, Ira Rothstein, and Gregg Franklin for their great lectures and support during that time.

My physics path would not have been possible without the guidance and help of my high school physics professor, Didona Niculescu, who has inspired me and started my love for physics. I thank her with all my heart.

I would also like to thank my family, my parents and my sister for always believing in me and for giving me the necessary strength to reach my highest dreams, my parents and brother in law for their love and encouragements, and my husband, *Dragoş*, for his love, his support during my time as a graduate student and for helping me solve many programming issues. My results would not have been possible without our long discussions about physics projects and without his great help. Finally, I would like to thank my son, *Gabriel*, for enlightening my last year of graduate studies and for giving a new and more profound sense to my life.

CONTENTS

LIST OF TABLES

LIST OF FIGURES

1. INTRODUCTION

Nonequilibrium surface growth and interface dynamics represent an area of research that has received much attention in the last two decades [1, 2]. A large number of discrete atomistic growth models [3, 4, 5, 6, 7, 8, 9, 10] and stochastic growth equations [11, 12, 13, 14, 15, 16] have been found [17] to exhibit *generic scale invariance* characterized by power law behavior of several quantities of interest, such as the interface width as a function of time (measured in units of deposited layers) and space- and time–dependent correlation functions of the interface height. Much effort has been devoted to the classification of growth models and equations into different universality classes characterized by the values of the exponents that describe the dynamic scaling behavior implied by these power laws. A variety of experimental studies [17, 18] have confirmed the occurrence of dynamic scaling in nonequilibrium epitaxial growth. Among the various experimental methods of surface growth, molecular beam epitaxy (MBE) is especially important because it plays a crucial role in the fabrication of smooth semiconductor films required in technological applications. Under usual MBE growth conditions, desorption from the film surface is

negligible and the formation of bulk vacancies and overhangs is strongly suppressed. It is generally believed that nonequilibrium surface growth under these conditions is well–described by a *conserved* nonlinear Langevin–type equation [14, 15, 16] and related atomistic models [4, 6, 10, 16] that form the so–called "MBE universality class".

Surface growth is an example of a general class of problems involving the dynamics of non–Markovian, spatially extended, stochastic systems. In recent years, the concept of *persistence* [19], which is closely related to first–passage statistics [20, 21, 22], has proven to be very useful in analyzing the dynamical behavior of such systems [23, 24, 25, 26, 27, 28, 29, 30]. Loosely speaking, a stochastic variable is *persistent* if it has a tendency to maintain its initial characteristics over a long period of time. The *persistence probability* $P(t)$ is typically defined as the probability that a characteristic feature (e.g. the sign) of a stochastic variable does not change at all over a certain period of time t. Although the mathematical concept of persistence was introduced a long time ago in the context of the "zero–crossing problem" in Gaussian stationary processes [31], it is only very recently that this concept has received attention in describing the statistics of first–passage events in a variety of spatially extended nonequilibrium systems. Examples of such applications of the concept of persistence range from the fundamental classical diffusion equation [23] and diffusion in a random velocity field [24] to the zero temperature Glauber dynamics of the ferromagnetic Ising and q–state Potts models [25, 26, 27, 32] and phase ordering kinetics [28]. Recently, a generalization of the persistence concept (i.e., the probability of persistent large deviations) has been introduced [32]. A closely re-

lated idea, that of sign–time distribution, was developed in Ref. [33]. An increasing number of experimental results are also available for persistence in systems such as coalescence of droplets [34], coarsening of two–dimensional soap froth [35], twisted nematic liquid crystal [36], and nuclear spin distribution in laser polarized Xe^{129} gas [37].

Recent work of Krug and collaborators [29, 30] has extended the persistence concept to the first–passage statistics of fluctuating interfaces. Persistence in the dynamics of fluctuating interfaces is of crucial importance in ultra–small scale solid–state devices. As the technology advances into the nanometric regime, questions such as how long a particular perturbation that appears in an evolving interface persists in time and what is the average time required for a structure to first fluctuate into an unstable configuration become important. The persistence probability can provide quantitative predictions on such questions. Recent experiments [38, 39, 40, 41] have demonstrated the usefulness of the concept of persistence in the characterization of the equilibrium fluctuations of steps on a vicinal surface. Analysis of experimental data on step fluctuations on Al/Si(111) surfaces [38, 41], on Ag(111) films grown on mica [39, 41], and on screw dislocations on the facets of Pb crystallites [39, 40] has shown that the long–time behaviors of the persistence probability and the probability of persistent large deviations in these systems agree quantitatively with the corresponding theoretical predictions. These results show that the persistence probability and related quantities are particularly relevant for describing and understanding the long–time dynamics of interface fluctuations. More complex theoretical models that describe the dynamics of coupled fluctuating interfaces [42],

for example, can be understood by performing a persistence analysis.

The persistence probability $P(t)$, defined as the probability that the position ("height") of the step edge at a point along a fluctuating step *does not return to its initial value (at time $t = 0$)* over time t is found [29, 30, 38, 39, 40] in these studies to decay in time as a power–law, $P(t) \propto t^{-\theta}$, for large t, where θ is the so-called *persistence exponent*. Similar power-law behavior of the persistence probability has also been found in experiments for other physical processes [34, 35, 36, 37]. It turns out that the precise definition of $P(t)$ is absolutely crucial for the power-law behavior discussed in the recent surface fluctuations literature. If, instead of considering the probability of not returning to the initial position, one defines a *survival probability*, $S(t)$, as the probability of the dynamical step height (at a fixed but arbitrary spatial location) not returning in time t to its average ("equilibrium") level, then, quite surprisingly, it was found in a recent experimental study [38] of thermal fluctuations of surface steps that $S(t)$ actually manifests, in sharp contrast to the power-law behavior of $P(t)$, an exponential decay, $S(t) \propto \exp(-t/\tau_s)$, at long times, where τ_s is the survival time scale. This exponential behavior of $S(t)$ has been explained theoretically and verified numerically in Ref. [43] and its generalization is presented in Ref. [44].

Another quantity of interest in the study of the statistics of spatially extended systems is the natural analog of the temporal persistence (survival) probability, the *spatial persistence (survival) probability*. This idea has been investigated theoretically [45] in the context of the persistence of $(d+1)$–dimensional Gaussian interfaces with dynamics described by linear Langevin equations, where the variable undergo-

ing stochastic evolution is the height $h(x,t)$ of the interfacial sites (x is the lateral position along the interface and t is the time). The spatial survival probability of fluctuating interfaces has not been approached before.

Motivated by the tremendous resources of the first–passage statistical concepts (such as persistence, survival, persistent large deviations and generalized survival probabilities) for understanding the spatial/temporal evolution of a variety of stochastic variables, we show in this work how these concepts apply to fluctuating growing surfaces and interfaces and what type of information they provide. We investigate in detail their scaling behaviors, emphasizing the effect of the sampling procedure on the interpretation of the first–passage probabilities and correlation functions. Below we describe the stochastic growth equations relevant for surface growth phenomena and interface dynamics, belonging to different universality classes, and the atomistic models associated with these classes. We also introduce the definitions of the first–passage statistical concepts mentioned above. In Chapter 2, we show the numerical results for $P(t)$ corresponding to several growth models, emphasizing the results for the growth models in the nonlinear MBE universality class. Chapter 3 presents the generalization of $P(t)$ using the concept of persistent large deviations probability and its associated family of persistent large deviations exponents. In Chapters 4 and 5, we discuss the survival probability and its generalization, respectively. The spatial persistence and survival probabilities are described in Chapter 6 and finally, in Chapter 7, we show how particular temporal and spatial first–passage statistical concepts can be related to each other through an isomorphic mapping procedure. Our conclusions and outlook for future open questions

are presented in Chapter 8. In the Appendix section we present the transient and steady–state behaviors of the autocorrelation functions relevant for surface growth phenomena. We also describe the persistence properties of the fractional Brownian motion and give hints on the calculation of the persistence exponent for simple stochastic processes.

1.1 Stochastic growth equations and dynamic scaling

The dynamic scaling behavior of stochastic growth equations may be classified into several universality classes. Each universality class is characterized by a set of scaling exponents [1, 2] which depend on the dimensionality of the problem. These exponents are (α, β, z), where α is the roughness exponent describing the dependence of the amplitude of height fluctuations in the steady–state regime ($t \gg L^z$) on the sample size L, β is the growth exponent that describes the initial power law growth of the interface width in the transient regime ($1 \ll t \ll L^z$), and z is the dynamical exponent related to the system size dependence of the time at which the interface width reaches saturation. Note that $z = \alpha/\beta$ for all the models considered in this work. To describe the interface evolution we use the single–valued function, $h(\mathbf{r}, t)$, which represents the height of the growing sample at position $\mathbf{r}$ and deposition time t. The interfacial height fluctuations are described by the root–mean–squared height deviation (or interface width) which is a function of the substrate size L and deposition time t:

$$W(L, t) = \langle (h(\mathbf{r}, t) - \bar{h}(t))^2 \rangle^{1/2}, \tag{1.1.1}$$

where $\bar{h}(t)$ is the average sample thickness. The width $W(L,t)$ scales as $W(L,t) \propto t^{\beta}$ for $t \ll L^z$ and $W(L,t) \propto L^{\alpha}$ for $t \gg L^z$ [46], L^z being the equilibration time of the interface, when its stationary roughness is fully developed.

Since it is convenient to write the evolution equations in terms of the deviation of the height from its spatial average value, $h(\mathbf{r},t) - \bar{h}(t)$, from now on we will denote by $h(\mathbf{r},t)$ the interface height fluctuation measured from the average height. Extensive studies of dynamic scaling in kinetic surface roughening (for an extended review see Ref. [17]) have revealed the existence of (at least) four universality classes that are described, in the long wavelength limit, by the following continuum equations and sets of scaling exponents (α, β, z), shown for the 1+1(2+1)–dimensional cases, respectively:

(1) The Edwards–Wilkinson (EW) second order linear equation: $1/2,\ 1/4,\ 2$ (0 (log), 0 (log), 2)

$$\frac{\partial h(\mathbf{r},t)}{\partial t} = \nu_2 \nabla^2 h(\mathbf{r},t) + \eta(\mathbf{r},t), \tag{1.1.2}$$

(2) The KPZ second order nonlinear equation: $1/2,\ 1/3,\ 3/2$ ($\simeq 0.4,\ \simeq 0.24,\ \simeq 1.67$)

$$\frac{\partial h(\mathbf{r},t)}{\partial t} = \nu_2 \nabla^2 h(\mathbf{r},t) + \lambda_2 |\nabla h(\mathbf{r},t)|^2 + \eta(\mathbf{r},t), \tag{1.1.3}$$

(3) The Mullins–Herring (MH) fourth order linear equation: $3/2,\ 3/8,\ 4$ ($1,\ 1/4,\ 4$)

$$\frac{\partial h(\mathbf{r},t)}{\partial t} = -\nu_4 \nabla^4 h(\mathbf{r},t) + \eta(\mathbf{r},t), \tag{1.1.4}$$

and

(4) The MBE fourth order nonlinear equation: $\simeq 1, \simeq 1/3, \simeq 3$ ($\simeq 2/3, \simeq 1/5,$

$\simeq 10/3$)

$$\frac{\partial h(\mathbf{r},t)}{\partial t} = -\nu_4 \nabla^4 h(\mathbf{r},t) + \lambda_{22} \nabla^2 |(\nabla h(\mathbf{r},t)|^2 + \eta(\mathbf{r},t), \tag{1.1.5}$$

where ν_i (i=2, 4) and λ_j (j=2, 22) are constant. The quantity $\eta(\mathbf{r},t)$ represents the noise term which accounts for the random fluctuations in the deposition rate. We assume that the noise has Gaussian distribution with zero mean and correlator

$$\langle \eta(\mathbf{r}_1,t_1)\eta(\mathbf{r}_2,t_2)\rangle = D\delta(\mathbf{r}_1-\mathbf{r}_2)\delta(t_1-t_2), \tag{1.1.6}$$

D being a constant related to the strength of the bare noise. Note that we do not include the (trivial) constant external deposition flux term in the continuum growth equations since that is easily eliminated by assuming that the height fluctuation h is always measured with respect to the average interface which is growing at a constant rate.

The concepts of universality classes and scaling exponents have been widely used in the literature to analyze the kinetics of surface growth and fluctuations. Our study based on persistence probabilities is motivated by the possibility that the concept of persistence may provide an additional (and complementary) tool to analyze the surface growth kinetics. It addresses fundamental questions such as: is persistence an independent (and new) conceptual tool for studying surface fluctuations or essentially equivalent (or perhaps complementary) to dynamic scaling? and does persistence lead to the definition of new universality classes on the basis of the values of the persistence exponent? To answer these questions, we consider in Chapter 2, for each of the four universality classes mentioned above (i.e. Eqs. (1.1.2)–(1.1.5)), at least one growth model and investigate how the associated persistence exponents

are related to the dynamic scaling exponents mentioned above.

In this work we also consider the 1–dimensional model characterized by $\beta = 1/8$ which describes an equilibrium surface relaxing through surface diffusion (known as the step–edge diffusion (SED) mechanism [47]), corresponding to $z = 4$, $\alpha = 1/2$ and volume conserving noise with correlator:

$$\langle \eta_c(x,t)\eta_c(x',t')\rangle \propto \nabla^2\langle \eta(x,t)\eta(x',t')\rangle \equiv \nabla^2\delta(x-x')\delta(t-t'). \tag{1.1.7}$$

This case applies to low temperature step fluctuations dominated by atomic diffusion along the step edge, described by a fourth order conserved linear Langevin equation:

$$\frac{\partial h(x,t)}{\partial t} = -\frac{\partial^4 h(x,t)}{\partial x^4} + \eta_c(x,t). \tag{1.1.8}$$

1.2 Atomistic growth models

Besides the stochastic continuum growth equations that describe the interface at large length scales and focus on its asymptotic coarse–grained properties, one can also use atomistic growth models to study the kinetics of surface growth and fluctuating interfaces.

In this study we use different atomistic limited–mobility growth models for simulating surface growth processes. In these models, the substrate consists of a collection of lattice sites labeled by the index j ($j = 1, 2, \ldots, L^d$) and the height variables $h(x_j)$ take integral values. The term "limited–mobility" is meant to imply that in these models, each adatom is characterized by a finite diffusion length which is taken to be one lattice spacing in most of the models we consider here. Thus, a

deposited atom can explore only a few neighboring lattice sites according to a set of specific mobility rules before being incorporated into the growing film. The solid–on–solid constraint is imposed in all these models, so that defects such as overhangs and bulk vacancies are not allowed. In most of the models considered in this work, the possibility of desorption is neglected, thereby making the models "conserved" in the sense that all deposited atoms are incorporated in the film; the noise (given by Eq. (1.1.6)) is of course nonconserved since the system is open to the deposition flux.

The deposition process is described by a few simple rules in these models. An atomic beam drops atoms on the substrate in a random manner. Once a lattice site on the substrate is randomly chosen, the diffusion rules of the model are applied to the atom dropped at the chosen site to determine where it should be incorporated. The allocated site is then instantaneously filled by the adatom. We consider both (1+1)– and (2+1)– dimensional models (one or two spatial dimensions and one temporal dimension) defined on substrates of length L in units of the lattice spacing. The deposition rate is taken to be constant and equal to L^d particles per unit time in our simulations of the Family (F), larger curvature (LC), Das Sarma–Tamborenea (DT), Wolf–Villain (WV) and controlled Kim–Das Sarma (CKD) models (see below). In these simulations, one complete layer is grown in each unit of time. In the RSOS Kim–Kosterlitz (KK) and Kim–Park–Kim (KPK) models described below, the diffusion rules are replaced by a set of local restrictions on nearest-neighbor height differences, which have to be satisfied after the deposition. The randomly chosen deposition site is rejected (the atom is not deposited) if these restrictions

are not satisfied. As a consequence, the number of deposition attempts does not coincide with the number of successful depositions in the KK model, although they are linearly related.

All conserved growth models satisfy the conservation law

$$\frac{\partial h(\mathbf{r},t)}{\partial t} = -\nabla \cdot \mathbf{j}(\mathbf{r},t) + \eta(\mathbf{r},t), \tag{1.2.1}$$

where $\mathbf{j}$ is the surface current and η is the noise term. Using different expressions, dictated primarily by symmetry considerations, for the current $\mathbf{j}$, one can obtain all the conserved Langevin equations discussed in Sec. 1.1. The atomistic growth models considered in our work provide discrete realizations of these continuum growth equations.

It is known that some of the discrete growth models we study here have complicated transient behavior [48, 49]. For this reason, obtaining the dynamic scaling exponents that show the true universality classes of these models is often quite difficult. To make this task easier, the noise reduction technique [50, 51] was introduced in simulations of such models. It has been shown [52] that this technique helps in suppressing high steps in the models and reduces the corrections in the scaling behavior, so that the true asymptotic universality classes of the growth models can be seen in simulations that cover a relatively short time. This makes it interesting to examine whether the persistence probabilities in these discrete models also exhibit similar transient behavior, and whether the noise reduction technique can help in bringing out the true persistence exponents of these models. To investigate this, we have applied the noise reduction technique to some of the discrete models studied

in this work.

The noise reduction technique can be easily incorporated in the simulation of any discrete growth model by a small modification in the diffusion process [52]. When an atom is dropped randomly, the regular diffusion rules for the growth model are applied and the final allocated site is chosen. Instead of adding the atom at that final site, a counter at that site is increased by one but the height of that site remains unchanged. When the counter of a lattice site increases to the value of a pre–determined noise reduction factor, denoted by m, the height at that lattice site is increased by one and the counter of that site is reset back to zero. The value of the noise reduction factor m should be chosen carefully. If m is too small, the suppression of the noise effect is not enough and the true universality class is not seen. However, if m is too large, the kinetically rough growth becomes layer–by–layer growth [53] and the universality class of the model cannot be determined.

The atomistic models considered in our work are defined below.

(i) **Family model**: The Family (F) model [3] is an extensively studied SOS discrete stochastic model, rigorously known to belong to the same dynamical universality class as the EW equation. It allows the adatom to explore within a fixed diffusion length to find the lattice site with the smallest height where it gets incorporated. If the diffusion length is one lattice constant (this is the value used in our simulations), the application of this deposition rule to a randomly selected site j involves finding the local minimum height value among the set: $h(x_{j-1})$, $h(x_j)$ and $h(x_{j+1})$ (in (1+1)–dimensions). The height of the site with the minimum height is then increased by one.

(ii) **Larger curvature model**: The Kim–Das Sarma model [6] is a more complex one which allows the atomic surface current $\mathbf{j}$ to be written as a gradient of a scalar field K, $\mathbf{j} = -\nabla K$, which can depend on h, $\nabla^2 h$, $|\nabla h|^2$ and so on. In the particular case when $K = -\nabla^2 h$, one obtains the so–called larger curvature (LC) model. As the name suggests, the diffusion rules applied to a randomly selected site j allow the adatom to get incorporated at the site in the neighborhood of site j where the local curvature (given by $h(x_{j+1}) + h(x_{j-1}) - 2h(x_j)$ in (1+1)–dimensions) has the largest value. The LC model asymptotically rigorously belongs to the MH universality class described by Eq. (1.1.4).

(iii) **Wolf–Villain model**: The diffusion rules of the Wolf–Villain (WV) model [5] allow the adatom to diffuse to its neighboring sites in order to maximize its local coordination number which, for the (1+1)–dimensional case, varies between 1 and 3 when the bond with the atom lying below the site under consideration is taken into account. In contrast to the F model, in this case the surface develops deep valleys with high steps almost perpendicular to the substrate. For the range of times and sample sizes used in the present study, the WV model may be considered to belong to the MBE universality class [5, 48] described by Eq. (1.1.5). However, recent studies [52, 54] have shown that the asymptotic universality class of this model in (1+1)–dimensions is the same as that of the EW equation. In contrast, in (2+1)–dimensions, studies based on the noise reduction technique [55] have revealed that the WV model exhibits at very long times unstable (mounded) dynamic universality which cannot really be described by any of the continuum equations (Eqs. (1.1.2)-(1.1.4)) given above.

(iv) **Das Sarma–Tamborenea model**: The Das Sarma–Tamborenea (DT) model [4] is characterized by diffusion rules that are slightly different from those in the WV model. In this case, the diffusing atom tries to *increase* its coordination number, not necessarily to *maximize* it. For example, if a randomly selected deposition site has its local coordination number equal to 1 (i.e. no lateral neighbor in (1+1)–dimensions), and the two neighbors of this site have coordination numbers equal to 2 and 3, the deposited atom does not necessarily move to the neighboring site with the larger local coordination number: it moves to one of the two neighboring sites with equal probability (the atom would necessarily move to the site with coordination number 3 in the WV model). This minor change in the local diffusion rules actually changes the asymptotic universality class: the (1+1)–dimensional DT model belongs to the MBE universality class [52, 55] corresponding to the nonlinear continuum dynamical equation of Eq. (1.1.5). However, the (2+1)–dimensional DT model asymptotically belongs to the EW universality [55] at very long times.

(v) **Controlled Kim–Das Sarma model**: The Kim–Das Sarma model mentioned above provides a discrete realization of the continuum equation of Eq. (1.1.5) if the scalar field K is chosen to be $K = -\nabla^2 h + \lambda_{22}(\nabla h)^2$. However, the discrete treatment of the spatial gradients produces strong instabilities in the growth process due to uncontrolled growth of isolated structures, such as pillars or grooves. These instabilities can be easily controlled by introducing higher order nonlinear terms [16]. We call this new model the *controlled* Kim–Das Sarma (CKD) model. In this model, the scalar field K is chosen to be $K = -\nabla^2 h + \lambda_{22} f(|\nabla h|^2)$, where

the nonlinear function f is given by

$$f(|\nabla h|^2) = \frac{1 - e^{-c|\nabla h|^2}}{c}, \tag{1.2.2}$$

with $c > 0$ being the control parameter. The CKD diffusion rules for a randomly chosen deposition site, j, imply the minimization of the scalar field K, using the standard discretization scheme for the lattice derivatives $\nabla^2 h$ and ∇h:

$$(\nabla^2 h)_{|j} = h(x_{j+1}) + h(x_{j-1}) - 2h(x_j)\,, \tag{1.2.3a}$$

$$|\nabla h|^2_{|j} = \frac{1}{4}\left[h(x_{j+1}) - h(x_{j-1})\right]^2\,, \tag{1.2.3b}$$

in (1+1)–dimensions. By carefully choosing the values for c and λ_{22} [16], one can remove the nonlinear growth instabilities completely and ensure an overall behavior of the CKD model similar to that of the DT model.

(vi) **Kim–Kosterlitz and Kim–Park–Kim models**: For completeness, we also present in this chapter the results for the RSOS Kim–Kosterlitz (KK) [8, 9] and Kim–Park–Kim (KPK) [10] models which are known to belong asymptotically to the KPZ and MBE universality classes, respectively. The common feature of these two models is the replacement of the usual diffusion rules of the SOS models described above by local restrictive conditions controlling nearest–neighbor height differences.

In the KK model, deposition sites are randomly chosen, but the incorporation of the adatoms into the substrate is subject to a specific restriction: the deposition event occurs if and only if the absolute value of the height difference between the randomly selected deposition site, j, and *each* of its nearest–neighboring sites remains

smaller than or equal to a positive integer n after deposition (our simulations were done for $n = 1$). If this strict constraint is not satisfied, the attempted deposition of an adatom is rejected, and the random selection of the deposition site is repeated until the deposition is successfully done. Since every attempt to deposit an adatom is not successful, the definition of "time" in this model is not quite the same as that in the other models where every deposition attempt leads to the incorporation of a new adatom in the growing film. In the KK model, the "time" is equivalent to the average height, which is not the same as the number of attempted depositions per site (these two quantities are the same in the other models considered here). The KK model is known to belong to the KPZ universality class, and in fact provides the most numerically efficient and accurate method for calculating the KPZ growth exponents.

Kim *et al.* [10] discovered that a slight change in the algorithm for choosing the incorporation site transforms the KK model into a new one, the KPK model, that belongs to the MBE universality class. The change consists of extending the search for appropriate incorporation sites (i.e, sites where the constraint on the absolute values of the nearest–neighbor height differences would be satisfied after the incorporation of an adatom) to the neighbors of the originally selected deposition site j. If the original site does not satisfy the constraint, then the neighboring sites ($j \pm 1$ in (1+1) –dimensions) are checked, and an adatom is incorporated at one of these sites if the incorporation does not violate the constraint. Otherwise, the search is extended to the next–nearest–neighbors of j, and so on until a suitable incorporation site is found. We mention that in our implementation of this process, if, for example,

both the sites $j-k$ and $j+k$ are found to be suitable for incorporation, then one of them is chosen randomly without any bias. Application of this algorithm in (2+1)–dimensions involves extending the search for suitable incorporation sites to those lying inside circles of increasing radii around the randomly selected deposition site j. The diffusion and incorporation rules of the KPK model [10] lead essentially to a conserved version of the Kim–Kosterlitz RSOS model, and as such the continuum growth equation corresponding to the KPK model is the conserved KPZ equation (with nonconserved noise), which is precisely the MBE equation; Eq. (1.1.5) is the conserved version of Eq. (1.1.4) with nonconserved noise in both.

(vii) **Racz model**: The Racz model, introduced in Ref. [56], provides a discrete realization of the continuum equation of Eq. (1.1.8) with conserved noise, which means that the volume enclosed by the interface is conserved. In this model the nearest–neighbor height differences are restricted to:

$$|h_{j+1} - h_j| \leq 2. \tag{1.2.4}$$

In one simulation step a site j is randomly chosen. A diffusion move to a randomly chosen neighbor takes place if the above restrictive condition is satisfied, otherwise a new random site is selected and the procedure follows in the same way.

1.3 First–passage statistics of fluctuating interfaces

1.3.1 Transient and steady–state persistence probabilities

Let us introduce the definitions of the positive and negative persistence probabilities ($P_{\pm}(t_0, t_0+t)$) for a growing (fluctuating) interface in the transient and steady–state regimes. These definitions can be extended to any stochastic variable. Here t_0 is the initial time, and we are interested in evaluating the probability of the height at a fixed position remaining persistently above (P_+) or below (P_-) its initial value (i.e. its value at t_0 by definition) during the time period between t_0 and $t_0 + t$. If one considers the special case $t_0 = 0$, when the interface is completely flat, then the quantity of interest is the probability that the interfacial height (measured from its spatial average) does not return to its initial zero value up to time t. This case is known as the *transient* (T) regime. For values of t that are small compared to the time scale for saturation of the interface width ($t_{sat}(L) \propto L^z$), the persistence probabilities in this regime are expected to exhibit a power law decay in time:

$$P_{\pm}^{T}(0,t) \propto \left(\frac{1}{t}\right)^{\theta_{\pm}^{T}}, \tag{1.3.1}$$

where $\theta_{\pm}^{T}$ are called the transient positive and negative persistence exponents. In the particular case of *linear* continuum growth equations, these exponents are equal because the symmetry under a change of sign of $h(\mathbf{r}, t)$ remains valid at all stages of the growth process. However, in the case of dynamics governed by nonlinear continuum equations, the lack of this "up–down" interfacial symmetry implies that P_+ and P_- (and therefore, the exponents θ_+^T and θ_-^T) would, in general, be differ-

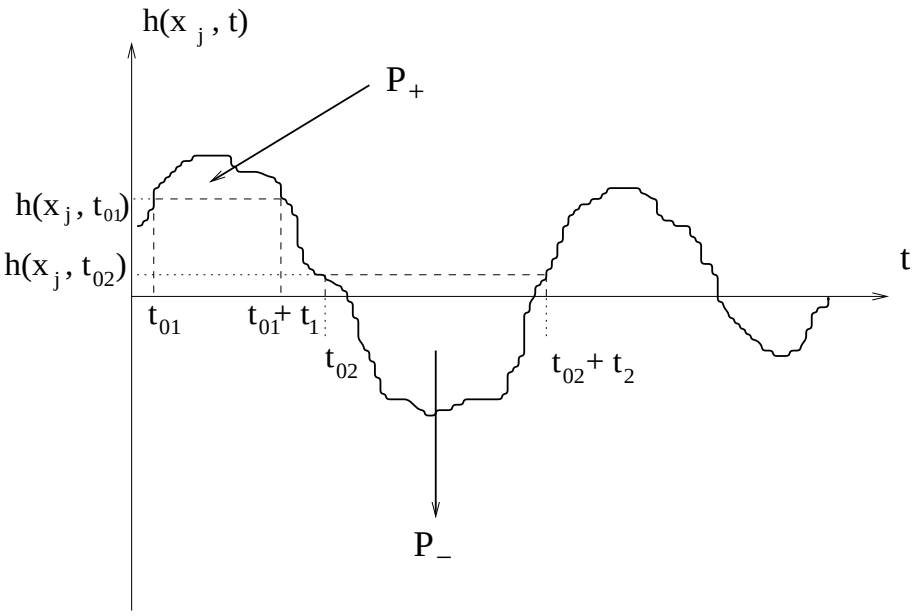

Figure 1.1: Schematic representation of the positive and negative persistence probabilities calculation for a stochastic variable $h(x_j, t)$ at a fixed point x_j.

ent from each other. No universal relationship between the transient positive and negative persistence exponents and the dynamic scaling exponents is known to exist for any one of the four universality classes mentioned above. On the other hand, if one considers t_0 larger than $t_{sat}(L)$, then the quantity of interest is the probability that the interfacial height at a fixed position does not return to its specific value at initial time t_0 during the subsequent time interval between t_0 and $t_0 + t$. Instead of being flat, the interface morphology at time t_0 has completely developed roughness, which produces persistence exponents that are different from the transient exponents defined earlier. This case is known as the *steady–state* (S) regime. If $t \ll L^z$, one expects to obtain in this regime the steady–state persistence probability with a

power law decay in time [29]

$$P_{\pm}^{S}(t_0, t_0 + t) \propto \left(\frac{1}{t}\right)^{\theta_{\pm}^{S}}, \tag{1.3.2}$$

where $\theta_{\pm}^{S}$ are the steady–state positive and negative persistence exponents. It has been pointed out by Krug *et al.* [29] that for systems described by *linear* Langevin equation, the steady–state persistence exponents are related to the dynamic scaling exponent β in the following way:

$$\theta_{+}^{S} \equiv \theta_{-}^{S} = 1 - \beta. \tag{1.3.3}$$

The exponent β is well known for linear Langevin equations for surface growth dynamics, and is given in d–dimensions by $\beta = (1 - d/z)/2$ for nonconserved white noise (Eq. (1.1.6)), where z, the dynamical exponent, is here precisely equal to the power of the gradient operator entering the linear continuum dynamical growth equation (i.e. $z = 2$ in Eq. (1.1.2); $z = 4$ in Eq. (1.1.4)). The relation defined by Eq. (1.3.3) holds true for the Langevin equations of Eqs. (1.1.2) and (1.1.4), which are obviously linear, as well as for the special case of the (1+1)–dimensional KPZ equation of Eq. (1.1.3) [30], which, despite its nonlinearity, behaves as the linear EW equation in the steady state. Since the positive and negative exponents are expected to be different for general nonlinear Langevin equations, the relation of Eq. (1.3.3) can not be valid for both θ_{+}^{S} and θ_{-}^{S} in systems described by such nonlinear equations. Therefore, at least one (or perhaps both) of these two persistence exponents must be non–trivial in the sense that it is not related to the usual dynamic scaling exponents. For this reason we pay particular attention to the MBE nonlinear equation and

investigate in Chapter 2 whether its persistence exponents can be related to the dynamic scaling exponents.

For a better understanding of the persistence probability concept we show in Fig. 1.1 two intervals where the height variable is always *above* its initial value, i.e., $P_+(t_1) = 1,\ \forall\ \ t_{01} < t' < t_{01} + t_1$, and also always *below* the original value, i.e., $P_-(t_2) = 1,\ \forall\ \ t_{02} < t' < t_{02} + t_2$, respectively. In real calculations, the probabilities are averaged over all the possible choices of the initial times t_{0n}, with $n = 1, 2, ...$, and all the realizations of the height stochastic variable.

1.3.2 Generalized persistence: Probability of persistent large deviations

The step height $h(x,t)$ can be alternatively described by a new stochastic variable, $S(t) \equiv$ sign $[h(x, t_0 + t) - h(x, t_0)]$. We can average it and obtain the so–called average sign variable, $S_{\rm av}(t) \equiv t^{-1} \int_0^t dt'\ S(t')$. Then, the probability of persistent large deviations, $P(t,s)$, is defined as the probability for the "average sign" $S_{\rm av}$ of the height fluctuation to remain above a certain pre-assigned value "s" up to time t:

$$P(t,s) \equiv \text{Prob}\ \{\ S_{\rm av}(t') \geq s,\ \forall t' \leq t\ \}. \tag{1.3.4}$$

The calculation of $P(t,s)$ is shown schematically in Fig. 1.2. Since $S_{\rm av}(t) \in [-1,1]$, the probability $P(t,s)$ is defined for $-1 \leq s \leq 1$. For $s = 1$ we recover the usual persistence probability: $P(t) \equiv P(t, s = 1)$ measures the probability of the height fluctuation remaining above zero ("positive") throughout the whole time interval.

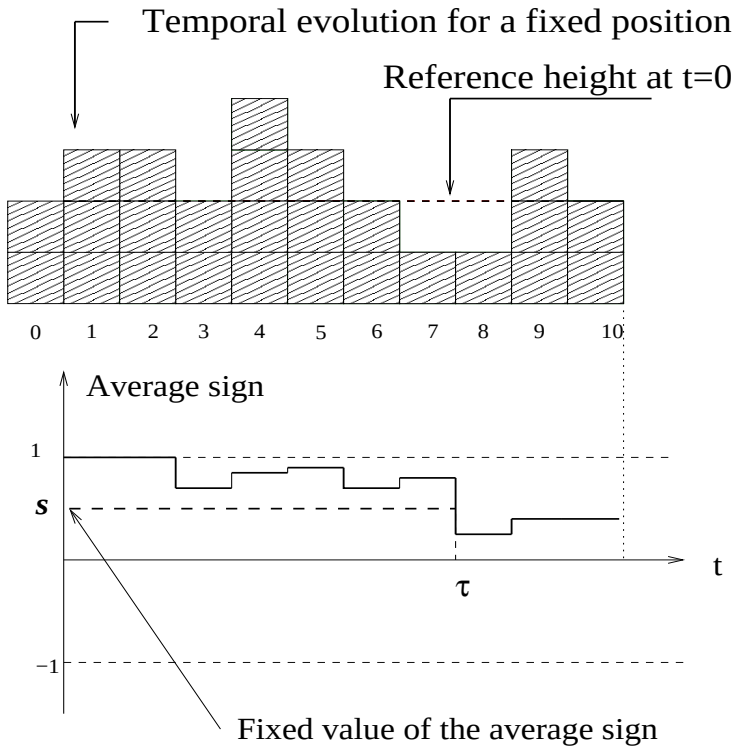

Figure 1.2: Temporal evolution of the height variable $h(x_j, t)$ at a fixed position x_j (top) and the representation of the associated average sign variable vs. time (bottom). At time $t = \tau$ the persistent large deviations probability vanishes because the average sign becomes smaller than s.

For $s = -1$ the probability $P(t, s = -1)$ is trivially equal to unity for all t. We will show in Chapter 3 that the evolution of $P(t, s)$ in time follows a power–law, $P(t, s) \sim t^{-\theta_l(s)}$, where $\theta_l(s)$ represents the family of persistent large deviations exponents, making this probability an extremely useful concept for probing the universality class of the underlying dynamic process. $P(t, s)$ and $\theta_l(s)$ are natural generalizations of the persistence probability $P(t)$ and the persistence exponent θ, respectively, to the broader concept of distribution of residence times with limiting behavior (i.e. $s = 1$) determining the usual persistence exponent.

1.3.3 Survival probability

Instead of considering the probability of not returning to the initial position, we define a *survival probability*, $S(t)$, as the probability of the dynamical step height (at a fixed but arbitrary spatial location) not returning in time t to its average ("equilibrium") level (denoted by $\bar{h}$). In a recent experimental study [38] of thermal fluctuations of surface steps, it was found that $S(t)$ has an exponential decay, $S(t) \propto \exp(-t/\tau_s)$, at long times, where τ_s is the survival time scale. The formal definition of this probability reads:

$$S(t) \equiv \text{Prob } \{ \ h(x, t') > \ \bar{h}, \ \forall \ t_0 \leq t' \leq t_0 + t \ \}. \tag{1.3.5}$$

The calculation of both persistence and survival probabilities is depicted in Fig. 1.3. $h(t)$ is the height stochastic variable and δt is the sampling time (i.e., the interval between two successive measurements of the height value). The persistence/survival clock ticks as long as the probability remains equal to 1. We see that the persistence

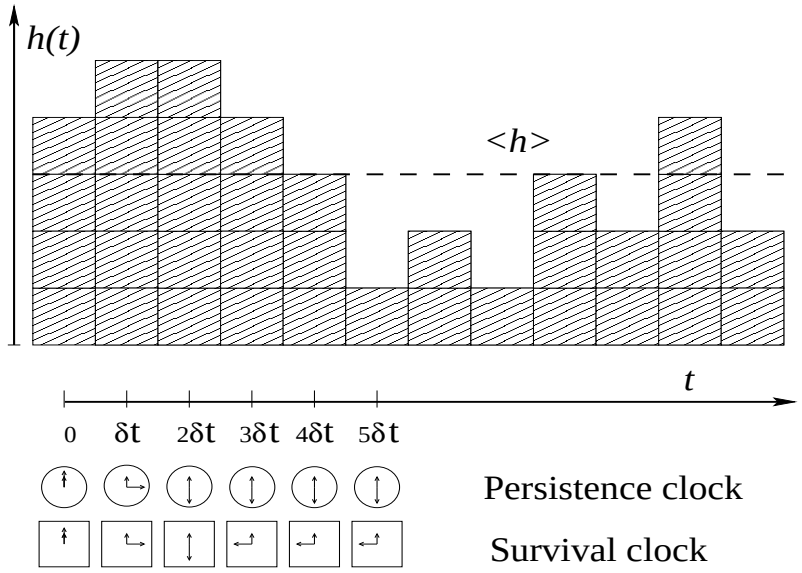

Figure 1.3: Schematic representation of the survival probability calculation for a stochastic variable $h(t)$. The clock, shown in the bottom of the figure, runs if the probability remains 1 (i.e., if the average height level has *not* been reached). The persistence probability clock is shown for comparison.

clock stops at $t = 2\delta t$ because the height reaches its original value for $t > 2\delta t$. However, the survival clocks continues to run until $t = 3\delta t$ and afterwards, since the average value $\bar{h}$ is reached at $t = 4\delta t$, the survival probability vanishes.

1.3.4 Generalized survival probability

For equilibrium step fluctuations, we define the generalized survival probability with respect to the height reference level R, $S(t, R)$, as the probability for the height variable to remain consistently *above* a certain pre-assigned value "R" over time t:

$$S(t, R) \equiv \text{Prob } \{\ h(x, t') > \ R,\ \forall\ t_0 \leq t' \leq t_0 + t\ \}, \tag{1.3.6}$$

where $h(x, t)$ is the dynamical height of the interface at a fixed lateral position x at time t, and t_0 is the initial time of the measurement. Although the above definition involves the dynamical variable $h(x, t)$ defined for a particular lateral position x, we take a statistical ensemble average over all lateral positions to obtain a purely time dependent stochastic dynamical quantity $S(t, R)$. Obviously, another quantity that can be measured is the probability for the height stochastic variable to remain *below* the reference level up to time t. Since we will consider the dynamics of the interface fluctuations obeying a linear stochastic equation, the interface preserves the up-down symmetry along the direction perpendicular to the step edge. As a consequence, the average of the probabilities of remaining always above R and below $-R$, with $R \geq 0$, will be our measured generalized survival probability. For $R = 0$ we obtain the usual survival probability.

1.3.5 Spatial persistence and survival probabilities

Obviously, the same type of persistence and survival questions, addressed previously to the temporal evolution of the variable $h(x,t)$, can now be formulated in terms of the stochastic spatial evolution at a fixed time. The spatial persistence probability of fluctuating interfaces, denoted by $P(x_0, x_0+x)$, is simply the probability that the height of a steady-state interface configuration, measured at a fixed time t_0, *does not* return to its "original" value $h(x_0,t_0)$ at the initial point x_0 within a distance x measured from x_0 along the interface. In the long-time, steady-state limit, the spatial persistence probability, which depends only on x for a translationally invariant interface, has been shown [45] to exhibit a power-law decay, $P(x_0, x_0+x) \sim x^{-\theta}$. One of the interesting results reported in Ref. [45] is that the spatial persistence exponent θ can take two values determined by the initial conditions or selection rules imposed on the starting point x_0: 1) $\theta = \theta_{SS}$, the "steady state" (SS) persistence exponent if x_0 is sampled uniformly from *all* the sites of a steady-state configuration; and 2) $\theta = \theta_{FIC}$, the so-called *finite-initial-conditions* (FIC) persistence exponent if the sampling of x_0 is performed from a *subset* of steady-state sites where the height variable and its spatial derivatives are *finite*. The spatial persistence probabilities obtained for these two different ways of sampling the initial point are denoted by $P_{SS}(x_0, x_0+x)$ and $P_{FIC}(x_0, x_0+x)$, respectively, and their definitions are:

$$P_{SS}(x_0, x_0+x) \equiv \text{Prob}\ \{\ \text{sign}\,[h(x_0+x') - h(x_0)] = \text{constant}\,, \\ \forall\ 0 < x' \leq x\ ,\ \forall\ x_0 \in \mathcal{S}_{SS}\ \}\,, \qquad (1.3.7)$$

and

$$P_{FIC}(x_0, x_0 + x) \equiv \text{Prob } \{ \text{ sign } [h(x_0 + x') - h(x_0)] = \text{ constant }, \\ \forall\ 0 < x' \leq x\ ,\ \forall\ x_0 \in \mathcal{S}_{FIC}\ \}\,. \qquad (1.3.8)$$

The spatial survival probabilities corresponding to the SS and FIC conditions are calculated similarly to the corresponding persistence probabilities, except that the stochastic variable under consideration becomes $h(x_0 + x') - \langle h \rangle$. Thus,

$$S_{SS}(x_0, x_0 + x) \equiv \text{Prob } \{ \text{ sign } [h(x_0 + x') - \langle h \rangle] = \text{ constant }, \\ \forall\ 0 \leq x' \leq x\ ,\ \forall\ x_0 \in \mathcal{S}_{SS}\ \}\,, \qquad (1.3.9)$$

and

$$S_{FIC}(x_0, x_0 + x) \equiv \text{Prob } \{ \text{ sign } [h(x_0 + x') - \langle h \rangle] = \text{ constant }, \\ \forall\ 0 \leq x' \leq x\ ,\ \forall\ x_0 \in \mathcal{S}_{FIC}\ \}\,. \qquad (1.3.10)$$

2. PERSISTENCE IN NONEQUILIBRIUM SURFACE GROWTH

As we have seen in Chapter 1, in the context of surface growth and fluctuations, the persistence probability $P(t_0, t_0 + t)$ may be defined as the probability that starting from an initial time t_0, the interfacial height $h(\mathbf{r}, t')$ at spatial position $\mathbf{r}$ does not return to its original value at any point in the time interval between t_0 and $t_0 + t$. This probability is clearly the sum of the probabilities of the height $h(\mathbf{r}, t')$ always remaining above (the *positive* persistence probability P_+) and always remaining below (the *negative* persistence probability P_-) its specific initial value $h(\mathbf{r}, t_0)$ for all $t_0 < t' \leq t_0 + t$. This concept quantifies the tendency of a stochastic field (in our case the interface height) to persistently conserve a specific feature (the sign of the interfacial height fluctuations). The persistence probability $P(t_0, t_0 + t)$ would, in general, depend on both t_0 and t. In the early stage of the growth process starting from a flat interface (transient regime), the interface gradually develops dynamical roughness [1, 2] due to the effect of fluctuations in the beam intensity. In this regime, the choice of the initial time t_0 is clearly important: it determines the degree of

roughness of the configuration from which the interface evolves. At long times, the growing interface enters into a new evolution stage, called the steady–state regime, characterized by fully developed roughness that does not increase further in time. In this regime, the choice of t_0 is expected to be unimportant.

The work of Krug *et al.* [29] shows that for a class of *linear* Langevin–type equations for surface growth and atomistic models belonging in the same dynamical universality class as these equations, the persistence probability decays as a power law in time for long times in both transient and steady–state regimes. These power laws define the positive and negative persistence exponents, $\theta_{\pm}^{T}$ and $\theta_{\pm}^{S}$, for positive and negative persistence in the transient and steady–state regimes, respectively. The $h \to -h$ symmetry of the linear growth equations implies that $\theta_{+}^{T} = \theta_{-}^{T}$ and $\theta_{+}^{S} = \theta_{-}^{S}$ in these systems. In Ref. [29], it was pointed out that the persistence exponent in the steady state of these linear models is related to the dynamic scaling exponent β, that describes the growth of the interface width W as a function of time t in the transient regime ($W \propto t^{\beta}$), through the relation $\theta_{+}^{S} = \theta_{-}^{S} = 1 - \beta$. The validity of this relation was confirmed by numerical simulations. Since the exponent β is the same for all models in the same dynamical universality class, this result implies that the persistence exponent in the steady–state regime of these *linear* models is also universal. Numerical results for the persistence exponent in the transient regime, for which no analytic predictions are available, also indicate a similar universality. Kallabis and Krug [30] carried out a similar calculation for (1+1)–dimensional Kardar–Parisi–Zhang (KPZ) [13] interfaces. They found that the nonlinearity in the KPZ equation that breaks the $h \to -h$ symmetry is reflected in *different* values of

the positive and negative persistence exponents, θ_+^T and θ_-^T, in the transient regime. The values of the steady–state persistence exponents θ_+^S and θ_-^S were found to be equal to each other, and equal to $1-\beta$ within the accuracy of the numerical results. This is expected because the $h \to -h$ symmetry is dynamically restored in the steady state of the (1+1)–dimensional KPZ equation. This is, however, a specific feature of the (1+1)–dimensional KPZ model, which for nongeneric reasons, turns out to be up–down symmetric in the steady state. Nonlinear surface growth models (e.g. the higher dimensional KPZ model, the nonlinear MBE growth model) are generically expected to have different values of $\theta_\pm$ in both transient and steady–state regimes.

In this chapter, we present the results of a detailed numerical study of the persistence behavior of several atomistic, solid–on–solid (SOS) models of surface growth in (1+1) and (2+1) dimensions. While we concentrate on models in the MBE universality class, results for a few other models, some of which have been studied in Refs. [29] and [30] are also presented for completeness. The highly non–trivial nature of the persistence probability, in spite of a deceptive simplicity of the defining concept, arises from the complex temporal non–locality ("memory") inherent in its definition. In fact, there are very few stochastic problems where an analytical solution for the persistence probability has been achieved. These include the classical Brownian motion [57], the random acceleration problem [58] and the one dimensional Ising and q-state Potts models [26]. In general, the highly nonlocal nature of the temporal correlations in a non–Markovian stochastic process makes it extremely difficult to obtain exact results for the persistence probability even for

seemingly simple stochastic processes[1]. Even for the simple diffusion equation, the persistence exponent is known only numerically, or within an independent interval approximation [23] or series expansion approach [59]. However, it is fairly straightforward in most cases to directly simulate the persistence probability to obtain its stationary power law behavior at large times, and thus to numerically obtain the approximate value of the persistence exponent. For this reason, we use stochastic (Monte Carlo) simulations of the atomistic growth models to study their temporal persistence behavior in the transient and steady–state regimes. These models are defined in terms of random deposition and specific cellular–automaton–type local diffusion or relaxation rules. Some of these models are of the "limited–mobility" type in the sense that the surface diffusion rules or local restrictions limit the characteristic length over which a deposited particle can diffuse to just one or a few lattice spacings. The models in the MBE universality class considered in our study are: the Das Sarma–Tamborenea model [4], the Wolf–Villain model [5] [2], the Kim–Das Sarma model [6] and its "controlled" version [16], and the restricted solid–on–solid (RSOS) model of Kim *at al.* [10]. We also present results for the Family model [3] that is known to belong to the Edwards–Wilkinson [12] universality class and the

[1]In the appendix we explain in detail why the analytical calculation of θ is difficult for surface growth models.

[2]The asymptotic long–time behavior of the (1+1)–dimensional Wolf–Villain model is known to be in the Edwards–Wilkinson universality class. However, its behavior in the relatively short–time regime considered here is expected to be similar to that of other models in the MBE universality class.

restricted solid–on–solid (RSOS) model of Kim and Kosterlitz [8] that is in the KPZ universality class.

The main objective of this chapter is to examine the effects of the nonlinearity in the MBE growth equation [14, 15] on the persistence behavior. Unlike the (1+1)–dimensional KPZ equation, the nonlinearity in the MBE growth equation persists in the steady state in the sense that the height profile exhibits a clear asymmetry between the positive and negative directions (above and below the average height). Therefore, the positive and negative persistence exponents θ_+^S and θ_-^S are expected to have different values in these models. If this is the case, then the relation between the steady–state persistence exponent and the dynamic scaling exponent β found in linear models can not be valid for both θ_+^S and θ_-^S, indicating that at least one of these exponents is a new, nontrivial one not related to the usual dynamic scaling exponents. The values of θ_+^S and θ_-^S and their relation to β, as well as the values of the transient persistence exponents θ_+^T and θ_-^T are the primary questions addressed in our study. We also investigate the universality of these exponents by measuring them for several models that are known to belong in the same universality class as far as their dynamic scaling behavior is concerned. To obtain accurate values of the exponents, the "noise reduction" technique [52] is employed in some of the simulations of (1+1)–dimensional models. We also address some questions related to the methodology of calculating persistence exponents from simulations. Since the value of the dynamical exponent z is relatively large for models in the MBE universality class, the time required for reaching the steady state grows quickly as the sample size L is increased ($t_{sat} \propto L^z$). As a result, it is difficult to reach the

steady state in simulations for large L. It is, therefore, useful to find out whether the value of the steady–state persistence exponents can be extracted from calculations of $P(t_0, t_0 + t)$ with $t_0 \ll t_{sat} \propto L^z$. Another issue in this context involves the effects of the finiteness of the sample size L and the sampling time δt (the time interval between two successive measurements of the height profile) on the calculated persistence probability. An understanding of these effects is needed for extracting reliable values of the persistence exponents from simulations that *always* involve finite values of L and δt. Understanding the effects of L and δt on the persistence analysis is not only important for our simulations, but is also important in the experimental measurements of persistence which invariably involve finite system size and sampling time.

The main results presented in this chapter are as follows. We find that the positive and negative steady–state persistence exponents for growth models in the MBE universality class are indeed different from each other, reflecting the asymmetry of the interface arising from the presence of nonlinearities in the underlying growth equation. Our results for these exponent values are: $\theta_+^S = 0.66 \pm 0.02$ and $\theta_-^S = 0.78 \pm 0.02$, respectively, in (1+1) dimensions; $\theta_+^S = 0.76 \pm 0.02$ and $\theta_-^S = 0.85 \pm 0.02$ in (2+1) dimensions. The values of the positive and negative persistence exponents for different models are clearly correlated with the asymmetry of the "above" and "below" (defined relative to the mean interface height) portions of the interface. We show analytically that the *smaller* one of the two steady-state persistence exponents should be equal to $(1 - \beta)$. Thus, the relation $\theta = 1 - \beta$ derived in Ref. [29] for linear surface growth models is expected to be satisfied by

θ_+^S for the nonlinear models considered here. Our numerical results are consistent with this expectation: we find that the positive persistence exponent is indeed close to $(1-\beta)$, while the negative one is significantly higher. Similar asymmetry is found for the persistence exponents in the transient regime with $\theta_+^T < \theta_-^T$ in MBE growth. Within the uncertainties in the numerically determined values of the exponents, they are universal in the sense that different models in the same dynamic universality class yield very similar values for these exponents. For the models in the Edwards–Wilkinson and KPZ universality classes, we find results in agreement with those of earlier studies [29, 30].

Our simulations also reveal that a measurement of the steady–state persistence exponents is possible from simulations in which the initial time t_0 is much smaller than the time ($\sim L^z$) required for the interfacial roughness to saturate. A similar result was reported in Ref. [29] where it was found that the steady–state persistence exponent may be obtained from a calculation of $P(t_0, t_0+t)$ with $t \ll t_0 \ll L^z$. We find that the restriction $t \ll t_0$ is not necessary for seeing a power law behavior of $P_\pm(t_0, t_0+t)$ – a power law with the steady–state exponents is found even if t is close to or somewhat larger than t_0. We exploit this finding in some of our persistence simulations for (2+1)–dimensional growth models which are more relevant to experiments. These results, however, also imply that it would be extremely difficult to measure the transient persistence exponents from real surface growth experiments. Finally, we show that the dependence of the steady–state persistence probability on the sample size L and the sampling time δt is described by a simple scaling function of the variables t/L^z and $\delta t/L^z$. This scaling description is similar to that found

recently [43] for a different "persistence probability", the survival probability, that measures the probability of the height not returning to its *average value* (rather than the initial value) over a certain period of time. Although the "persistence" and the "survival" [43] probability seem to be qualitatively similar in their definitions, the two are mathematically quite unrelated, and in fact, no exponent can be defined for the survival probability, as we will see in Chapter 4. In this chapter we only discuss the persistence probability and the persistence exponent for surface growth processes.

2.1 Simulation results and discussion

2.1.1 Persistence exponents in (1+1) dimensions

Simulations for (1+1)–dimensional discrete growth models were carried out for $\beta =$ 1/4, 3/8 and 1/3. The value $\beta = 1/4$ corresponds to the F model that has a relatively small equilibration time (of the order of L^2). The remaining conservative models, characterized by $\beta = 3/8$ (LC) and $\simeq 1/3$ (WV, DT, CKD and KPK), have a much slower dynamics (with z values 4 or 3). So their corresponding equilibration time intervals, required for the interface roughness to reach saturation, are of the order of L^4 and L^3, respectively. For this reason, the largest values of L for which the steady state could be reached in reasonable simulation time are considerably shorter in these models than in the F model. The fastest equilibration occurs in the KK model ($\beta = 1/3$) where $z = 3/2$.

In calculations of the transient persistence probabilities, the initial configura-

tion of the height variables is taken to be perfectly flat, i.e. $h_j(t_0) = 0$ $(j = 1, L)$. The lattice size was in the range $10^4 \leq L \leq 10^6$, and the duration of the deposition process, measured in units of number of grown monolayers (ML), was $\sim 10^3$. The results were averaged over $\sim 10^3$ independent runs. For measurements in the steady–state situation, a saturation of the interface roughness was first obtained by depositing a large number (of the order of L^z) of monolayers and subsequent time evolution from one of the steady–state configurations obtained this way was used for measuring the persistence probabilities. A much smaller lattice length ($L = 1000$ for the F model, $L = 500$ for the KK model, $L = 200$ for the KPK model, and $L = 40$ for the LC, WV, DT and CKD models) was used in these calculations in order to reach the steady–state saturation within reasonable simulation times.

The positive (negative) persistence probabilities in both transient and steady–state regimes were obtained as the fraction of sites that maintain the values of their heights persistently above (below) their initial values, averaged over a large number ($\sim 10^4$) of independent runs. The persistence exponents were obtained from power law fits to the decay of these probabilities, as shown in Figs. 2.1–2.4 and 2.6–2.8 for the transient and steady–state regimes, respectively.

For all the models studied here, we have also measured the value of the growth exponent β in both transient and steady–state simulations. Since the latter simulations were carried out for smaller values of the system size L, these measurements provide useful information about the dependence of the measured exponent values on the lattice size. Similar information is also provided by the values of the transient persistence exponents obtained from measurements in the initial stage of the

Model	L	θ_+^T	θ_-^T	β	Universality class
F	10^6	1.57 ± 0.10	1.49 ± 0.10	0.25 ± 0.01	EW
KK	5×10^4	1.68 ± 0.02	1.21 ± 0.02	0.33 ± 0.01	KPZ
LC	10^4	0.84 ± 0.02	0.84 ± 0.02	0.37 ± 0.01	MH
WV	10^4	0.94 ± 0.02	0.98 ± 0.02	0.37 ± 0.01	MBE
DT	10^4	0.95 ± 0.02	0.98 ± 0.02	0.38 ± 0.01	MBE
CKD	10^4	0.98 ± 0.02	0.93 ± 0.02	0.35 ± 0.01	MBE
KPK	10^4	1.04 ± 0.02	1.01 ± 0.02	0.31 ± 0.01	MBE

Table 2.1: Positive and negative persistence exponents, θ_+ and θ_-, for the transient (T) regime, measured for seven different discrete growth models (identified in the first column) using kinetic Monte Carlo simulations with relatively large system sizes (L). The measured growth exponent, β, and the universality class of the model are indicated in the last two columns, respectively.

Model	L	θ_+^T	θ_-^T	θ_+^S	θ_-^S	β
F	10^3	1.67 ± 0.10	1.56 ± 0.10	0.78 ± 0.02	0.76 ± 0.02	0.25 ± 0.01
KK	5×10^2	1.70 ± 0.02	1.27 ± 0.02	0.71 ± 0.02	0.71 ± 0.02	0.30 ± 0.01
LC	40	0.98 ± 0.02	0.96 ± 0.02	0.67 ± 0.02	0.67 ± 0.02	0.32 ± 0.01
WV	40	0.94 ± 0.02	0.99 ± 0.02	0.65 ± 0.02	0.70 ± 0.02	0.35 ± 0.01
DT	40	0.98 ± 0.02	1.01 ± 0.02	0.64 ± 0.02	0.72 ± 0.02	0.36 ± 0.01
CKD	40	1.11 ± 0.02	0.99 ± 0.02	0.78 ± 0.02	0.66 ± 0.02	0.33 ± 0.01
KPK	2×10^2	1.16 ± 0.02	1.09 ± 0.02	0.70 ± 0.02	0.68 ± 0.02	0.28 ± 0.01

Table 2.2: Positive and negative persistence exponents, θ_+ and θ_-, for the transient (T) and the steady state (S) regimes of our seven different discrete growth models, obtained from simulations with relatively small samples sizes (L). To illustrate the effects of reduced system sizes on the measured exponents, we have shown the values of β obtained from these simulations in the last column.

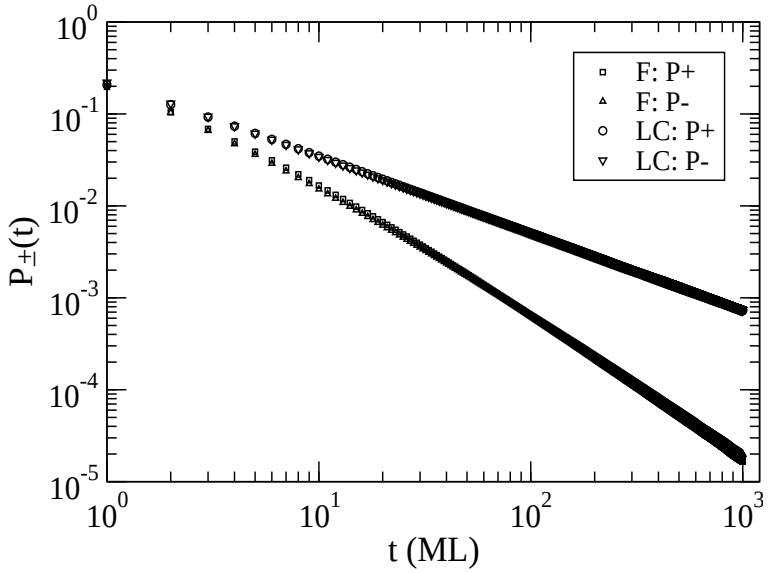

Figure 2.1: Transient persistence probability for the (1+1)–dimensional linear F and LC growth models. As expected, the positive and negative persistence probabilities are identical in these models. The system size is $L = 10^6$ for the F model and $L = 10^4$ for the LC model, and an average over 10^3 independent runs was performed. The slopes of the double–log plots yield the values of the transient persistence exponents shown in Table 2.1.

steady–state simulations. The transient exponent values obtained from the large–L simulations are listed in Table 2.1, and both transient and steady–state exponent values obtained from simulations of relatively small samples are shown in Table 2.2. The measured values of the growth exponent β are also shown in these Tables.

Estimation of the probable error in the measured values of the growth and persistence exponents is a delicate task (and surely depends on precisely how the exponent error is defined), since there is not a traditional accepted method to evaluate the error in dynamical simulations. To solve this problem we did the following simulations. We decreased the number of independent runs used for the averaging procedure by a factor of 2, keeping the size of the system constant. Under these circumstances, we have measured the exponents corresponding to the two different numbers of independent runs and the differences between the obtained values of the exponents were used as error estimates for β and θ, respectively. Approximately the same size of the error bar was obtained from the estimations of fluctuations in the value of the local slope of the double–log plots. We have also noticed that a reduction of the lattice size (imposed for the steady–state persistence calculations) produces lower values of the growth exponents, as shown in Table 2.2. This is because the downward bending (approach to saturation) of double–log width versus time plots occurs at shorter times in simulations of smaller systems. However, the smaller–L simulations seem to lower the measured values of the growth exponents by a maximum of about 10% percent. So we conclude that this effect is not dramatic and that the steady–state results reported below are reliable.

The measured values of β agree reasonably well with the expected ones (see

Section 1.1) within their errors. As expected, the agreement is better in the case of larger values of L. For the larger–L simulations ($L \sim 10^4$), we have found that the growth exponents of the F, LC and KK models are in excellent agreement with their corresponding expected values of 1/4, 3/8 and 1/3, respectively (see Table 2.1). The DT and WV models are found to behave similarly at early (transient) stages of their interface growth, at least in (1+1)–dimensions, their growth exponents being: $\beta_{WV} \approx 0.37$ and $\beta_{DT} \approx 0.38$. The closeness of these values to the value of 3/8, which corresponds to the MH universality class, suggests that the nonlinear term that appears in the associated dynamic equation (i.e. Eq. (1.1.5)) has a very weak effect for the range of lattice sizes used in our study. In addition, we have found that the CKD model characterized by the nonlinear coefficient $\lambda_{22} = 2$ and control parameter $c = 0.02$ has a growth exponent $\beta_{CKD} \sim 0.35$, in agreement with Ref. [16]. These particular parameter values ensured the elimination of any interfacial instability, thus allowing a calculation of the steady–state persistence properties. Regarding the conserved KPK model, we have observed that the growth exponent has a value that is slightly smaller than 1/3, a result that agrees with Ref. [10].

The temporal behavior of the transient persistence probability in our models is shown in Figs. 2.1–2.4. From these measurements, we obtained the transient persistence exponents by fitting the linear middle regions (excluding the small–t and large–t ends, typically using the data for $20 < t < 800$) of the double–log plots to straight lines. As expected, due to the invariance of the interfaces of the F and LC models (which are characterized by *linear* continuum equations) under a change of sign of the height variables, we obtained equal positive and negative transient

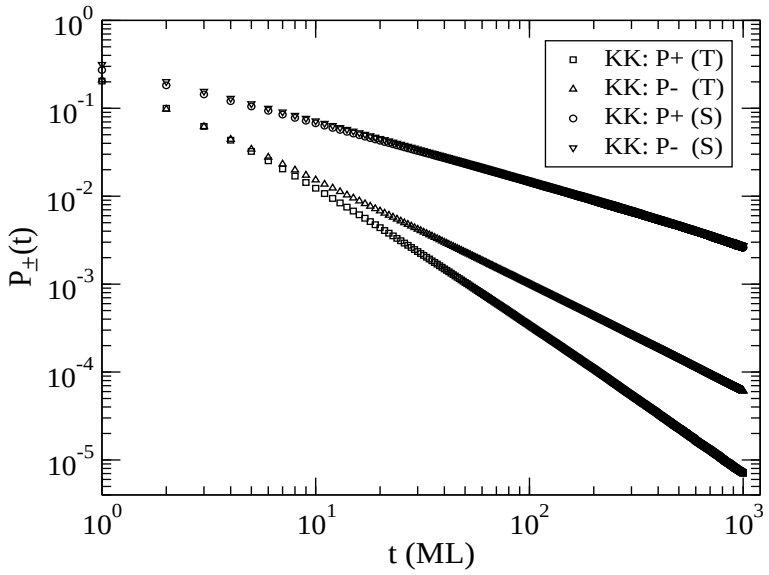

Figure 2.2: Positive and negative transient (bottom two curves) and steady–state (top two curves, mostly overlapped) persistence probabilities for the (1+1)–dimensional RSOS KK model. The faster decay of the positive persistence probability in the transient regime is due to the negative sign of λ_2 in the equivalent continuum equation of Eq. (1.1.3). In the transient case, systems of size $L = 5 \times 10^4$ were averaged over 5×10^3 independent runs. The steady–state simulation was done for $L = 500$ and a similar average was performed.

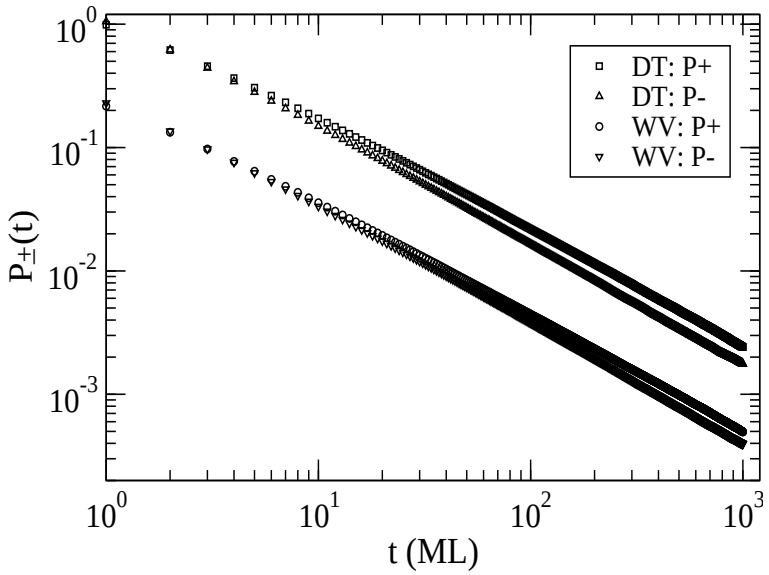

Figure 2.3: Positive and negative transient persistence probabilities for the (1+1)–dimensional nonlinear DT and WV growth models. We note that despite the difference in their local diffusion rules, these two models behave identically as far as the transient persistence probability is concerned. The curves corresponding to the DT model have been shifted upward in order to avoid a complete overlap of the plots for the two models. The system size is $L = 10^4$ and an average over 10^3 independent runs was performed. The slopes of the double–log plots yield the transient persistence exponents given in Table 2.1.

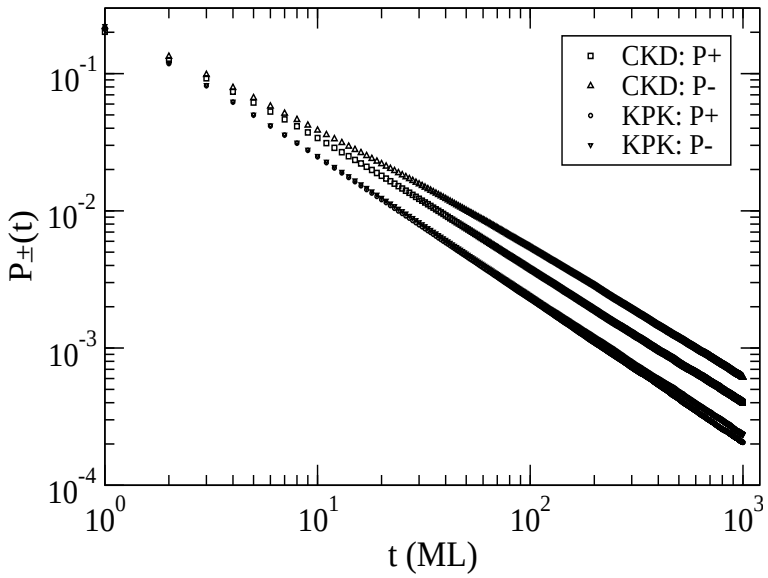

Figure 2.4: Positive and negative transient persistence probabilities for the (1+1)–dimensional CKD (the upper two curves) and RSOS (the lower two, almost overlapped curves) models that belong to MBE universality class. In both cases the system size was $L = 10^4$ and an average over 10^3 independent runs was performed. The slopes of the double–log plots yield the transient persistence exponents given in Table 2.1.

persistence exponents within the error bars, as displayed in Fig. 2.1. However, we mention that the F model has a rather slow convergence of the positive and negative exponents towards their long–time value of ~ 1.55 observed in much longer simulations. The results for F and LC models, that correspond to $\beta = 1/4$ and $3/8$, respectively, agree well with the values reported by Krug *et al.* [29]. The same level of agreement is also found in the case of the KK model [30], shown in Fig. 2.2, for which the transient persistence exponents are $\theta_+^T \approx 1.68$ and $\theta_-^T \approx 1.21$ in (1+1)–dimensions. We note that the negative persistence probability has a slower decay than the positive one. This is due to the constant coefficient, λ_2, of the nonlinear term $|\nabla h(\mathbf{r},t)|^2$ of the KPZ equation (which provides a continuum description of the KK model) having a negative sign [30].

For the models described by the fourth–order nonlinear MBE equation (i.e. WV, DT, CKD and KPK models), we expect to find different positive and negative transient persistence exponents due to the fact that their morphologies violate the up–down interfacial symmetry with respect to the average level. No information about how different these two exponents should be is available in the literature. In most of these growth models, we observe that the two exponents are not very different from each other, especially during the transient regime. Fig. 2.3 shows the transient regime results for DT and WV models, which are indeed very similar – their persistence probability curves have almost identical behavior. We note here that the negative persistence probability has a faster decay than the positive persistence probability. This indicates a negative sign of λ_{22}, the coefficient that multiplies the nonlinear term $\nabla^2|\nabla h(\mathbf{r},t)|^2$ of the MBE equation. However, the relative order of

the values of these exponents is reversed when $\lambda_{22} > 0$, which is the case in the CKD and KPK models, as shown in Fig. 2.4. To clarify this aspect, we show in Fig. 2.5 the interfacial morphologies of DT and CKD models. We used a lattice of $L = 10^4$ sites (but only a portion of 1000 sites is shown in each case) and the displayed configurations correspond to a time of 10^3 ML. The interface of the DT model is characterized by deep grooves, while the profile in the CKD model exhibits the distinct feature of high pillars. Both morphologies display strong up–down interfacial asymmetry, but their representative features (i.e. deep grooves and high pillars) are opposite in "sign", indicating a reversal of the sign of the coefficient λ_{22} (note that a reversal of the sign of λ_{22} in Eq. (1.1.5) is equivalent to changing the sign of the height variable $h(\mathbf{r}, t)$).

As summarized in Table 2.1, the DT, WV and CKD models show very similar values for the transient persistence exponents when the above mentioned effect of the sign of λ_{22} is taken into account. However, some deviation from the exponent values for this group of models is observed in the RSOS KPK model which shows the smallest difference between the positive and negative persistence exponents. Finite size effects appear to be stronger in this case. These effects also cause an increase in the measured values of the persistence exponents above the expected values. A similar behavior is found in the steady–state results as well, as described below.

Our calculations of WV, DT, CKD and KPK persistence exponents illustrate the feasibility of studying this type of nonequilibrium statistical probabilities for a large class of nonequilibrium applications described by nonlinear dynamical equations. Until now, the only nonlinear equation for which persistence exponents have

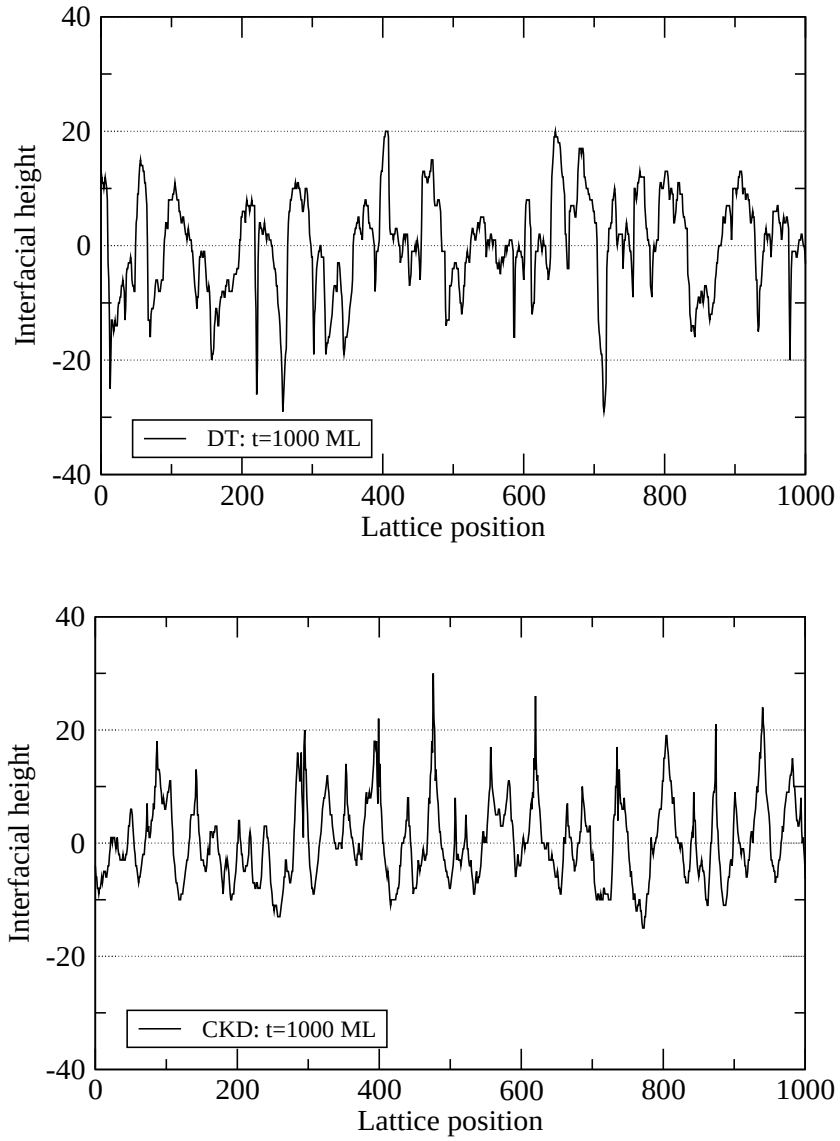

Figure 2.5: Morphologies of the (1+1)–dimensional DT (top) and CKD (bottom) stochastic models for $L = 10^4$ (only a portion of 1000 sites is shown) and $t = 10^3$ ML. In the DT model, we notice a breaking of up–down symmetry due to the formation of deep grooves, while in the CKD model, the representative asymmetric feature corresponds to high pillars.

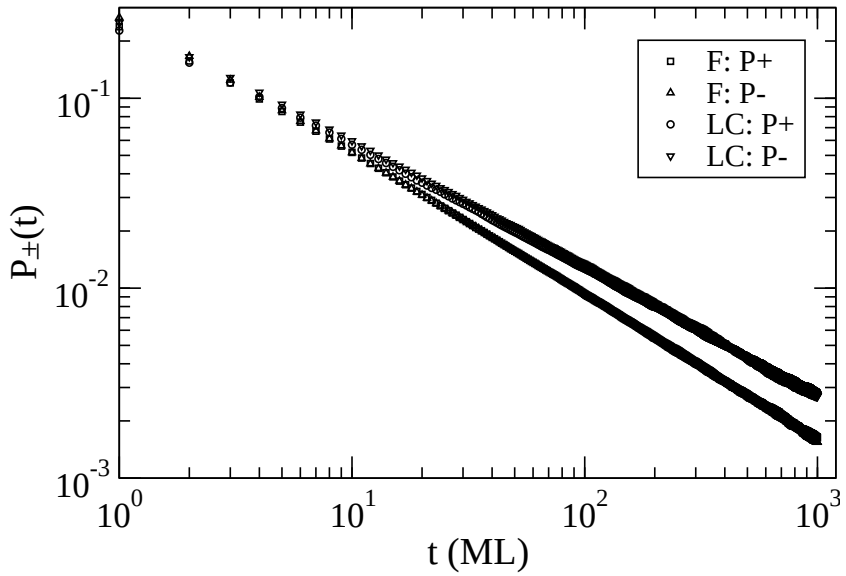

Figure 2.6: Positive and negative steady–state persistence probabilities for the (1+1)–dimensional F and LC models which are governed by linear continuum dynamical equation. The temporal decay of the persistence probability is slower in the LC model which has a larger growth exponent ($\beta_{LC} = 3/8$, $\beta_F = 1/4$). We used $L = 1000$ and $t_0 = 4 \times 10^6$ ML for the F model, and $L = 40$, $t_0 = 10^6$ ML for the LC model. The displayed results were averaged over 5000 independent runs. The measured slopes of the double–log plots yield the steady–state persistence exponents shown in Table 2.2.

been calculated [30] is the KPZ equation, which is arguably the simplest nonlinear Langevin equation. Further, the nonlinearity in the KPZ equation becomes irrelevant in the steady–state regime in (1+1)–dimensions. So, the effects of nonlinearity are not reflected in the steady–state persistence behavior of (1+1)–dimensional KPZ systems. An immediate concern would be that more complex nonlinear dynamic equations might be less approachable from the point of view of persistence probability calculation. Our results for four nonlinear models eliminate this possibility and illustrate the applicability and usefulness of persistence probability calculations in the study of surface fluctuations.

Figures 2.6–2.8 display our results for the steady–state persistence probabilities. The values of the growth and persistence exponents obtained from the steady–state simulations are summarized in Table 2.2. The values of the steady–state persistence exponents in the F and LC models, corresponding, respectively, to the ∇^2 and ∇^4 linear equations, (see Fig. 2.6) are consistent with the values of the corresponding growth exponents (as predicted by Eq. (1.3.3)) obtained from the same small–L simulations. For the WV and DT models, as shown in Fig. 2.7, we obtain very similar positive and negative persistence exponents. In the case of the KK model we find, as expected, identical positive and negative exponents ($\theta_{\pm}^{S} \approx 0.71$), as shown in Fig. 2.2.

Among the models belonging to the MBE universality class, the KPK model exhibits steady–state persistence exponents that are systematically higher than the ones obtained for the remaining three (WV, DT and CKD) models. Our study of the dynamical scaling behavior of the KPK model indicates that both α (~ 0.9) and z

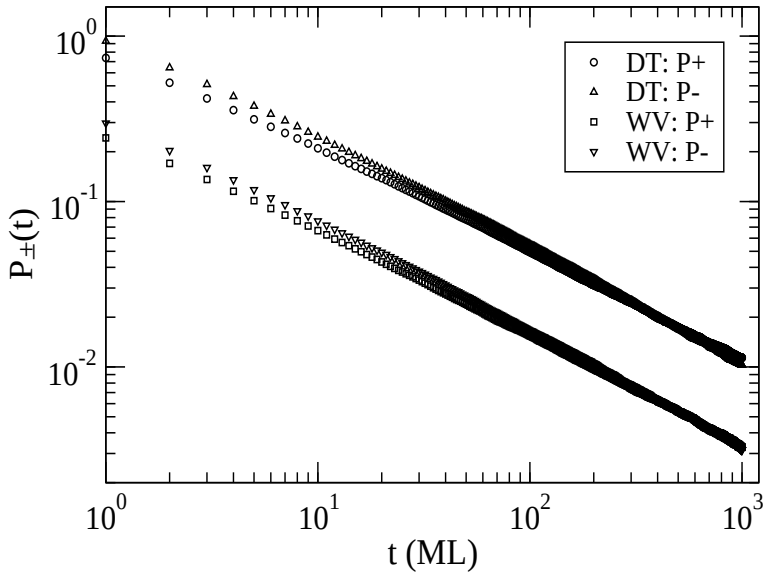

Figure 2.7: Steady–state persistence probabilities for two (1+1)–dimensional models in the MBE universality class – the DT and WV models. As in the transient case, these two models exhibit almost identical persistence behavior in the steady state. The effects of the nonlinearity in their continuum dynamical description are not very prominent for the small lattice sizes considered here. For the data shown, systems of size $L = 40$ were equilibrated for $t_0 = 10^5$ ML, and the results were averaged over 5000 independent runs. The persistence plots for the DT model have been shifted up in order to make them distinguishable from the WV plots. The measured slopes of the double–log plots yield the steady–state persistence exponents shown in Table 2.2.

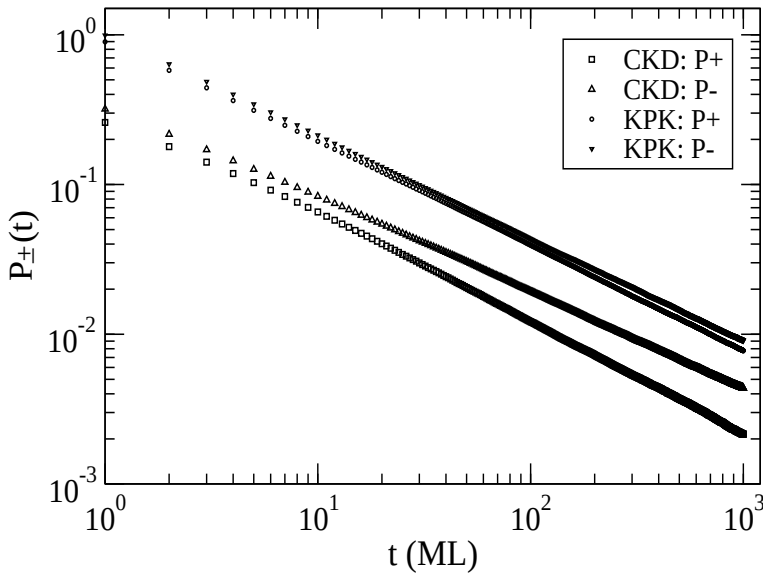

Figure 2.8: Double–log plots of the steady–state persistence probabilities of (1+1)–dimensional MBE class CKD and KPK (shifted up by a constant amount) models. While the KPK model does not show a clear effect of nonlinearity in the values of the persistence exponents, the CKD model shows positive and negative persistence exponents that are clearly different from each other. Systems of size $L = 40$ (CKD) and $L = 200$ (KPK) were equilibrated for $t_0 \sim 10^5$ ML. The results were averaged over 10^4 independent runs. The measured slopes of the double–log plots yield the steady–state persistence exponents shown in Table 2.2.

(~ 2.9) in this model are reasonably close to the expected values, in agreement with Ref. [10]. Therefore, the reason for the differences between the values of the steady–state persistence exponents for the KPK model and those in the other models in the MBE universality class is unclear. This discrepancy may very well be arising from subtle differences in finite size (and time) effects in the simulations for persistence exponents and dynamic scaling. Further investigation of the applicability of this RSOS model in understanding MBE growth is beyond the scope of the present study.

As shown in Fig. 2.8, a nice illustration of the presence of nonlinearity in the underlying dynamical equation is provided by the steady–state persistence exponents of the CKD model, characterized by distinct values, $\theta_+^S \approx 0.78$ and $\theta_-^S \approx 0.66$, of the positive and negative exponents. Although one must take into account the fact that these values might be slightly overestimated (by approximatively 5%) due to the smallness of the sample sizes used in the steady–state simulations, these exponents provide a good qualitative account of the nontrivial up–down asymmetric persistence behavior expected for nonlinear models belonging to the MBE universality class.

Next we investigate the influence of small sample sizes on the measured values of the persistence exponents. We mainly used the DT model to answer this question and we pursued the following two tests. First we decreased the size of the system from 10^4 to 100 and then to 40 and found the values of the growth and persistence exponents, as summarized in Table 2.3. We note that as the lattice length decreases to 40, the persistence exponents increase by $\sim 2\%$, while the growth exponents in-

L	θ_+^T	θ_-^T	β
10^4	0.95 ± 0.02	0.98 ± 0.02	0.38 ± 0.01
10^2	0.96 ± 0.02	0.99 ± 0.02	0.37 ± 0.01
40	0.98 ± 0.02	1.01 ± 0.02	0.36 ± 0.01

Table 2.3: Transient positive and negative persistence exponents, $\theta_\pm^T$, obtained for the DT model with different system sizes (L). The effect of the system size on the measured growth exponent, β, is displayed in the last column. No result for steady–state persistence exponents is available for system sizes larger than ~ 100, due to the impossibility of reaching saturation of the interface width for such values of L in time scales accessible in simulations. The results shown here were averaged over 500 (for $L = 10^4$), 5×10^4 (for $L = 100$) and 10^5 (for $L = 40$) independent runs.

crease by $\sim 5\%$. As a second test, we have applied the noise reduction technique to both the DT and WV models. It has been shown [52] that a noise reduction factor of $m = 5$ helps the DT model to recover quite accurately the universal exponents corresponding to the MBE universality class. In addition, the noise reduced WV model exhibits, at late evolution times, its true EW asymptotic universality, which is difficult to observe without applying noise reduction. Therefore, the DT model with the appropriate noise reduction factor is expected to provide the correct persistence exponents associated with the fourth–order nonlinear dynamical equation for MBE growth. The results obtained from the simulations with noise reduction are summarized in Table 2.4. We notice that the noise reduction scheme produces only a minor change in the persistence exponents and in addition, the results obtained for $m = 5$ agree within the error bars with those for the CKD model. We, therefore, conclude that the noise reduced DT model and the discrete CKD model provide a good representation of the MBE universality class, characterized by two different steady–state persistence exponents: $\theta_+^S \sim 0.66$ (positive persistence) and $\theta_-^S \sim 0.78$ (negative persistence). These nontrivial persistence exponents for this class have not been reported earlier, and it would be useful to check these results from further theoretical or experimental studies. Regarding the noise reduced WV model we mention that the convergence of θ^S towards the expected value of 3/4 is rather slow in the case of the positive exponent and probably a higher value of the noise reduction factor would be necessary to reveal the true EW universality. We did not explore this technical issue any further.

We note that among the positive and negative steady–state persistence expo-

Growth model	m	θ_+^S	θ_-^S
DT	1	0.64 ± 0.02	0.72 ± 0.01
DT	5	0.65 ± 0.02	0.77 ± 0.01
WV	1	0.65 ± 0.02	0.70 ± 0.01
WV	5	0.68 ± 0.02	0.75 ± 0.01

Table 2.4: Positive and negative persistence exponents, $\theta_\pm^S$, for the steady state of the DT and WV models for two different values of the noise reduction factor, m. Systems of size $L = 40$ were equilibrated for 10^5 ML and the results were averaged over 5000 independent runs.

nents for these nonlinear growth models, the smaller one (for example, the positive exponent in the DT model or the negative exponent of the CKD model), turns out to be close to $(1 - \beta)$. In the next subsection, we show analytically that this relation between the smaller steady-state persistence exponent and the dynamic growth exponent is, in fact, exact. Our numerical studies suggest a connection of this result with the morphology that develops in the steady–state regime. As shown in Fig. 2.5, the characteristic feature of the DT morphology is the presence of deep grooves, while the CKD model exhibits high pillars. Loosely speaking, in the case of the DT model, we expect the relation of Eq. (1.3.3) to be more likely to be satisfied by the positive persistence exponent than the negative one because the preponderant grooves, responsible for the negative persistence exponent, represent the effects

of the nonlinearity of the underlying MBE dynamics. More work is clearly needed for a better understanding of the possible relationship between such "nonlinear" features of the interface morphology and the value of the persistence exponent.

2.1.2 An exact relation between steady-state persistence exponents and the growth exponent

As mentioned earlier, for interface heights $h(\mathbf{r},t)$ evolving via a Langevin equation that preserves $(h \to -h)$ symmetry (for example, any linear Langevin equation), the steady state persistence exponents satisfy the scaling relation $\theta_+^S = \theta_-^S = 1-\beta$, where β is the growth exponent [29]. In this subsection, we derive a generalized scaling relation,

$$\beta = \max\left[1-\theta_+^S, 1-\theta_-^S\right], \tag{2.1.1}$$

which is valid even in the absence of $(h \to -h)$ symmetry. When this symmetry is restored, Eq. (2.1.1) reduces to the known result [29], $\theta_+^S = \theta_-^S = 1-\beta$.

To derive the relation in Eq. (2.1.1), we start with a generic interface described by a height field $h(\mathbf{r},t)$ and define the relative height, $u(\mathbf{r},t) = h(\mathbf{r},t) - \overline{h}(\mathbf{r},t)$ where $\overline{h}(\mathbf{r},t) = \int h(\mathbf{r},t)d\mathbf{r}/V$ is the spatially averaged height and V is the volume of the sample. Let us also define the incremental correlation function in the stationary state,

$$C(t,t') = \lim_{t_0\to\infty} \langle [u(\mathbf{r},t+t_0) - u(\mathbf{r},t'+t_0)]^2 \rangle. \tag{2.1.2}$$

It turns out that for generic self-affine interfaces (which do not have to be Gaussian), this function $C(t,t')$ depends only on the time difference $|t-t'|$ (and not on the

individual times t and t') in a power-law fashion for large $|t-t'|$ [30, 60],

$$C(t,t') \sim |t-t'|^{2\beta}, \tag{2.1.3}$$

where β is the growth exponent.

This particular behavior of the correlation function in Eq. (2.1.3) is typical of a fractional Brownian motion (fBm). A stochastic process $x(t)$ with zero mean is called an fBm if its incremental correlation function $C(t_1,t_2) = \langle [x(t_1)-x(t_2)]^2 \rangle$ depends only on the time difference $|t_1-t_2|$ in a power-law fashion for large arguments [61],

$$C(t_1,t_2) = \langle [x(t_1)-x(t_2)]^2 \rangle \sim |t_1-t_2|^{2H}, \tag{2.1.4}$$

where $0 < H < 1$ is called the Hurst exponent of the fBm. For example, ordinary Brownian motion which evolves as $dx/dt = \eta(t)$, where $\eta(t)$ is a Gaussian white noise with zero mean and a delta function correlator, satisfies Eq. (2.1.4) with $H = 1/2$. Thus, an ordinary Brownian motion is a fBm with $H = 1/2$. It follows clearly by comparing Eqs. (2.1.3) and (2.1.4) that the relative height $u(\mathbf{r},t)$ of a generic interface at a fixed point $\mathbf{r}$ in space, in its stationary state, is also a fBm with Hurst exponent, $H = \beta$. Note that an fBm is not necessarily Gaussian.

We are then interested in the 'no return probability' to the initial value of the fBm process $u(\mathbf{r},t)$. So, the relevant random process is $Y(\mathbf{r},t) = u(\mathbf{r},t+t_0) - u(\mathbf{r},t_0)$. Clearly, $Y(\mathbf{r},t)$ is also a fBm with the same Hurst exponent β since the incremental correlation function of Y is the same as that of $u(\mathbf{r},t)$. We are then interested in the zero crossing properties of the fBm $Y(\mathbf{r},t)$. Now, consider the process $Y(\mathbf{r},t)$ as a function of time, at a fixed point $\mathbf{r}$ in space, from time t_0 to time t_0+t where $t_0 \to \infty$. There are two types of intervals between successive zero crossings in time,

the '+' type (where the process lies above 0) and the '−' type (where the process lies below 0).

In general, the statistics of the two types of intervals are different. Only, in special cases, where one has the additional knowledge that the process $Y(\mathbf{r}, t)$ is symmetric around 0 (i.e., processes which preserve the $(h \to -h)$ symmetry), the + and − intervals will have the same statistics. For such cases, a simple scaling argument was given in Ref. [29] to show that the length of an interval of either type has a power-law distribution, $Q(\tau) \sim \tau^{-1-\theta^S}$ (for large τ) with $\theta^S = 1 - H = 1 - \beta$. Note that this relation between the persistence exponent and the Hurst exponent is very general and holds for any symmetric fBm, i.e., any stochastic process with zero mean (not necessarily Gaussian) satisfying Eq. (2.1.4). Recently, other applications of this result have been found [62, 63]. For general nonsymmetric processes, however, one would expect that $Q_{\pm}(\tau) \sim \tau^{-1-\theta^S_{\pm}}$ for large τ, where θ^S_+ and θ^S_- are, in general, different. Here we generalize this scaling argument of Ref. [29] (derived for a symmetric process) to include the nonsymmetric cases and derive the result in Eq. (2.1.1).

The derivation of Eq. (2.1.1) follows more or less the same line of arguments as that used in Ref. [29] for the symmetric case. Let $P(Y, \tau)$ denote the probability that the process has value Y at time τ, given that it starts from its initial value 0 at $\tau = 0$. Then, it is natural to assume that the normalized probability distribution $P(Y, \tau)$ has a scaling form,

$$P(Y, \tau) = \frac{1}{\sigma(\tau)} f\left(\frac{Y}{\sigma(\tau)}\right), \tag{2.1.5}$$

where $\sigma(\tau)$ is the typical width of the process, $\sigma^2(\tau) = \langle Y^2(\tau)\rangle$. It follows from Eq. (2.1.3) that $\sigma(\tau) \sim \tau^\beta$ for large τ. The scaling function $f(z)$ is a constant at $z = 0$, $f(0) \sim O(1)$ (note that, in general, $f(z)$ is *not* a symmetric function of z) and should decrease to 0 as $z \to \pm\infty$. So, given that a zero occurs initially, the probability $\rho(\tau) = P(0, \tau)$ that the process will return to 0 after time τ (not necessarily for the first time) scales as

$$\rho(\tau) \sim \frac{1}{\sigma(\tau)} \sim \tau^{-\beta}, \tag{2.1.6}$$

as $\tau \to \infty$. This function $\rho(\tau)$ indeed is the density of zero crossings between τ and $\tau + d\tau$. Thus, the total number of zeros up to a time T is simply the integral,

$$N(T) = \int_0^T \rho(\tau) d\tau \sim T^{1-\beta}, \tag{2.1.7}$$

for large T.

Next, we relate the persistence probabilities to the number of zeros. Let $P_\pm(\tau)$ denote the probabilities that the process stays positive (or negative) over the interval $[0, \tau]$, given that it started from a zero. By definition, we have $P_\pm(\tau) \sim \tau^{-\theta^S_\pm}$ for large τ. Then, $Q_\pm(\tau) = -dP_\pm(\tau)/d\tau \sim \tau^{-1-\theta^S_\pm}$ (as $\tau \to \infty$) denote the probabilities that the process will cross zero next time (from the positive or the negative side respectively) between time τ and $\tau + d\tau$. Thus, $Q_\pm(\tau)$ are also the distribution of intervals of the two types of length τ.

Now, consider a total length of time T. Let $N(T)$ denote the total number of intervals in this period, half of them are + types and the other half − types, $N_\pm(T) = N(T)/2$. Let, $n_\pm(\tau)$ denote the number of $\pm$ intervals of length τ within the period T. Thus, the fraction of + (or −) intervals of length τ, $n_\pm(\tau)/N_\pm(\tau)$, by

definition, are the two distributions $Q_{\pm}(\tau)$ provided T is large. Thus, for large T, we have

$$n_{\pm}(\tau, T) = \frac{N(T)}{2} Q_{\pm}(\tau) \sim N(T)\tau^{-1-\theta_{\pm}^{S}}, \tag{2.1.8}$$

for $1 << \tau \leq T$. On the other hand, we have the length conservation condition (the total length covered by the intervals must be T),

$$\int_0^T d\tau\, \tau\, [n_+(\tau) + n_-(\tau)] = T. \tag{2.1.9}$$

Substituting the asymptotic behavior of $n_{\pm}(\tau)$ in Eq.(2.1.8) into the left-hand side of Eq.(2.1.9), we get

$$N(T) \left[\frac{T^{1-\theta_+^S}}{1-\theta_+^S} + \frac{T^{1-\theta_-^S}}{1-\theta_-^S} \right] \propto T. \tag{2.1.10}$$

We next use $N(T) \sim T^{1-\beta}$ for large T from Eq.(2.1.7). This gives, for large T,

$$\left[\frac{T^{1-\theta_+^S}}{1-\theta_+^S} + \frac{T^{1-\theta_-^S}}{1-\theta_-^S} \right] \sim T^{\beta}. \tag{2.1.11}$$

Taking $T \to \infty$ limit and matching the leading power of T in Eq. (2.1.11), we arrive at our main result in Eq. (2.1.1). Note that in the above derivation we have implicitly assumed a small-t cut-off and focused only on the distribution of large intervals. Our numerical results obtained for a class of nonlinear interfaces in both (1+1) and (2+1) dimensions (see Sec. 2.1.4 below) are consistent with the analytical result in Eq. (2.1.1).

2.1.3 Dependence of persistence probabilities on the initial configuration

We present in this section some surprising simulation results about the dependence of the persistence behavior (specifically, the values of the persistence exponents) on the choice of the initial configuration. In particular, we show that the steady–state exponents may be obtained with a fair degree of accuracy from simulations in which the interface *has not* yet reached the steady state. We also present some results that have bearing on the measurability of the transient persistence exponents from experimental data.

We recall that in Section 2.1.1 the transient persistence exponents were measured from simulations in which the initial configuration was completely flat, corresponding to $t_0 = 0$. To examine the dependence of the persistence probabilities on the choice of t_0, we evolved samples governed by F and DT atomistic diffusion rules for $t_0 = 10$, 100 and 1000 ML, starting from perfectly flat initial states and used the resulting configurations as starting points for measuring the persistence probability (the probability of the height at a given site not returning to its initial value at time t_0) as a function of t. We show the results of these simulations in Figs. 2.9 and 2.10 for the F and DT models, respectively. We find that even for the small value of $t_0 = 10$ ML [see panel a)], the observed persistence probabilities do not exhibit power law decay in time with the transient persistence exponents, despite the fact that the expected condition [29] for transient behavior, $t \gg t_0$, is well satisfied in a large part of the range of t used in these simulations. These

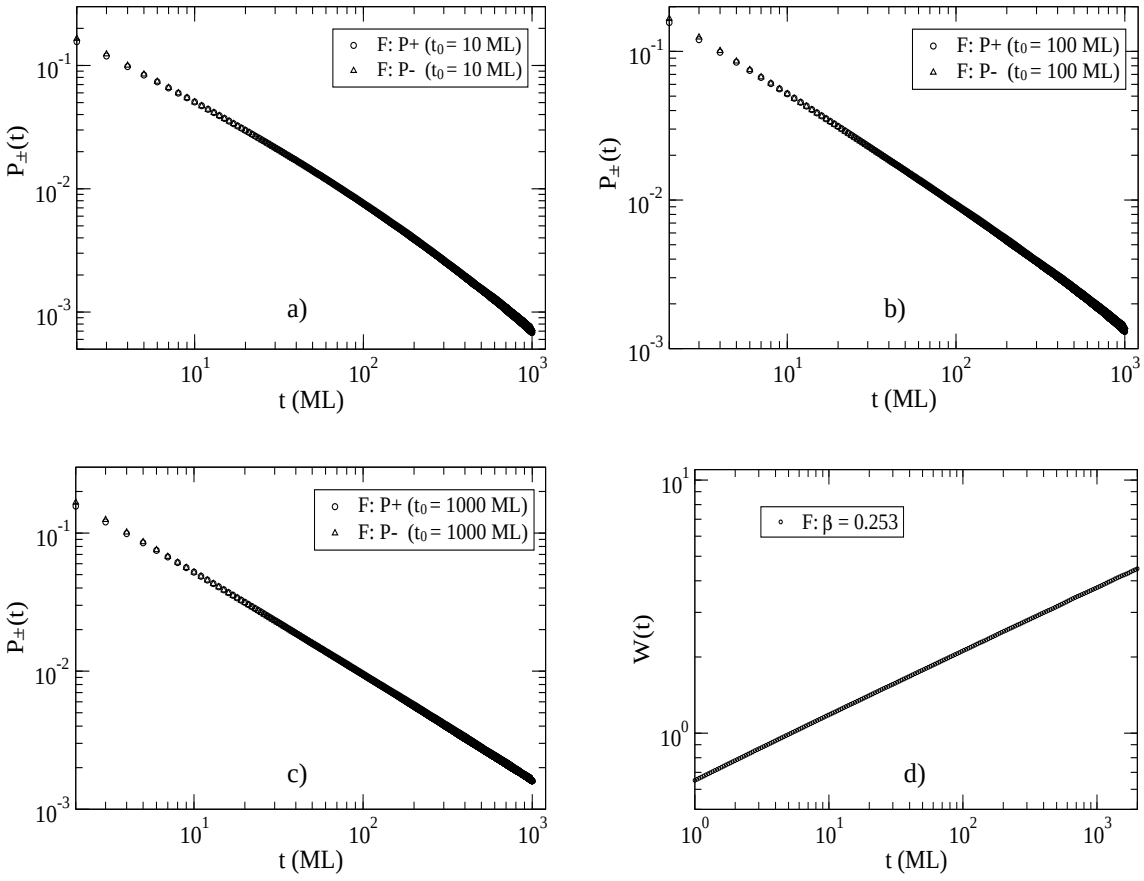

Figure 2.9: Log–log plots of the positive and negative persistence probabilities [panels (a)–(c)] for the F model, obtained using different values of the initial time t_0. Systems with $L = 10^4$ sites have been averaged over 500 independent runs. Persistence probabilities are computed starting from the configuration corresponding to: a) $t_0 = 10$ ML. We do not find a clear power law decay of the persistence curves. b) $t_0 = 100$ ML. As t_0 increases, a clearer power law behavior is observed. c) $t_0 = 1000$ ML. The power law decays are recovered and characterized by exponents in agreement with those corresponding to the steady–state regime: $\theta_{\pm}^{S} \approx 0.75$. d) Log–log plot of the interface width W as a function of time t (in units of ML). The value of the slope (equal to the growth exponent β) agrees with the expected value, $\beta = 0.25$.

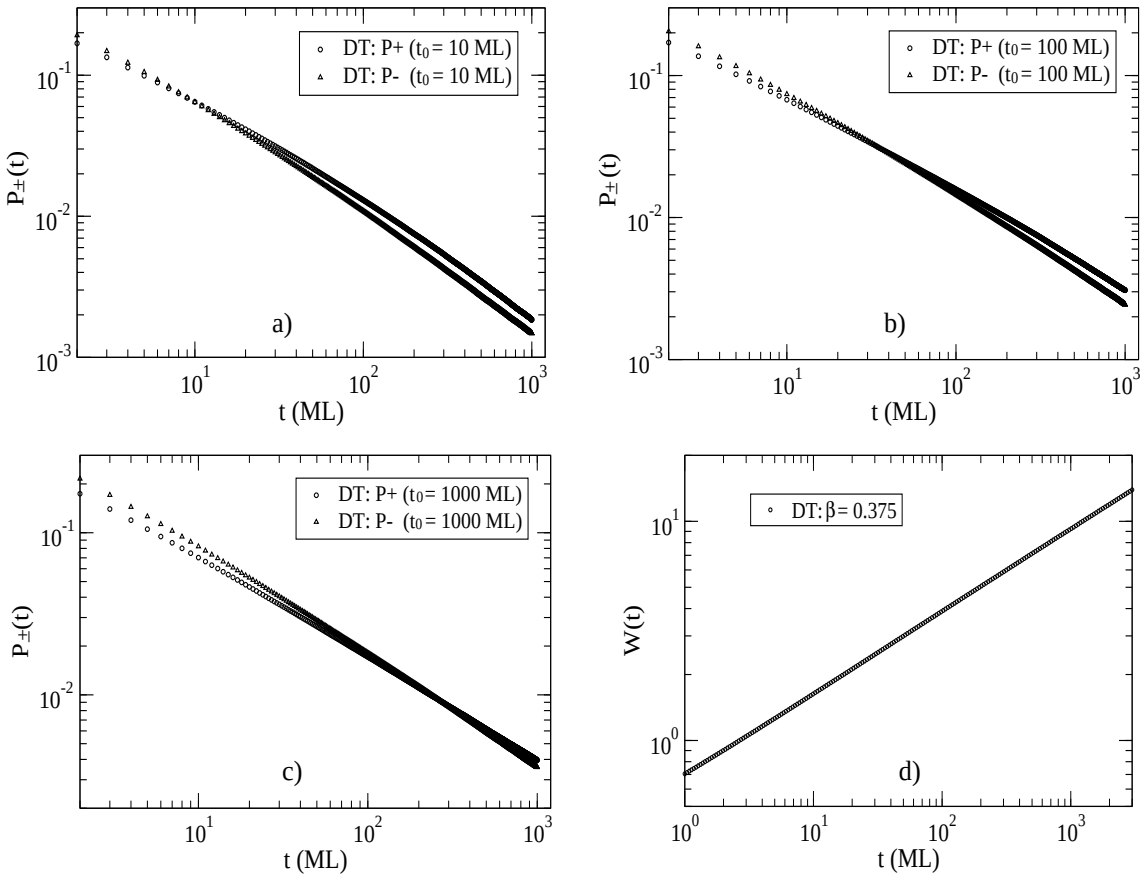

Figure 2.10: Positive and negative persistence probabilities [panels (a)–(c)] for the DT model, obtained using different values of the initial time t_0. Persistence probabilities are computed starting from the configuration corresponding to: a) $t_0 = 10$ ML. As in the case of the F model, we do not find a clear power law for the persistence curves. b) $t_0 = 100$ ML; c) $t_0 = 1000$ ML: Power law decays are recovered and characterized by exponents that are approximately equal to those corresponding to the steady–state regime, $\theta_+^S \approx 0.64$ and $\theta_-^S \approx 0.71$. d) Log–log plot of the interface width W as a function of time t (in units of ML). The slope gives a growth exponent of $\beta_{DT} \simeq 0.375$.

results point out a practical difficulty in obtaining experimental evidence for transient persistence behavior. Since perfectly flat initial configurations can hardly be achieved experimentally and experimental measurements are always started from a relatively rough substrate, the transient persistence exponents may very well not be measurable from experiments if the only way of measuring these exponents is to start from a perfectly flat morphology.

As the value of t_0 is increased to 100 ML, the persistence probabilities tend to show the expected power law behavior, as shown in Fig. 2.9(b) for the F model and in Fig. 2.10(b) for the DT model. Most surprisingly, as shown in Figs. 2.9(c) and 2.10(c), we find that for $t_0 = 1000$ ML, one recovers precisely the power law behavior, $P(t_0, t_0 + t) \propto t^{-\theta^S}$, and the exponents are essentially the same as the previously obtained steady–state ones shown in Table 2.2. This investigation, thus, reveals the fact that a measurement of the steady–state persistence exponents does not require the preparation of an initial state in the long–time steady–state regime where the interface width has reached saturation: an initial state in the pre–asymptotic growth regime where the interface width is still increasing as a power law in time [as illustrated in Figs. 2.9(d) and 2.10(d)] is sufficient for measurements of the steady–state persistence exponents. A similar result was reported in Ref. [29], but it was argued there that the measurement time t must be much smaller than t_0 for steady–state persistence behavior to be observed. Our results show that the steady–state persistence exponents are found even if t is of the order of (or even slightly larger than) the initial time t_0. This observation has an important practical benefit: it implies that one can easily obtain accurate estimates of the steady–state persistence

exponents using rather large systems ($L \sim 10^4$), and growing approximately up to $t_0 \sim 10^3$ ML, instead of having to use the very large values (of the order of L^z) of t_0 necessary for obtaining saturation of the interface width. At the same time, this observation also illustrates the above mentioned difficulty in obtaining the transient exponents from experimental measurements.

To investigate the effects of random imperfections in the initial substrate (which are always present in experimental studies) on the persistence behavior, we carried out simulations in which particles were deposited randomly on a perfectly flat substrate for 10 ML and the resulting configuration was used for further depositions using the diffusion rules of the F and DT models. Persistence probabilities were calculated starting from the configurations obtained after the random deposition of 10 ML. Figures 2.11 and 2.12 show the results for the F and DT models, respectively. We find that even when the persistence calculation starts from a configuration characterized by random deposition, there is an indication that one can still obtain the steady–state exponents during the last decade of t where the growth exponent reaches the values characteristic of the diffusion rules of the specific (F or DT) model being considered. Indeed, in the time region where the growth exponents are $\beta = 0.25$ for the F model [see Fig. 2.11(b)] and $\beta = 0.375$ for the DT model [see Fig. 2.12(b)], we have calculated the persistence exponents and recovered values very close to the steady–state ones. These observations confirm our earlier conclusions about the relatively easy measurability of the steady–state persistence exponents and the difficulty in measuring the transient exponents in experimental situations.

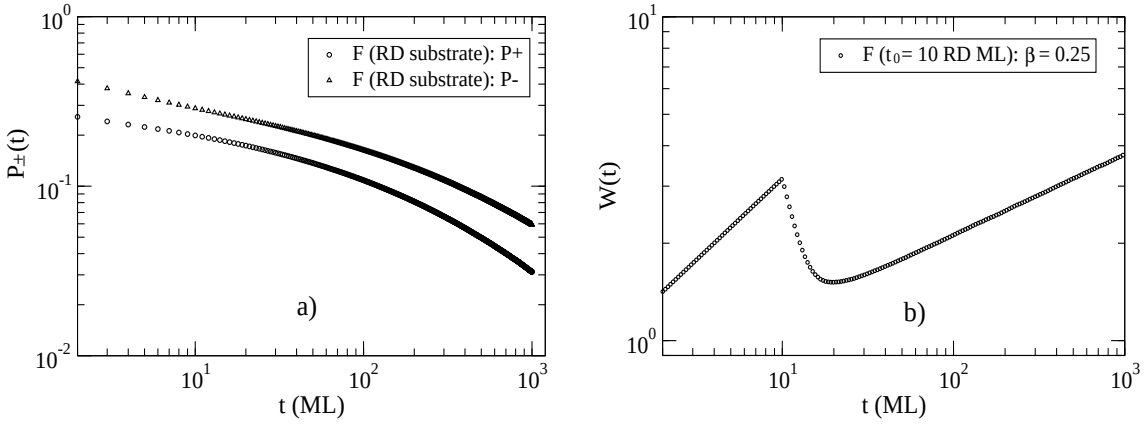

Figure 2.11: a) Positive and negative persistence probabilities for the F model. During the deposition of the first 10 ML, the growth process is random deposition. The diffusion rules of the F model are then used to evolve the interface. Persistence probabilities are computed starting from the configuration obtained after the random deposition of 10 ML. The positive and negative persistence exponents in the last growth decade are in the range 0.6 to 0.7, depending on the fitting region. b) Log–log plot of the interface width W as a function of t (in ML). The slope in the first decade of t is precisely the random–deposition value, $\beta = 0.5$. The second decade shows a crossover region where the systems undergoes a transformation towards a morphology governed by the F model diffusion rules, and the last decade is characterized by the expected growth exponent of the F model, $\beta = 0.25$.

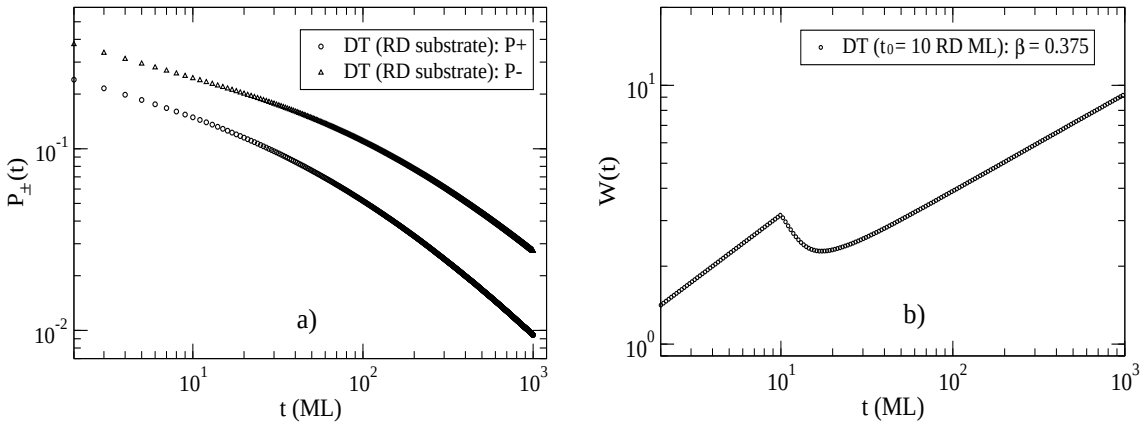

Figure 2.12: Positive and negative persistence probability curves for the DT model. During the deposition of the first 10 ML, the growth process is random deposition. The diffusion rules of the DT model are used to evolve the interface subsequently. Persistence probabilities are computed starting from the configuration obtained after the deposition of the first 10 ML. The positive and negative persistence exponents in the last growth decade are approximatively equal to 0.66 and 0.79 respectively. b) Log–log plot of the interface width W as a function of time t (in ML). Beyond the crossover regime, the last decade in t is characterized by the expected growth exponent of the DT model, $\beta \simeq 0.375$.

2.1.4 Persistence exponents in (2+1) dimensions

Our calculations in (2+1)–dimensions make use of our observation (discussed above) concerning the possibility of obtaining the correct steady–state exponents from simulations that avoid the time consuming process of reaching the true steady state where the interface width has saturated. The result that the persistence exponents obtained from (1+1)–dimensional simulations using fairly small values of t_0 and $t \sim t_0$ are quite close to the steady–state values allows us to extract numerically the steady–state persistence exponents in (2+1)–dimensions using systems with reasonably large sizes. If one had to run systems of size $L \sim 100 \times 100$ all the way to saturation in order to measure the steady–state persistence exponents, it would have been impossible to do the calculations within reasonable simulation time. In addition, decreasing the system size is not an acceptable solution because the results then become dominated by finite size effects.

Simulations for (2+1)–dimensional discrete growth models were carried out for the F model ($\beta = 0$) and the DT model ($\beta \simeq 1/5$). Simulations using systems of size $L = 200 \times 200$ revealed that the growth exponents, obtained from averages over 200 independent runs, are $\beta = 0.04 \pm 0.01$ and 0.20 ± 0.01 for the F and DT models, respectively, in agreement with Ref. [48]. In the DT model, we noticed a crossover from the initial value of 0.26 to the asymptotic expected value of 0.20, indicating that no additional noise reduction technique is necessary for obtaining results that reflect the correct universality class of this model. For both F and DT models we calculate the transient and steady–state persistence probabilities by

recording the fraction of sites which do not return to their initial height up to time t, as in the (1+1)–dimensional case. We used $t_0 = 0$ (perfectly flat initial state) in the calculation of the transient persistence probabilities, and three different values, such as $t_0 = 20$ ML, 200 ML and 2000 ML for the F model, in the calculation of the steady–state exponents.

We report the results for the transient probabilities just for the sake of completeness: the rapid decay of the persistence probabilities prevents us from obtaining accurate values of the associated persistence exponents. This fast decay of the transient persistence probability is a consequence of the reduced roughness of these higher dimensional models. This effect is particularly pronounced for the F model, for which the persistence exponent is found to be larger than 6 and the persistence probability decreases rapidly to zero for any deposition time larger than ~ 60 ML, as shown in Fig. 2.13. We also observe that the transient values of the positive and negative persistence exponents in the DT model are roughly 3 times larger than the values obtained in the $(1 + 1)$–dimensional case. The relative difference between the positive and negative persistence exponents remains approximately the same as that in the (1+1)–dimensional model. Our results for these (2+1)–dimensional persistence exponents are summarized in Table 2.5.

We now focus on the steady–state persistence exponents which, as discussed above, are found using relatively small values of t_0 and $t \approx t_0$. In Fig. 2.14(a), we show that for $t_0 \ll t$ (e.g. for $t_0 = 20$ ML), the persistence probability of the F model does not exhibit a clear power law decay. However panels b) and c) of Fig. 2.14 reveal that once t_0 becomes of the order of the measurement time t, the expected power

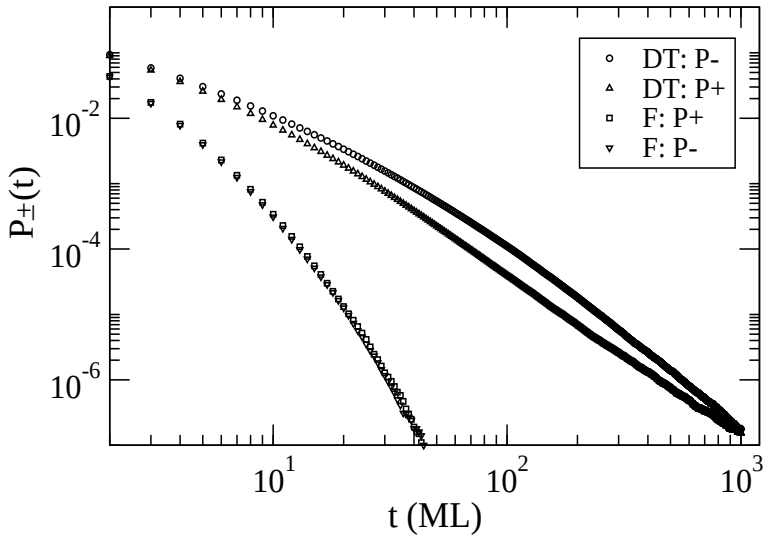

Figure 2.13: Transient persistence probabilities for the (2+1)–dimensional F and DT growth models. In the case of the F model, systems of size $L = 1000 \times 1000$ have been averaged over 200 independent runs, while for the DT model, systems of size $L = 500 \times 500$ have been averaged over 800 independent runs. The transient persistence probability for the F model exhibits a very fast decay, characterized by a persistence exponent $\theta^T \approx 6.9$ for the last decade of t. More accurate results (see Table 2.5) are obtained for the exponents in the DT model, although the statistics is not excellent.

Growth model	L	θ_+^T	θ_-^T	θ_+^S	θ_-^S	β
FM	200×200	> 6	> 6	1.02 ± 0.02	1.00 ± 0.02	0.04 ± 0.01
DT	200×200	2.84	2.44	0.76 ± 0.02	0.85 ± 0.02	0.20 ± 0.01

Table 2.5: Transient and steady–state persistence exponents, $\theta_\pm$, for two (2+1)–dimensional discrete growth models. The measured value of the growth exponent β is shown in the last column. The transient persistence exponents are measured with relatively low accuracy due to the rapid temporal decay of the persistence probabilities.

law is recovered and in addition the steady–state exponent for the linear F model, $\theta^S = 1.01 \pm 0.02$, which should be equal to $(1 - \beta)$ with $\beta = 0$, is recovered. The results for the DT model are presented in Fig. 2.15. The steady–state persistence exponents have been measured from the power law decays shown in Fig. 2.15(b). In this temporal regime, as shown in panel d), the growth exponent is equal to the asymptotic value of 1/5. The persistence behavior of the DT model in this regime is characterized by $\theta_+^S \approx 0.76$ and $\theta_-^S \approx 0.85$, indicating that the relation of Eq. (2.1.1) holds reasonably well for the (2+1)– dimensional nonlinear MBE dynamics, as in the (1 + 1)–dimensional case. It is important to mention that the same values of the persistence exponents have been obtained using a DT system with $L = 40 \times 40$, equilibrated for $t_0 = 10^5$ ML, as required in the traditional method (used in most of the (1+1)–dimensional simulations) of measuring the steady–state persistence

probabilities. Thus the "quick and easy" method of obtaining the steady–state persistence exponent again agrees well with the exponent extracted from the actually saturated interface, as discussed above.

We have also performed some preliminary persistence calculations for the (2+1)–dimensional CKD model in order to check the validity of our reported (2+1)–dimensional MBE persistence exponents. Using $L = 100 \times 100$ and $t_0 = 1000$ ML, we find that the values of the positive and negative persistence exponents depend to some extent on the chosen values for the coefficient λ_{22} of the nonlinear term and the control parameter c. For example, we obtain $\theta_+^S \approx 0.82$ and $\theta_-^S \approx 0.77$ using $\lambda_{22} = 5.0$ and $c = 0.085$, and $\theta_+^S \approx 0.88$ and $\theta_-^S \approx 0.83$ using $\lambda_{22} = 5.0$ and $c = 0.13$. Both cases are characterized by a growth exponent of 0.18 ± 0.01, in agreement with Ref. [64], which is consistent with the expected value of $1/5$. The results obtained in the latter case are displayed in panel c) of Fig. 2.15 for the purpose of illustrating the similarity between the DT and CKD models. From these observations, we conclude that the (2+1)–dimensional DT and CKD persistence results are consistent with each other, and they clearly reflect the nonlinearity of the MBE dynamical equation in the difference between the values of the positive and negative persistence exponents as expected for the up–down asymmetric generic nonlinear situation.

2.1.5 Scaling behavior of the persistence probability

Since all the results described above have been obtained from simulations of finite systems, it is important to address the question of how the persistence probabilities

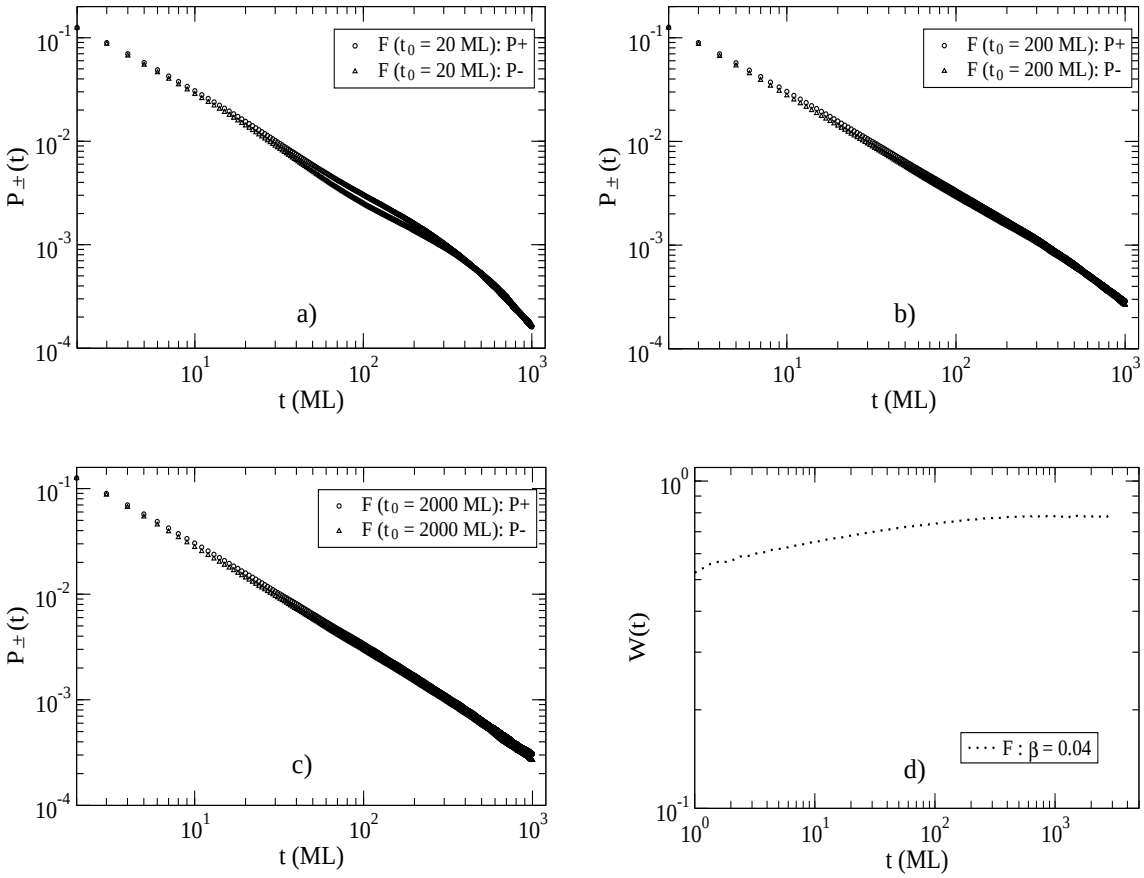

Figure 2.14: Persistence probabilities for the (2+1)–dimensional F model of size $L = 200 \times 200$, averaged over 200 runs, obtained from simulations with different values of the initial time t_0. a) $t_0 = 20$ ML. b) $t_0 = 200$ ML. c) $t_0 = 2000$ ML. The persistence probability curves in case c) show the expected power law decay characterized by the exponent values $\theta_+^S = 1.02 \pm 0.02$ and $\theta_-^S = 1.00 \pm 0.02$. d) Log–log plot of the interface width W vs deposition time t in units of ML. The slope in the intermediate growth decade is $\beta \simeq 0.04$ and thereafter it decreases to zero, as expected.

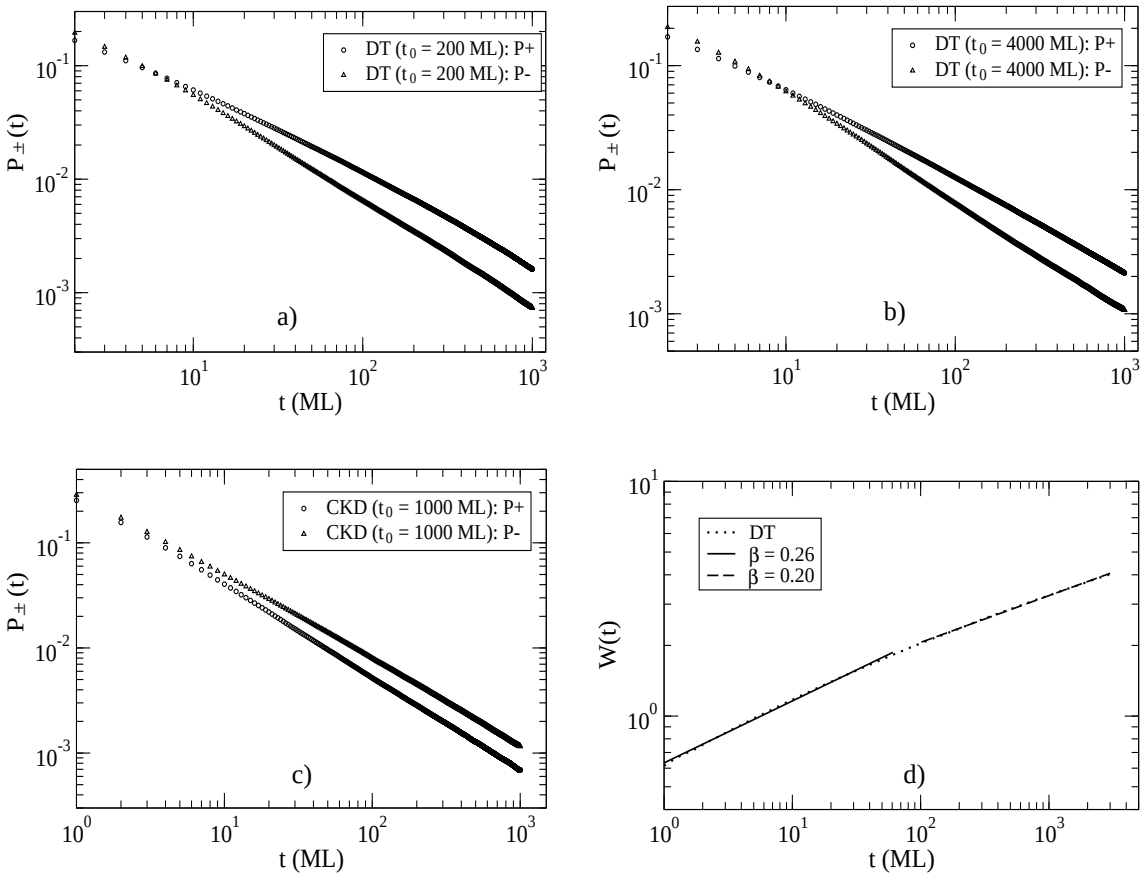

Figure 2.15: Persistence probabilities for the (2+1)–dimensional DT model of size $L = 200 \times 200$, averaged over 200 runs, obtained from simulations with different values of the initial time t_0. a) $t_0 = 200$ ML: The persistence probabilities do not exhibit clear power law decay. b) $t_0 = 4000$ ML: The persistence probability curves show the expected power law decay characterized by the exponent values $\theta_+^S = 0.77 \pm 0.02$ and $\theta_-^S = 0.85 \pm 0.02$. c) Results for the (2+1)–dimensional CKD model, obtained using $L = 100 \times 100$, $t_0 = 1000$ ML, $\lambda = 5$ and $c = 0.13$. d) Log–log plot of the interface width W vs deposition time t in ML for the DT model. The slope manifests a crossover from an initial value of ~ 0.26 to the asymptotic value of 0.20.

are affected by the finite system size. We have already encountered such effects in our study of persistence probabilities for (1+1)–dimensional models (see Table 2.3), where it was found that the measured values of the persistence exponents in the steady state increase slightly as the system size L is decreased, while the value of the growth exponent β decreases with decreasing L. We did not investigate finite size effects in our study of the transient persistence probabilities because these studies were carried out for large values of L and relatively small values of the time t.

The qualitative dependence of the measured values of the steady–state persistence exponents $\theta_{\pm}^{S}$ and the growth exponent β on the sample size L is not difficult to understand. The steady–state persistence probabilities $P_{\pm}^{S}(t_0, t_0 + t)$ exhibit a power law decay with exponent $\theta_{\pm}^{S}$ as long as the time t is small compared to the characteristic time scale $\tau(L)$ of the system which is proportional to L^z. The decay of $P_{\pm}^{S}$ becomes faster as t approaches and exceeds this characteristic time scale. Since this departure from power law behavior occurs at earlier times for smaller systems, the value of the persistence exponent extracted from a power law fit to the decay of the persistence probability over a fixed time window is expected to increase as the system size is reduced. In a similar way, the measured value of β is expected to be smaller for relatively small values of L because the precursor to the saturation of the width at long times occurs at shorter values of t in smaller systems. Thus, the general trends in the system size dependence of the persistence and growth exponents are reasonable. However, it would be useful to obtain a more quantitative description of these trends.

Since the characteristic time scale $\tau(L)$ ("equilibration" or "saturation" time)

of a system of linear size L is proportional to L^z, one expects, in analogy with the theory of finite size scaling in equilibrium critical phenomena, that the steady–state persistence probability $P_{\pm}^{S}(t)$ (in this discussion, we omit the initial time t_0 in the argument of $P_{\pm}^{S}$ because the steady–state persistence probability is independent of the choice of t_0) would be a function of the scaling variable t/L^z. Another time scale has to be taken into consideration in a discussion of the scaling behavior of the persistence probability. This is the sampling time δt which is the time interval between two successive measurements of the height at a fixed spatial point. In our simulations of the atomistic growth models, the smallest value of δt is 1 ML because the heights are measured after each deposition of one complete (ideal) monolayer. However, larger integral values of δt can also be used in the calculation of the persistence probabilities. Since experimental measurements are also carried out at discrete time intervals, the presence of a finite value of δt has to be accounted for in the analysis of experimental data also. Note that the persistence probability itself is mathematically defined, $P(t_0, t_0 + t)$, for continuous values of time t whereas measurements and simulations are necessarily done on discrete time.

It has been pointed out in Ref. [65, 66] that discrete–time sampling of a continuous–time stochastic process does affect the measured persistence probability. Such effects have been investigated in detail [43] in the context of a different stochastic probability (called the survival probability in Ref. [43]) that measures the probability of the interface height at a fixed position not returning to its time–averaged value within time t. As we will see in Chapter 4, we have found that the survival probability measured for a system of size L with sampling interval δt is a

function of the scaling variables t/L^z and $\delta t/L^z$. We expect a similar behavior for the steady–state persistence probabilities measured in our simulations. Thus, the expected scaling behavior of $P^S_\pm(t, L, \delta t)$ is

$$P^S_\pm(t, L, \delta t) = f_\pm(t/L^z, \delta t/L^z), \tag{2.1.12}$$

where the function $f_\pm(x_1, x_2)$ should decay as $x_1^{-\theta^S_\pm}$ for small x_1 and $x_2 \ll 1$.

To test the validity of this scaling ansatz, we have carried out calculations of the steady–state persistence probability in the linear F model (the positive and negative persistence probabilities are the same in this model) using different values of L and δt. Due to the linearity of the F model, we have computed a persistence probability $P^S(t)$ given by the average value of the positive and negative persistence probabilities. If the scaling description of Eq. (2.1.12) is valid, then plots of $P^S(t, L, \delta t)$ versus t/L^z for different values of L and δt should coincide if the value of δt for the different sample sizes are chosen such that the ratio $\delta t/L^z$ remains constant. As shown in Fig. 16, where we present the data obtained from simulations of the (1+1)–dimensional F model for three different values (200, 400 and 800) of L and three correspondingly different values of δt (4, 16 and 64, so that $\delta t/L^z$ with $z = 2$ is held fixed at 10^{-4}), plots of $P^S(t)$ versus $t/\delta t$ (which is proportional to t/L^z because δt is chosen to be proportional to L^z) for the three different sample sizes exhibit an excellent scaling collapse. These results confirm the validity of the scaling form of Eq. (2.1.12).

As shown in Fig. 2.16, the scaling function f exhibits the expected power law behavior for relatively small values of $t/\delta t$. Our results also show signatures of a

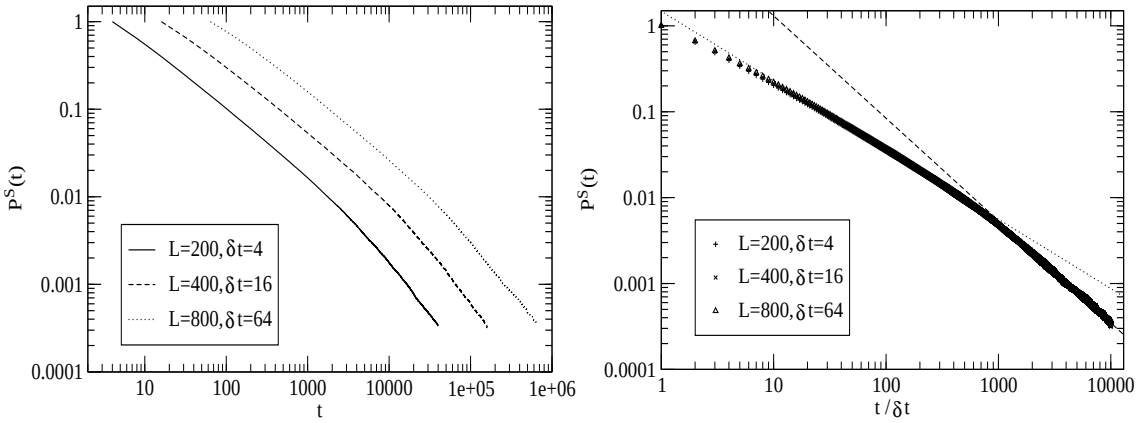

Figure 2.16: Persistence probability, $P(t)$, for the F model shown for different system sizes with different sampling times. Panel a): Double–log plot showing three different persistence curves vs. time corresponding to: $L = 100$ and $\delta t = 4$, $L = 400$ and $\delta t = 16$, $L = 800$ and $\delta t = 81$, respectively. Panel b): Finite size scaling of $P(t, L, \delta t)$. Results for persistence probabilities for three different sizes (as in panel a)) with the same value of $\delta t/L^z$ (i.e. $1/10^4$) are plotted versus $t/\delta t$ ($z = 2$). The dotted (dashed) line is a fit of the data to a power law with an exponent of ~ 0.75 (~ 1.0).

crossover to a power law decay with exponent 1 as t approaches and exceeds the characteristic time scale $\tau(L)$ (this crossover occurs near $t/L^z \simeq 0.1$ in the F model). We discuss below a possible explanation for this behavior.

Height fluctuations at times t_0 and $t_0 + t$ are expected to be completely uncorrelated if t is large compared to $\tau(L)$. Therefore, the persistence probability $P^S(t)$ for values of t much larger than $\tau(L)$ may be obtained by considering a collection of fluctuating variables which have the same probability distribution (since the system is in the steady state), and which are completely uncorrelated with one another. Let $x_0, x_1, x_2, \ldots$ represent such a collection of variables (these variables may be thought of as the height at a particular site measured at regularly spaced times with spacing larger than $\tau(L)$). For simplicity, we assume that each x_i is uniformly distributed between $-a$ and a. Then, given a particular value of x_0, the probability $P_+(x_0, n)$ that all the variables $x_i, 1 \leq i \leq n$ are larger than x_0 may be easily obtained as

$$P_+(x_0, n) = \left[\frac{1}{2a}\int_{x_0}^{a} dx\right]^n = [(a - x_0)/(2a)]^n. \tag{2.1.13}$$

The positive persistence probability $P_+(n)$ is obtained by averaging this probability over the probability distribution of x_0. Thus, we have

$$P_+(n) = \frac{1}{2a}\int_{-a}^{a} P_+(x_0, n) dx_0 = \frac{1}{n+1}, \tag{2.1.14}$$

which decays as a power law with exponent 1 for large n. This power law behavior does not depend on the form of the assumed probability distribution for the fluctuating variables $\{x_i\}$. Assuming a general probability distribution $p(x)$ with

$\int_{-\infty}^{\infty} p(x)dx = 1$, Eq. (2.1.14) can be written as

$$P_+(n) = \int_{-\infty}^{\infty} p(x_0) \left[\int_{x_0}^{\infty} p(x)dx \right]^n dx_0 = \int_{-\infty}^{\infty} p(x_0) \left[1 - \int_{-\infty}^{x_0} p(x)dx \right]^n dx_0. \tag{2.1.15}$$

For large n, the quantity that multiplies $p(x_0)$ in Eq. (2.1.15) is of order unity only for values of x_0 for which $\int_{-\infty}^{x_0} p(x)dx$ is of order $1/n$. Physically, this means that the positive persistence probability is nonzero for large n only if the initial value x_0 is very close to the lower limit of the allowed range of values. This effectively restricts the upper limit of the integral over x_0 to y_0 where y_0 satisfies the requirement that

$$\int_{-\infty}^{y_0} p(x)dx = C/n, \tag{2.1.16}$$

where C is a constant of order unity. Since the quantity that multiplies $p(x_0)$ in Eq. (2.1.15) is of order unity for such values of x_0, it follows that

$$P_+(n) \approx \int_{-\infty}^{y_0} p(x_0)dx_0 \propto \frac{1}{n}. \tag{2.1.17}$$

This simple analysis shows that the simulation results for the behavior of the scaling function of Fig. 16 for large values of $t/\delta t$ are quite reasonable.

While we have not carried out similar scaling analyses [Eq. (2.1.12)] for other models, we expect the scaling form of Eq. (2.1.12) to be valid in general. We expect that such scaling analysis of the persistence probability as a function of the system size L and the sampling time δt would be useful in the analysis of numerical and experimental data in the future. In fact, we believe that a direct experimental verification of the scaling ansatz defined by Eq. (2.1.12) will be valuable.

2.2 Concluding remarks

In this chapter, we have investigated the temporal first passage statistics, expressed in terms of temporal persistence probabilities, for a variety of atomistic models that provide discrete realizations of several linear and nonlinear Langevin equations for the stochastic dynamics of growing and fluctuating interfaces [67]. Using extensive kinetic Monte Carlo simulations, we have obtained transient and steady–state persistence exponents for these (1+1) and (2+1)–dimensional SOS and RSOS growth models. We have followed the methodology of Krug *et al.* [29, 30] and extended their numerical work to the nonlinear MBE dynamical equation by studying the persistence behavior of the atomistic DT, WV, CKD and KPK models. From these studies, we have identified two persistence exponents for each of the two temporal regimes (transient and steady–state) of the persistence probability. The difference between the values of the two exponents reflects the nonlinearity (and the resulting lack of up–down symmetry) of the MBE dynamical equation.

Among the models studied here, we find that in (1+1) dimensions and in the range of system sizes used in our simulations, WV and DT models are hardly distinguishable from the point of view of transient and steady–state persistence behavior: the persistence exponents obtained for these two models are very close to each other. We, therefore, conclude that in the range of simulation parameters used in this study, the (1+1)–dimensional DT and WV models belong to the same universality class (namely the MBE universality class) as far as their persistence behavior is concerned. A separate investigation is required in order to understand

the universality class of the WV model in (2+1) dimensions. The KPK model appears not to reflect well the nonlinear feature of the underlying dynamical equation in the values of the positive and negative persistence exponents. This is probably due to strong finite size effects arising from the small lattice sizes used in our traditional steady–state simulations (i.e. using $t_0 \sim L^z$). These finite size effects appear to lead to overestimated persistence exponents [and underestimated growth exponent, consistent with Eq. (1.3.3)].

We have also investigated the CKD model, which is another discrete model belonging to the MBE universality class, our main goal being a closer examination of how the nonlinearity of the underlying continuum equation is reflected in values of the transient and steady–state persistence exponents. In this case we have obtained clearly different values for the positive and negative persistence exponents. The predictions of the CKD model concerning the persistence exponents have been checked by applying the noise reduction technique to the DT model. We found that for the MBE universality class, the steady–state persistence exponents in (1+1) dimensions are: $\theta_+^S = 0.66 \pm 0.02$ and $\theta_-^S = 0.78 \pm 0.02$. These two values represent the average of the results obtained for the CKD and the noise reduced DT models. These results suggest that measurements of persistence exponents can be profitably used to detect the presence of nonlinearity in the continuum equations underlying surface growth and fluctuation phenomena.

The observed difference between the positive and negative steady–state persistence exponents for the models in the MBE universality class implies that the relation of Eq. (1.3.3), known to be valid for linear Langevin equations (our results

for the linear F and LC models are in agreement with this relation), can not be satisfied by both these exponents. Thus, it is clear that at least one of these steady–state persistence exponents is not related to the usual dynamic scaling exponents in a simple way. We have found that the relation of Eq. (1.3.3) is approximately satisfied (within the error bars of our numerical results) by the smaller one of the two steady–state persistence exponents in all the (1+1)– and (2+1)–dimensional discrete stochastic growth models studied in this study. We have also shown analytically that this relation between the smaller persistence exponent and the growth exponent is, in fact, exact. The smaller exponent appears to correspond to the positive (negative) persistence probability if the top (bottom) part of the steady–state interface profile is smoother. This observation suggests a deep (and potentially important) connection between the surface morphology and the associated persistence exponent, which has no simple analog in the dynamic scaling approach where the critical exponents (α, β, $z = \alpha/\beta$) by themselves do not provide any information about the up–down symmetry breaking in the surface morphology. Further investigation of this aspect would be very interesting and highly desirable, particularly if experimental information on persistence properties of nonequilibrium surface growth kinetics becomes available.

Our investigation of the effects of the initial configuration on the persistence probabilities indicates that the transient persistence exponents can be obtained only if the interface is completely flat at the initial time. This restriction puts severe limits on the possibility of measuring the transient persistence exponents in real experiments where it would be very difficult, if not impossible, to meet the requirement

of zero initial roughness. We have also found the surprising and useful result that the steady–state persistence exponents can be accurately measured even if the initial configuration corresponds to a value of t_0 that is much smaller than the time required for the interface to reach saturation. In other words, the persistence probabilities exhibit their steady–state behavior for measurement times comparable to the initial time t_0 even if the value of t_0 is much smaller than L^z. This behavior was found in both (1+1) and (2+1) dimensions, in all the linear and nonlinear models we studied. This finding is very useful because it opens up the possibility of numerically calculating the steady–state persistence exponents for large systems and for higher dimensions as well. In fact, this observation enabled us to calculate the steady–state persistence exponents for (2+1)–dimensional models belonging to the EW and MBE universality classes. For the MBE universality class, we have considered the DT model and found the positive and negative persistence exponents in the steady–state to be ≈ 0.76 and ≈ 0.85, respectively, in (2+1) dimensions.

We have also examined in detail the dependence of the measured steady–state persistence probability in the (1+1)–dimensional F model on the sample size L and the sampling interval δt which is always finite in simulations and experimental measurements. We found that this dependence is described by a simple scaling form. The scaling function was found to exhibit power law decay with exponent 1 for times larger than L^z. We have proposed a simple explanation for this behavior. We believe that such scaling analysis would prove to be useful in future numerical and experimental studies of persistence properties.

3. INFINITE FAMILY OF PERSISTENCE EXPONENTS FOR INTERFACE FLUCTUATIONS

The concept of persistence has been used in Refs. [29, 30, 38, 39, 40] to study the interesting problem of thermally fluctuating interfaces where steps on vicinal surfaces undergo random thermal motion in equilibrium [47]. The step persistence probability is the probability $P(t_0, t_0 + t)$ that a given lateral step position x with a height (i.e. step fluctuation measured from the equilibrium step position) $h(x, t_0)$ at time t_0 does not return to this value up to a later time $t_0 + t$. With no loss of generality we will set $t_0 = 0$ from now on, assuming that thermal equilibrium has been achieved in the step fluctuations and we are discussing steady-state stationary properties. The resulting persistence probability $P(t) \equiv P(0, t)$ of fluctuating steps has recently been studied experimentally using dynamical scanning tunneling microscopy (STM) in two systems: Al steps on Si (111) surface at high temperatures ~ 970K [38] and Ag (111) surface at low temperatures ~ 320K [39]. In the first case, the step fluctuations dominated by atomistic attachment and detachment (AD) at the step edge are known [47] to be well described by the coarse-grained second-order

non-conserved linear Langevin equation

$$\frac{\partial h(x,t)}{\partial t} = \frac{\partial^2 h(x,t)}{\partial x^2} + \eta(x,t), \tag{3.1}$$

where $\eta(x,t)$ with $\langle \eta(x,t)\eta(x',t') \rangle \propto \delta(x-x')\delta(t-t')$ is the usual uncorrelated random Gaussian noise corresponding to the non-conserved white noise associated with the random AD process. Low temperature step fluctuations dominated by the step edge diffusion (SED) mechanism are, on the other hand, described by a fourth order conserved linear Langevin equation:

$$\frac{\partial h(x,t)}{\partial t} = -\frac{\partial^4 h(x,t)}{\partial x^4} + \eta_c(x,t), \tag{3.2}$$

where $\eta_c(x,t)$ with $\langle \eta_c(x,t)\eta_c(x',t') \rangle \propto \nabla^2 \delta(x-x')\delta(t-t')$ is a conserved noise associated with atomic diffusion along the step edge. From a quantitative analysis of the digitized STM step images as a function of time, the persistence exponent was found to be $\theta = 0.77 \pm 0.03$ [38] and $\theta = 0.87 \pm 0.02$ [39], respectively, for the high-temperature AD mechanism and low-temperature SED mechanism. These measured step fluctuation persistence exponents agree reasonably well with those found [29] from kinetic Monte Carlo simulations of the corresponding discrete solid-on-solid models: $\theta \simeq 0.75$ (for Eq. (3.1)) and $\theta \simeq 0.86$ (for Eq. (3.2)). These results are in agreement with the relation $\theta = 1 - \beta$ (in the steady–state regime) since $\beta = 1/4$ for Eq. (3.1) and $\beta = 1/8$ for Eq. (3.2).

This striking agreement between experimentally obtained and theoretically predicted values of the persistence exponent demonstrates the overall excellent consistency among theory, experiment, and simulations in this problem, but also brings

up a key question regarding persistence studies [29, 38, 39, 40] of surface fluctuations: Is persistence really an independent (and new) conceptual tool in studying surface fluctuations, or, is it just an equivalent (perhaps even complementary) way of studying dynamic scaling [1, 47, 68] of height correlations? In this chapter, we present new theoretical and experimental persistence results on surface step fluctuations that fundamentally transcend any dynamic scaling considerations, establishing in the process the existence of a novel and nontrivial infinite family (i.e. a continuous set) of persistence exponents for equilibrium step fluctuations. We carry out quantitative analyses of (digitized) dynamical STM images of step fluctuations both for high-temperature (Al/Si) and low-temperature (Ag) equilibrium surfaces, and compare in details the experimental results with those we have obtained from numerical integration of the corresponding Langevin equations and discrete stochastic Monte Carlo simulations of corresponding atomistic cellular automata type models in the same dynamical universality classes [1, 47, 68]. All three sets of persistence results (experimental, continuum Langevin equation, discrete stochastic simulation) agree very well for both high and low temperature equilibrium step fluctuations, establishing persistence (particularly, the infinite family of persistence exponents) as a potentially powerful tool (rivaling, perhaps even exceeding, in utility the well-studied dynamic scaling approach) in studying dynamical interface fluctuation processes.

3.1 The generalized persistence probability: persistent large deviations probability

The infinite family of persistence exponents we study here is based on the concept of *persistence of large deviations* introduced recently by Dornic and Godreche [32] in the context of kinetic Glauber-Ising dynamics of magnetization coarsening (a closely related idea, that of sign-time distribution, was developed in Ref. [33]). For equilibrium step fluctuations, we define the probability of persistent large deviations, $P(t,s)$, as the probability for the "average sign" $S_{\rm av}$ of the height fluctuation to remain above a certain pre-assigned value "s" up to time t:

$$P(t,s) \equiv \text{Prob } \{ \ S_{\rm av}(t') \geq s, \ \forall t' \leq t \ \}, \tag{3.3}$$

where

$$S_{\rm av}(t) \equiv t^{-1} \int_0^t dt' \ S(t'), \tag{3.4}$$

and

$$S(t) \equiv \text{sign } [h(x,t_0+t) - h(x,t_0)], \tag{3.5}$$

where with no loss of generality, we set $t_0 = 0$. Although the dynamical variable $S(t)$ above is defined for a particular lateral position x, we take a statistical ensemble average over all lateral positions to obtain a purely time dependent dynamical quantity $P(t,s)$. Since $S_{\rm av}(t) \in [-1,1]$, the probability $P(t,s)$ is defined for $-1 \leq s \leq 1$. For $s = 1$ we recover our earlier simple definition of persistence used in Refs. [29, 30, 38, 39]: $P(t) \equiv P(t, s=1)$ measures the probability of the height fluctuation remaining above zero ("positive") throughout the whole

time interval. For $s = -1$ the probability $P(t, s = -1)$ is trivially equal to unity for all t. The generalized probability function, $P(t, s)$, defined in Eqs. (3.3) –(3.5) above, leads to a continuous family or hierarchy of persistent *large* deviations exponents, $\theta_l(s)$, *provided* the steady-state decay of $P(t, s)$ in time follows a power law, $P(t, s) \sim t^{-\theta_l(s)}$. As we show below, this indeed happens for equilibrium step fluctuation phenomena, allowing us to define and measure the non-trivial persistence exponent $\theta_l(s)$, $-1 \leq s \leq 1$, that varies continuously between $\theta_l(s = -1) \equiv 0$ and $\theta_l(s = +1) \equiv \theta$ where θ is the usual persistence exponent. Clearly, $P(t, s)$ and $\theta_l(s)$ are natural generalizations of the persistence probability $P(t)$ and the persistence exponent θ, respectively, to the broader concept of distribution of residence times with limiting behavior (i.e. $s = 1$) determining the usual persistence exponent.

3.2 Numerical results and discussions

We have carried out the first application of the persistent large deviations concept to the equilibrium step fluctuations phenomenon. We also report the first experimental measurements of $P(t, s)$ and θ_l for *any* stochastic system. Our results for the two distinct types of step fluctuation processes (the high-temperature AD and low-temperature ED situations, described [47] by Eqs. (3.1) and (3.2), respectively) are shown in Figs. 3.1 and 3.2. The details of the experimental procedure for extracting the persistence probability from the digitized dynamical STM images are described in Refs. [38, 39] for the same two systems, and are therefore not repeated here. We only mention that in order to obtain the probability of persistent large

deviations, we had to use a substantially larger number (~ 100) of STM data sets than that used in Refs. [38, 39, 40]. As mentioned earlier, we compare the experimental results with two theoretical models in each case: The continuous Langevin equation (Eq. (3.1) or (3.2)) and a discrete stochastic model which is theoretically known [1, 29, 38, 39, 40, 47, 68] to belong to the same universality class (in the dynamic scaling sense) as the continuum equation. For the high-temperature AD step fluctuations, described on a coarse-grained scale by Eq. (3.1) (sometimes referred to as the Edwards–Wilkinson equation [1]), the discrete stochastic model we use is the extensively studied solid-on-solid Family model [1, 3]. For the low-temperature ED case, described on a coarse-grained scale by Eq. (3.2) (sometimes referred to as the Mullins–Herring equation with conserved noise [1]), the discrete stochastic model we use is the well-studied Racz model [56]. Our results are obtained from numerical integration of the Langevin equations using the simple Euler scheme [29], and standard Monte Carlo simulation [29] of the atomistic models. Typical system sizes used in the numerical work are ~ 1000 for Eq.(3.1) and ~ 100 for Eq.(3.2), and the number of independent runs used in the calculation of persistence probabilities is ~ 1000.

In Fig. 3.1 we show in the top two panels our measured (panel (b)) and calculated (panel (a), main figure and inset) persistent large deviation probability $P(t, s)$ as a function of time t for the high-temperature step fluctuations case. Each panel shows eight different log-log plots of $P(t, s)$ against t for eight different values of the average sign parameter s ($= +1, +0.75, ..., -0.75$ from the bottom to the top). As mentioned before, the case $s = +1$ (the bottom-most curve) corresponds to

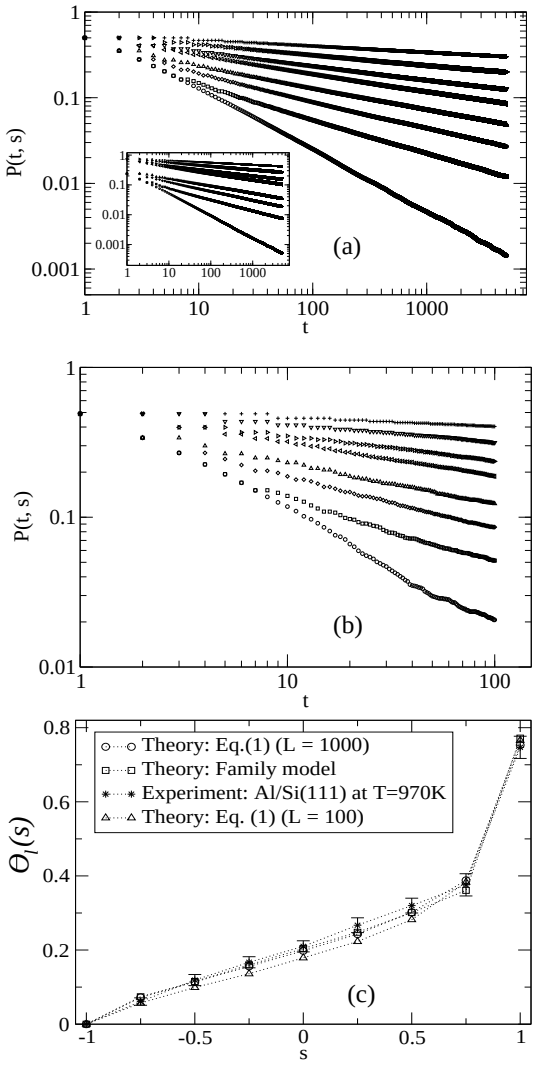

Figure 3.1: Log-log plots of $P(t,s)$ vs. t for high-temperature surface step fluctuations via the AD mechanism, shown for different values of s: $s = 1.0, 0.75, 0.5, 0.25, 0, -0.25, -0.5, -0.75$ (from the bottom to the top). (a) Eq.(3.1) (main figure) and the Family model (inset); (b) experimental data from STM step images of Al on Si(111) surface; and (c) comparison of the various sets of results for θ_l as a function of s. The error bars shown for the experimental data are obtained from variations of the local slope of the $\log P(t,s)$ vs. $\log t$ plots. Simulation results for two sample sizes are shown to illustrate that the use of small samples leads to an underestimation of $\theta_l(s)$.

the usual persistence probability $P(t)$, and therefore the results shown in Fig. 3.1 for $s = 1$ are already known. The results for all the other values of s are new and non-trivial. The linearity of the log-log $P(t, s)$ vs. t plots immediately implies that $P(t, s) \sim t^{-\theta_l(s)}$. The different sets of results for θ_l as a function of s are shown in Fig. 3.1(c). The excellent agreement among the various data sets shown in Fig. 3.1(c) is the most important new quantitative result of our work. This means that the high-temperature step fluctuation phenomenon via the AD mechanism is indeed described by the Edwards–Wilkinson equation (and therefore also by the discrete Family model), not just in the sense of the dynamical universality class (as defined by specific exponent values, e.g. β and θ) but more importantly for the infinite family of persistent large deviations exponents as defined by the continuous *function* $\theta_l(s)$. This striking agreement between experiment and theory for a continuous family of exponents definitely establishes persistent large deviations studies as a new and effective tool for studying dynamical fluctuations of nanoscale systems.

In Fig. 3.2 we present results similar to those in Fig. 3.1, but now for the ED mechanism step fluctuation data along with the corresponding theoretical results for the continuum Langevin equation defined by Eq. (3.2) and the discrete stochastic Racz model which are known [29, 39, 47, 3] to be in the same dynamic universality class as the low-temperature step fluctuation process. The same description and explanation given above for Fig. 3.1 apply now to Fig. 3.2 where $\theta_l(s = 1) \approx 0.875$, which agrees with recent experimental measurements [39] of the usual persistence exponent of low-temperature step fluctuations on Ag and Pb surfaces. The experimental and theoretical results for the continuous function $\theta_l(s)$, shown in Fig. 3.2(c),

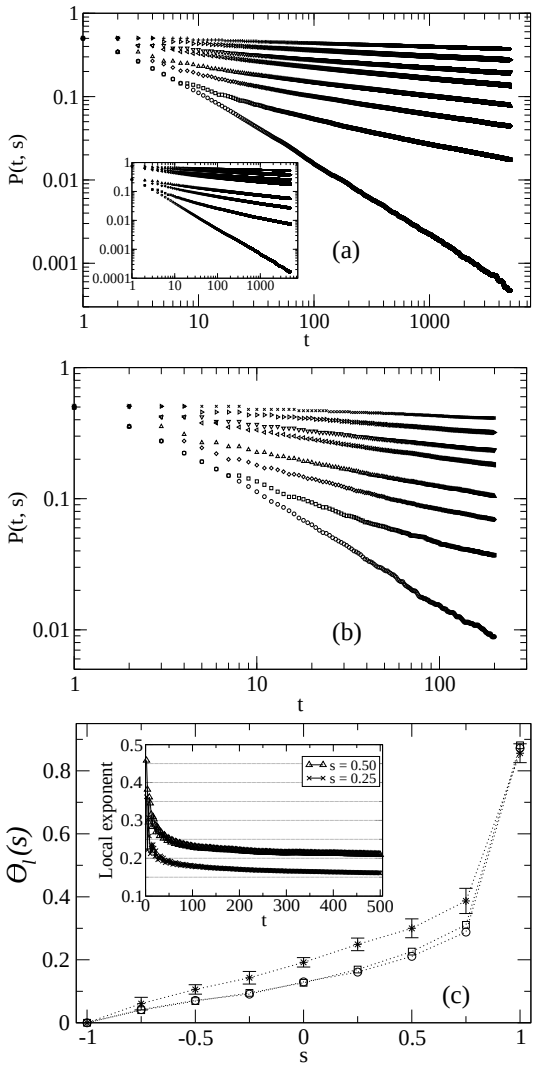

Figure 3.2: The same as in Fig. 3.1 for the low-temperature step fluctuations via the ED mechanism. (a) The continuum Langevin equation of Eq. (3.2) (main figure) and the discrete stochastic Racz model (inset); (b) experimental data for the Ag(111) step fluctuations; and (c) comparison of the three sets of results for θ_l: experiment (star), stochastic Racz model (square) and Eq. (3.2) (circle). The inset shows the time-dependence of the *local* exponent $\theta_l(s,t)$ obtained from simulations of the Langevin equation for $s = 0.25$ and $s = 0.50$.

exhibit qualitative agreement, with the experimental exponent values for $s < 1$ being slightly larger than the theoretical ones. There are several possible explanations for this difference between experimental and theoretical results. There are reasons to expect that increasing the dynamic range of the experimental $P(t, s)$ beyond two decades in t (this range is limited by noise problems inherent in dynamic STM imaging) would bring theory and experiment into closer agreement. To illustrate this possibility, we show in the inset of Fig. 3.2(c) the time-dependence of the *local* exponent $\theta_l(s, t) = d \log[P(s, t)]/d \log t$, obtained from simulations of the Langevin equation for two values of s for which the difference between theory and experiment is large. The local exponent is found to *decrease* with time before reaching a constant value at large t. We have checked that the experimental data show similar behavior for all $s < 1$, which implies that the effective exponent values obtained from power-law fits of relatively short-time data would be larger than the true long-time values. Indeed, we have found that fits of the simulation data over the range $20 \leq t \leq 200$ (this is the range used in obtaining $\theta_l(s)$ from the experimental data) yield values of $\theta_l(s)$ that are higher and closer to the experimental values. A second possibility is that the smallness of the sample size used in the simulations leads to an underestimation of the values of $\theta_l(s)$, as in Fig. 3.1(c). Unfortunately, the impossibility of equilibrating much larger samples of these models with very slow dynamics prevents us from checking this explicitly. Another possibility that we can not rule out is that the Ag(111) equilibrium step fluctuations do not precisely follow the theoretical models of edge-diffusion limited kinetics. Further experimental and theoretical investigations would be needed for settling this issue. We should

emphasize, however, that given the severe complexity in measuring any power law exponents associated with surface step fluctuation dynamics, the overall agreement between theory and experiment is quite good.

3.3 Conclusion

In summary, we have established the concept (and the usefulness) of an infinite family of persistent large deviations exponents for height fluctuations in equilibrium surface step dynamics phenomenon. The impressive agreement between theory and experiment indicates that the persistent large deviations probability (and the corresponding exponents) may very well be an extremely powerful tool in characterizing and understanding other stochastic fluctuation phenomena, e.g., kinetic surface roughening in nonequilibrium growth. In contrast to other dynamical approaches, the technique developed in this chapter leads to a continuous family of exponents (a continuous function rather than one or two isolated independent exponents, as in the dynamic scaling approach) and is therefore a much more stringent test of theoretical ideas, and also perhaps provides a deeper level of probing the dynamics of fluctuation problems.

4. SURVIVAL PROBABILITY: A DIFFERENT FIRST–PASSAGE STATISTICAL CONCEPT

As mentioned before, recent experimental STM measurements of step fluctuations [38] have revealed that the survival probability of the dynamical step height (at a fixed but arbitrary spatial location) not returning in time t to its average ("equilibrium") level, has an exponential behavior, $S(t) \propto \exp(-t/\tau_s)$, where τ_s is the survival time scale. In this chapter, we provide a definitive theoretical explanation for this exponential temporal behavior of the surface fluctuation survival probability using rigorous (analytical) arguments and direct (numerical) simulations. We note that survival and persistence turn out to be *identical* in problems related to Ising spin dynamics, where one is interested in the probability that a spin has not changed its sign (has not "flipped") up to time t[1]. This is due to the *discrete* nature of Ising spin

[1]Unfortunately, rather confusing terminology has been used in the spin dynamics literature to describe this probability, including persistence, survival, and non-zero-crossing probability. Further confusion is caused by the fact that even in the surface dynamics problem, persistence and survival become the same if one starts from the initial condition of a "flat surface" (which cannot be achieved experimentally) and defines "survival" with respect to the average surface which is also "flat"

dynamics, where a spin flip ensures a change of sign with respect to both the initial and the average (or any other reference) value of the stochastic variable. In contrast, the *continuous* nature of surface fluctuation dynamics, where the step height is a continuous variable, leads to a fundamental qualitative difference between $P(t)$ and $S(t)$. This qualitative difference was noted as an experimental fact and an unsolved puzzle in Ref. [38] for equilibrium step fluctuations on Al/Si(111)[2]. We emphasize that the probabilities $P(t)$ and $S(t)$ provide completely different physical information about surface step fluctuations: while persistence characterizes the universality class of the dynamical process through the persistence exponent θ, survival, as discussed in this chapter, provides useful information about the physical mechanisms (and their characteristic time scales) underlying step fluctuations in the long-time limit.

Another time scale that invariably enters experimental and numerical measurements of any statistical quantity is *the sampling time* δt (the interval between successive measurements of the step position). An understanding of the effects [65, 66] of a finite δt on the measured survival probabilities is necessary for comparing experimental and numerical results with theoretical predictions.

We present the results of a detailed study of the behavior of $S(t)$ for two linear Langevin equations that describe [1, 69] step fluctuations under attachment/detachment ("high-temperature") and edge-diffusion ("low temperature") limited kinetics. We

[2]We point out in this context that in Ref. [38] both of these probabilities were unfortunately called persistence probability (with respect to the average position and the initial position, respectively) causing perhaps some confusion.

first show analytically that if the equilibrium autocorrelation function $C(t)$ of height fluctuations decays exponentially at long times, then $S(t)$ must also decay exponentially with a time scale that is proportional to the correlation time (the time scale of the decay of $C(t)$). This prediction is verified from numerical simulations of the Langevin equations. The simulation results also provide information about the dependence of the measured survival probability on the sampling time δt. We show that the survival probability $S(t, L, \delta t)$ exhibits simple scaling behavior in both models. Finally, we use available experimental data [38, 39, 70] to calculate $C(t)$ and $S(t)$ for two physical systems that are believed to be described by these two Langevin equations and show that the experimental results are consistent with our predictions.

4.1 Autocorrelation function of height fluctuations

High-temperature step fluctuations dominated by atomistic attachment and detachment at the step edge are known [69, 1] to be well described by the second-order non-conserved linear Langevin equation

$$\frac{\partial h(x,t)}{\partial t} = \frac{\Gamma_a \tilde{\beta}}{k_B T} \frac{\partial^2 h(x,t)}{\partial x^2} + \eta(x,t). \tag{4.1}$$

Here, $h(x,t)$ is the dynamical height fluctuation (position of the step edge measured from its equilibrium value) at lateral point x along the step and time t, Γ_a is the "step mobility", $\tilde{\beta}$ is the step-edge stiffness, and $\eta(x,t)$ is a nonconserved Gaussian noise satisfying $\langle \eta(x,t)\eta(x',t')\rangle = 2\Gamma_a \delta(x-x')\delta(t-t')$. Low-temperature step fluctuations dominated by the step edge diffusion mechanism are, on the other hand, described

by the fourth order conserved Langevin equation

$$\frac{\partial h(x,t)}{\partial t} = -\frac{\Gamma_h \tilde{\beta}}{k_B T} \frac{\partial^4 h(x,t)}{\partial x^4} + \eta_c(x,t), \tag{4.2}$$

with $\langle \eta_c(x,t)\eta_c(x',t')\rangle = -2\Gamma_h \nabla_x^2 \delta(x-x')\delta(t-t')$.

Space- and time-dependent correlation functions of height fluctuations in these two *linear* equations may be calculated [1, 69] easily by Fourier transforms. We assume that height fluctuations are measured from the spatial average of $h(x,t)$, so that the $k=0$ Fourier component of $h(x,t)$ is zero at all times. The autocorrelation function of $\tilde{h}(k,t)$, the Fourier transform of $h(x,t)$, has the following form in the long-time equilibrium state:

$$\langle \tilde{h}(k,t_1)\tilde{h}(-k,t_2)\rangle = \frac{k_B T}{\tilde{\beta} k^2} \exp(-\Gamma \tilde{\beta} k^z |t_1 - t_2|/k_B T), \tag{4.3}$$

where $z=2$, $\Gamma = \Gamma_a$ for Eq. (4.1), and $z=4$, $\Gamma = \Gamma_h$ for Eq. (4.2). The autocorrelation function of height fluctuations at equilibrium is then given by

$$\begin{aligned} C(t) &= \langle h(x,t_1)h(x,t_2)\rangle \\ &= \frac{2k_B T}{\tilde{\beta}} \int_{k_{min}}^{\infty} \frac{dk}{2\pi} \frac{\exp(-\Gamma \tilde{\beta} k^z |t|/k_B T)}{k^2} \end{aligned} \tag{4.4}$$

where $t = t_1 - t_2$ and $k_{min} = 2\pi/L$ for a finite system of linear dimension L. This implies that $C(t)$ exhibits an exponential decay at long times, $C(t) \propto \exp(-t/\tau_c)$[3], where the correlation time τ_c is equal to $k_B T L^z/(2\pi)^z \Gamma \tilde{\beta}$.

There are other physical mechanisms that may lead to an exponential decay of $C(t)$ at long times. The fluctuations of a particular step are affected by its

[3]For details, see Ref. [70]

interaction with neighboring steps. These interaction effects, which are negligible at relatively short time scales if the spacing between neighboring steps is large, may become important at long times. If one assumes that the step fluctuates in a harmonic confining potential [69], $(\lambda/2)\int h^2(x)dx$, then one obtains an additional term, $-\lambda\Gamma_a h(x,t)/k_BT$, in the right-hand of Eq. (4.1), and $\lambda\Gamma_h\nabla_x^2 h(x,t)/k_BT$ in Eq. (4.2). The function $C(t)$ is then given by

$$C(t) = 2k_BT\int_{k_{min}}^{\infty}\frac{dk}{2\pi}\frac{\exp[-\Gamma(\tilde{\beta}k^z + \lambda k^{z-2})|t|/k_BT)]}{\tilde{\beta}k^2 + \lambda}. \tag{4.5}$$

This, again, leads to an exponential decay of $C(t)$ at long times, with the correlation time τ_c a function of λ and L.

4.2 Survival probability

There exists a rigorous theorem [71] that states that if the autocorrelation function $C(t)$ of a stationary Gaussian process decays exponentially in time, then its survival probability $S(t)$ must also decay exponentially for large t,

$$S(t) \propto \exp(-t/\tau_s), \tag{4.6}$$

with the survival time scale τ_s proportional to the correlation time τ_c. The constant of proportionality, $c \equiv \tau_s/\tau_c$, which must be less than unity and independent of the system size L, is usually nontrivial, being determined by the full functional form of $C(t)$. Since the height fluctuations in our models represent a stationary Gaussian process at equilibrium, this rigorous result applies for the survival probability of these fluctuations. Thus, we arrive at a very general, exact result that the

survival probability of equilibrium step fluctuations should decay exponentially at long times if the autocorrelation function does so. This is the first important result of this chapter. Further, measurements of the ratio c of the two time scales may provide valuable information about the nature of the processes involved in the step fluctuations.

4.3 Numerical results

We have investigated these aspects in a detailed numerical study in which a simple Euler scheme [29] is used to numerically integrate spatially discretized versions of Eqs. (4.1) and (4.2). All the results reported here were obtained in the equilibrium regime. $S(t)$ is measured as the probability that the height fluctuation h_i at a particular site i does not cross the average step height (which is conveniently chosen as the "zero" of the height stochastic variable) over time t, averaged over all sites and many ($\sim 10^4 - 10^6$) independent runs. $C(t)$ is calculated exactly using discretized versions of Eqs. (4.4) and (4.5).

Typical results for $C(t)$ and $S(t)$ are shown in Fig. 4.1 (a-c) for Eq. (4.1) and in Fig. 4.2 (a-c) for Eq. (4.2) [$\lambda = 0$ in both cases]. As indicated in the figures, we used several different values of the sampling time δt in the measurement of $S(t)$ [$C(t)$ is, of course, independent of δt]. It is clear from the plots that both $C(t)$ and $S(t)$ decay exponentially at long times. The time scales τ_c and τ_s are extracted from exponential fits shown in the semi-log plots as dashed straight lines. The dependence of τ_c on L is given exactly by $\tau_c(L) = (L/2\pi)^z$. The results for different

values of L shown in Figs. 4.1 and 4.2 indicate that τ_s also increases rapidly as L is increased. However, we find that the calculated values of τ_s extracted from the $S(t)$ data obtained for different L using *the same sampling time* δt exhibit small but clear deviations from the expected proportionality to L^z. These small deviations result from a weak dependence of $S(t)$ on the sampling time δt. As shown in Fig. 4.1c) and Fig. 4.2b), the rate of the exponential decay of $S(t)$ at large t depends weakly on the value of δt used in the measurement of S. This is in accordance with the analytic predictions of Refs. [65, 66]. Since the only time scale in the problem is τ_c (as mentioned above, τ_s should be proportional to τ_c), the dependence of $S(t)$ on the sampling time δt should involve the scaling combination $\delta t/\tau_c$. Since $\tau_c(L) \propto L^z$ in our models, this argument suggests that the sampling time should be chosen to be proportional to L^z if the survival probabilities for different values of L are to be tested for scaling. Indeed, as shown in Fig. 4.1d), the values of $S(t)$ obtained for L = 100, 200 and 400 using δt = 0.625, 2.5 and 10.0, respectively, (so that $\delta t \propto L^z$ with $z = 2$) all fall on the same scaling curve when plotted as functions of t/L^z with $z = 2$. As shown in Fig. 4.2d), a similar scaling collapse is obtained for Eq. (4.2). Here, the sampling times for different L are chosen to be proportional to L^4, and the best scaling collapse is obtained when the data for different L are plotted against t/L^z with $z \simeq 3.95$. These results establish that the *full function* $S(t, L, \delta t)$ (not just the asymptotic long-time part) has the scaling form

$$S(t, L, \delta t) = f(t/L^z, \delta t/L^z), \tag{4.7}$$

where the function $f(x, y)$ decays exponentially for large values of x and the rate of

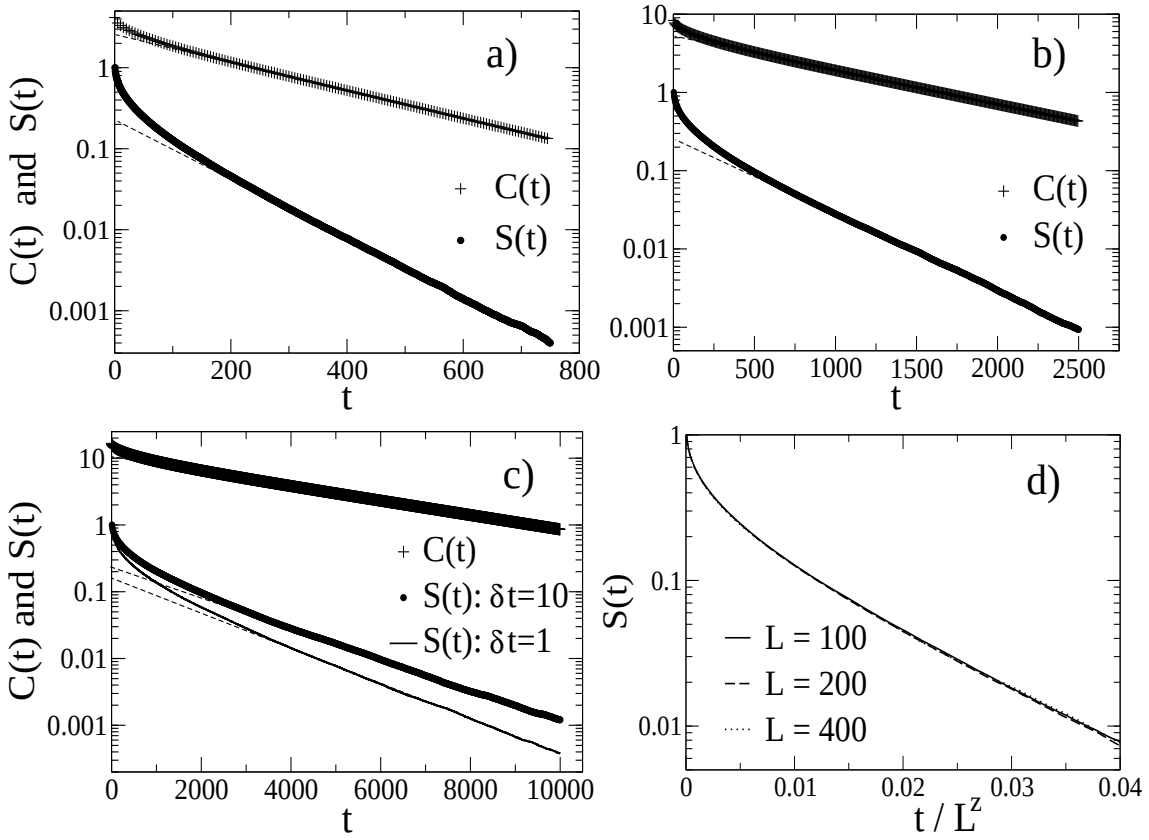

Figure 4.1: $S(t)$ and $C(t)$ for the Langevin equation of Eq.(1). The dashed lines are fits of the long-time data to an exponential form. In panels (a-c), the uppermost plots show the data for $C(t)$. Panel (a): $L = 100$, $\delta t = 0.625$. Panel (b): $L = 200$, $\delta t = 2.5$. Panel (c): $L = 400$, $\delta t = 10.0$ (upper plot) and $\delta t = 1.0$ (lower plot). Panel (d): Finite-size scaling of $S(t, L, \delta t)$. Results for S for 3 different sample sizes with the same value of $\delta t/L^z$ ($z = 2$) are plotted versus t/L^z.

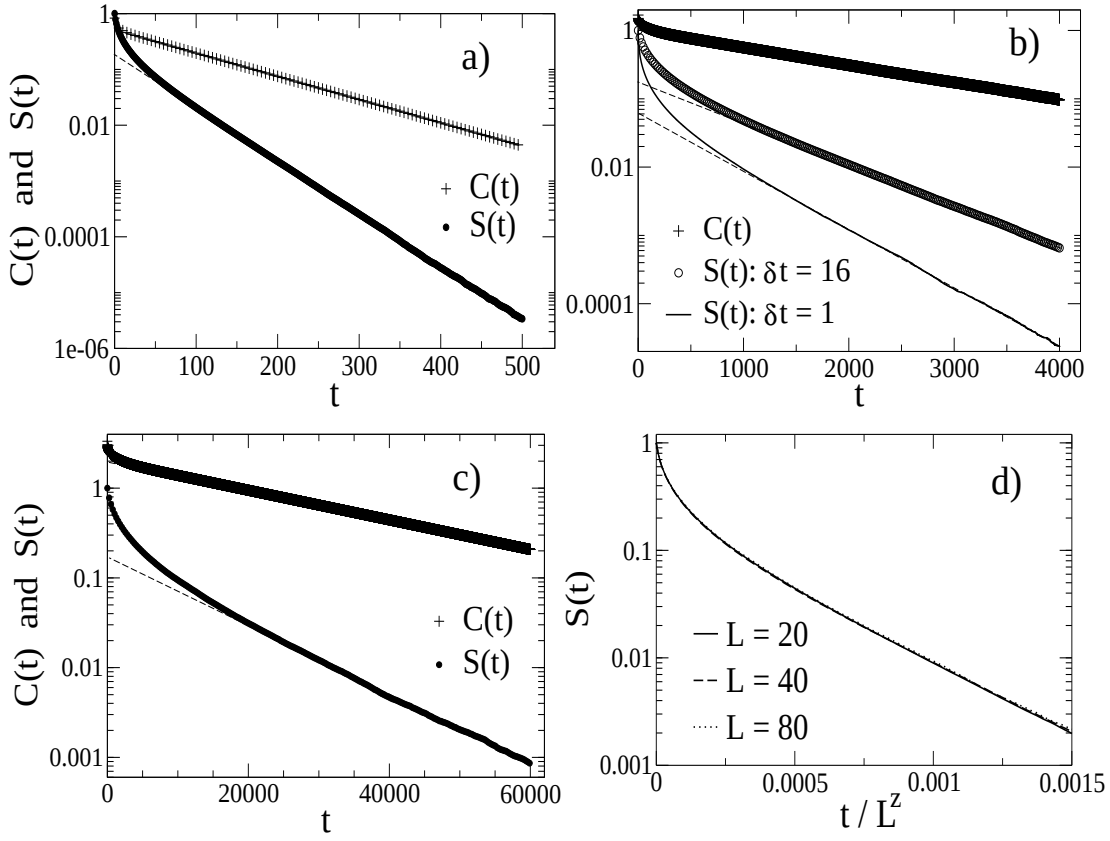

Figure 4.2: $S(t)$ and $C(t)$ for the Langevin equation of Eq.(2). In panels (a-c), the uppermost plots show the results for $C(t)$. The dashed lines are fits of the long-time data to an exponential form. Panel (a): $L = 20$, $\delta t = 1$. Panel (b): $L = 40$, $\delta t = 16$ (upper plot) and $L = 40$, $\delta t = 1$ (lower plot). Panel (c): $L = 80$, $\delta t = 256$. Panel (d): Finite-size scaling of $S(t, L, \delta t)$. Results for S for 3 different sample sizes with the same value of $\delta t/L^z$ ($z = 4$) are plotted versus t/L^z.

this decay increases slowly as y is decreased. This finite-size scaling behavior of S, which represents the second important result of our study, is similar to that found [72] for the persistence probability in a coarsening system. However, the dependence on the sampling time, *essential* in our scaling considerations, was not analyzed in Ref. [72].

We have also studied the behavior of $C(t)$ and $S(t)$ for Eq. (4.1) when the value of τ_c is primarily determined by the presence of a nonzero λ associated with step-step interaction (cf. Eq. (4.5) above). By varying λ and δt for a system with $L = 400$, we find that $S(t, \lambda, \delta t)$ exhibits excellent scaling behavior as a function of t/τ_c if the quantity $\delta t/\tau_c$ is held constant. Therefore, we conclude that S is a function of the scaling variables t/τ_c and $\delta t/\tau_c$, irrespective of the origin of the finite value of the correlation time τ_c.

For $\lambda = 0$, the ratio $c = \tau_s/\tau_c$ for Eq. (4.1) decreases from about 0.57 to about 0.41 as the ratio $\delta t/\tau_c$ is decreased from 0.025 to 2.5×10^{-4}, indicating that $c \simeq 0.4$ in the $\delta t \to 0$ limit. For relatively large L and nonzero λ, where τ_c is determined primarily by the value of λ, we find that $c \simeq 0.47$ for $\delta t/\tau_c = 0.025$. The difference between the values of c for the same value of $\delta t/\tau_c$ in the two cases reflects the expected dependence of c on the details of $C(t)$. For Eq. (4.2) with $\lambda = 0$, the value of c decreases from about 0.44 to about 0.30 as $\delta t/\tau_c$ is decreased from 0.01 to 6×10^{-4}. The qualitative behavior of c as a function of $\delta t/\tau_c$ is similar in all the cases we have considered, and is consistent with the general predictions of Refs. [65, 66].

We have also used dynamical STM data to calculate $C(t)$ and $S(t)$ for two experimental systems: Al/Si(111) at relatively high temperatures, which is believed

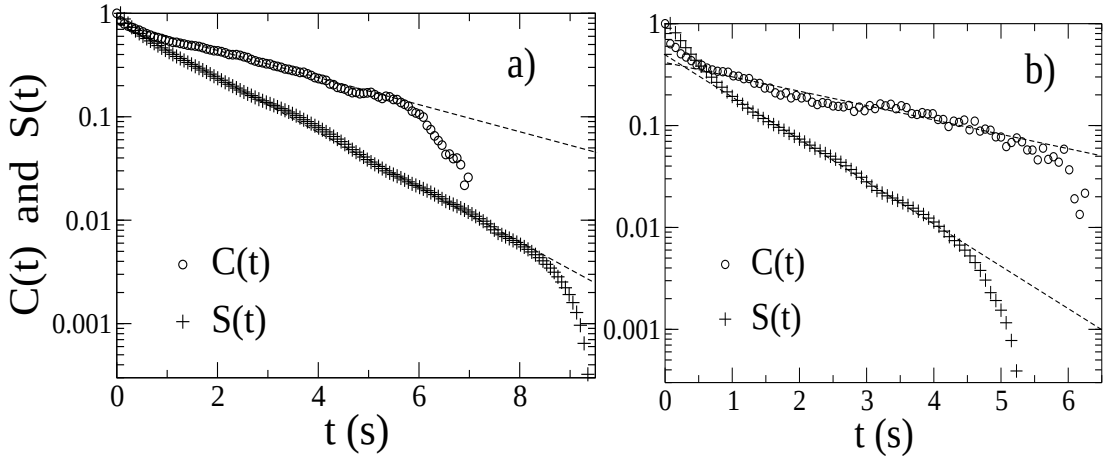

Figure 4.3: $S(t)$ and $C(t)$ for two experimental systems. The dashed lines are fits of the long-time data to an exponential form. Panel (a): Al/Si(111) at $T = 970$K. Panel (b): Ag(111) at $T = 450$K.

[38, 68, 73] to provide a physical realization of Eq. (4.1), and Ag(111) at relatively low temperatures where the step fluctuations are expected [39, 70] to be governed by the conserved Eq.(4.2). Some of the results of this analysis are shown in Fig. 4.3. For Al/Si(111) at 970K we find exponential decay of both $C(t)$ and $S(t)$. The value of the ratio c obtained from the estimates of τ_c and τ_s is close to 0.5. This value is right in the middle of the range of values of c obtained from our numerical study of Eq. (4.1). The Ag(111) at 450K data is characterized by $c \simeq 0.34$, which is again in the range of values obtained in the numerical study of Eq. (4.2). We, therefore, conclude that the available experimental data on $S(t)$ and $C(t)$ are consistent with our theoretical results.

Experimental data on the Al/Si(111) system are available at several temperatures between 770K and 1020K. As reported in Ref. [38], $S(t)$ decays exponentially

at long times at all these temperatures, with τ_s decreasing from 3.6s to 0.9s as T is increased from 770K to 1020K. Using these values of τ_s (actually, the corresponding values of τ_c obtained from the relation $\tau_s/\tau_c \simeq 0.5$) together with the values of the parameters Γ and $\tilde{\beta}$ obtained from other measurements [68, 73], we have calculated an "effective length" L_{eff} that would lead to the observed finite value of τ_c if it resulted from a finite length of the sample. The value of L_{eff} is found to decrease from $4020\mathring{A}$ to $389\mathring{A}$ as T is decreased from 1020K to 770K. These values are much smaller than the nominal step lengths in the experimental sample. The observed T-dependence of L_{eff} is inconsistent with the possibility that the finite values of τ_c are due to a nonzero value of the parameter λ: the length scale associated with λ should increase [69] as T is decreased. It is possible that L_{eff} is a measure of the typical length of a step edge between adjacent points that are held fixed by some kind of pinning centers. Since pinning becomes more effective at low T, this mechanism would provide a qualitative explanation of why L_{eff} decreases as T is reduced. Yet another possibility is that L_{eff} is a measure of the length scale over which step edge fluctuations are effectively equilibrated.

4.4 Conclusion

To conclude, we have shown analytically and numerically that the survival probability of equilibrium step fluctuations on vicinal surfaces decays exponentially at long times, and have established a relation between the time scales characterizing the exponential decay of the survival probability and the autocorrelation function.

Our theory explains the puzzling experimental finding of an exponential decay of $S(t)$ reported in Ref. [38]. We have also shown that the survival probability exhibits simple scaling as a function of the system size and the sampling time, which plays a very important role in the measurement of $S(t)$. Similar scaling features are displayed by the generalized survival probability, as we will see in the next chapter.

5. GENERALIZED SURVIVAL IN EQUILIBRIUM STEP FLUCTUATIONS

In this chapter, we introduce the concept of a generalized survival probability which enables us to probe deeper into the nature of the stochastic process of interface step fluctuations. The generalized survival probability is the probability $S(t, R)$ that a given lateral step position x with a height (i.e., step fluctuation measured from the equilibrium step position) $h(x, t)$ at time t does never cross a pre-assigned reference level of the height, R, throughout the entire evolution. We have seen in Chapter 4 that the particular case with $R = 0$ (i.e., the probability of the dynamical step height not returning in time t to its average ("equilibrium") $R = 0$ level) has been studied [43] both analytically and experimentally, and it has been shown to exhibit an exponential decay at large times, $S(t) \propto \exp(-t/\tau_s)$, where τ_s is the survival time scale that provides information about the underlying kinetics. The resulting surface step fluctuation survival probability $S(t) = S(t, R = 0)$ and the associated time scale τ_s have also recently been studied experimentally using dynamical scanning tunneling microscopy (STM) on different metallic systems: Al

steps on Si (111) surface at high temperatures, and Ag and Pb (111) surfaces at relatively low temperatures [70]. In this chapter, we show numerically that $S(t, R)$ also has an exponential behavior at large time, $S(t, R) \propto \exp(-t/\tau_s(R))$, where $\tau_s(R)$ is the generalized survival time scale. Our study reveals the dependence of $\tau_s(R)$ on the system size L, sampling interval δt, and reference level position R, allowing us to establish the complete scaling form of $S(t, R)$. In particular, the sampling interval [65, 66] turns out to be an essential ingredient inherent in any real experimental measurement procedure. Also the study of the dependence of the generalized survival time scale on the choice of the reference level R, which turns out to be exponential, should have particular importance for understanding the effect of thermal fluctuations at the nanoscale.

We consider the case of the high-temperature step fluctuations dominated by atomistic attachment and detachment (AD), where the step edge is known [1] to be well described by the coarse-grained second-order non-conserved linear Langevin equation (i.e., the Edwards–Wilkinson (EW) equation [12]).

For equilibrium step fluctuations, we define the generalized survival probability with respect to the height reference level R, $S(t, R)$, as the probability for the height variable to remain consistently *above* a certain pre-assigned value "R" over time t:

$$S(t, R) \equiv \text{Prob } \{\ h(x, t') > \ R, \ \forall\ t_0 \leq t' \leq t_0 + t\ \}, \tag{5.1}$$

where $h(x, t)$ is the dynamical height of the interface at a fixed lateral position x at time t, and t_0 is the initial time of the measurement.

The generalized survival probability function, $S(t, R)$, defined in Eq. (5.1)

above, leads to a hierarchy of generalized survival time scales, $\tau_s(R)$, *if* the steady-state decay of $S(t,R)$ in time follows an exponential trend, $S(t,R) \sim e^{-t/\tau_s(R)}$. As we show below, this indeed is obtained for Edwards–Wilkinson equilibrium step fluctuation phenomena, allowing us to define and measure the non-trivial survival time scale $\tau_s(R)$, $0 \leq R \leq R_{max}$, that varies between $\tau_s(R=0)$ and $\tau_s(R_{max})$, where $\tau_s(R=0)$ is the usual survival time scale and $\tau_s(R_{max})$ is the survival time with respect to the highest reference level R_{max} that can be defined for a model with finite roughness (i.e. rms fluctuations of the height variable with respect to the average). R_{max} is limited by the maximum value of the height fluctuation amplitude. Obviously, $S(t,R)$ and $\tau_s(R)$ are natural generalizations of the survival probability $S(t)$ and the survival time scale τ_s, respectively, to the more complex concept of distribution of generalized survival times with limiting behavior (i.e. $R=0$) providing the usual survival time.

The exponential decay at large time of $S(t,R)$ that we find numerically is not surprising. The generalized survival probability with respect to the reference level R can be regarded as the probability $Z(t)$ of no zero crossing of the new stochastic variable $H(x,t) = h(x,t) - R$. What we are looking for is the probability for the stochastic variable $H(x,t)$ to remain positive up to time t (or, equivalently, the probability for $h(x,t) + R$ to remain negative over time t). This type of question for the Gaussian stationary processes with zero mean has been addressed by mathematicians for a long time [31]. The no zero crossing probability is traditionally investigated in conjunction with the autocorrelation function, $C_H \equiv \langle H(x,t_1)H(x,t_2)\rangle$ (where $\langle ...\rangle$ represents an average over all realizations of $H(x,t)$ arising from the

thermal noise source). It is known [71] that for a stationary Gaussian process (i.e. $C_H = f(|t_1 - t_2|) \equiv f(t)$) with an autocorrelation function decaying faster than $1/t$ at large t, the asymptotic behavior of the no zero crossing probability is exponential, $Z(t) \propto \exp(-\mu t)$. The autocorrelation function $C_H(t)$ itself has been shown [43] to be stationary at late times and to decay exponentially. This, along with the exponential decay of $Z(t)$, ensures an exponential decay for $S(t, R)$.

5.1 Numerical measurement of $S(t, R)$ for the atomistic stochastic Family model

In order to numerically simulate the process described by the attachment/detachment limited kinetics (i.e., Eq. (1.1.2), we have used discrete stochastic Monte Carlo simulations of the corresponding atomistic solid–on–solid model, the extensively studied Family model [1], which belongs asymptotically to the Edwards–Wilkinson universality class [12]. The Family model in (1+1)–dimensions (i.e. one spatial variable and one temporal variable) is characterized by $\beta = 1/4$, $\alpha = 1/2$ and $z = \alpha/\beta = 2$ [1], where the growth exponent β is the rate of change of interface width (or roughness) in the transient regime ($w(t) \sim t^{\beta}$), the roughness exponent α shows the saturation of the width for a system with fixed size L in the steady state regime ($w(L) \sim L^{\alpha}$) and z is the dynamical exponent. This model involves the traditional random deposition (at a rate of one complete monolayer during one unit of time) and surface relaxation such that the adatoms are searching for the sites with the minimum local height. We have taken the relaxation length to be the lattice constant

and we have applied the usual periodic boundary conditions. Typical sizes (i.e., number of lattice sites) used in this numerical work are $100-900$, and the averaging procedure implies a number of at least 10^5 independent runs. All the measurements correspond to the steady state regime where the interface roughness has reached a time independent equilibrium value (i.e., $t_0 \gg L^z$ in Eq. (5.1)). We also mention that the smallest value for the sampling time is 1. We emphasize that our use of Family model is just a matter of convenience in simulating the EW equation [1]; our results are simply an exact discrete stochastic simulation of the EW equation.

Our results for the generalized survival probability and the associated time scale are presented in Figs. 5.1 and 5.2. $S(t,R)$ is simply computed as the fraction of sites which, starting above (below) the level R $(-R)$ at time t_0, have not crossed the reference level up to a later time t_0+t. In Fig. 5.1 we show that, as expected, the generalized survival with respect to an arbitrary reference level R follows an exponential decay at large times. The only varying parameter in Fig. 5.1 is the reference level R. We have considered six values for R, $R=0,1,...,5$ (only the first four curves are displayed due to the limitations imposed by the quality of the statistics, since as R increases it is less probable to have a reasonable number of lattice sites with height variables above (below) R $(-R)$). The dashed lines are fits of the long-time data to an exponential form, $S(t,R) \propto \exp(-t/\tau_s(R))$. The upper curve has $R=0$ and corresponds to the usual survival probability previously studied in Ref. [43]. However, all the other curves are new and they prove that the generalized survival probability decays exponentially in the long-time limit, with an associated time scale, $\tau_s(R)$, which decreases with the reference level value. As

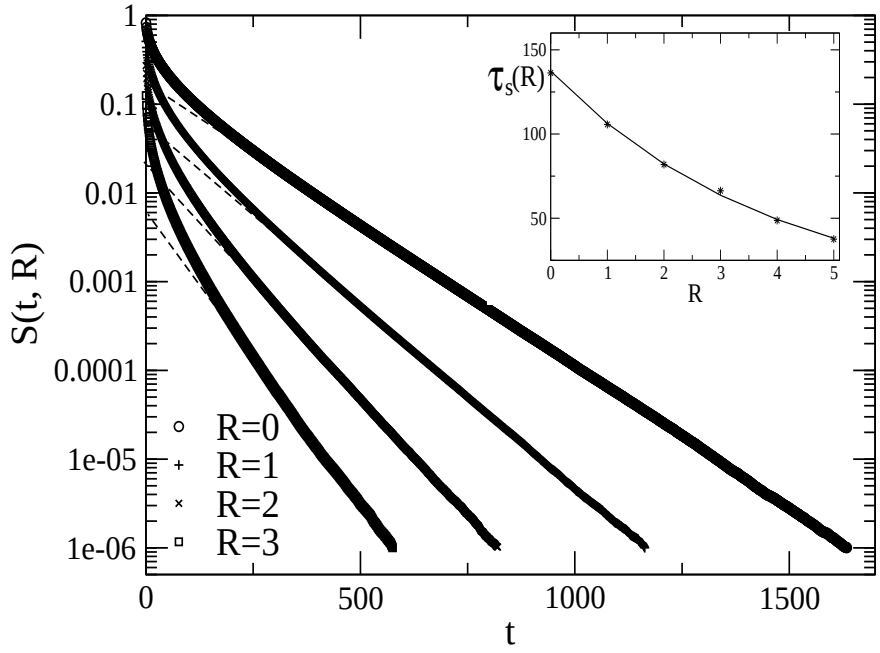

Figure 5.1: $S(t, R)$ for the discrete Family model. The dashed lines are fits of the long–time data to an exponential form. The system size is $L = 100$, the sampling time is $\delta t = 1.0$ and the reference level R takes four different values: 0, 1, 2 and 3 (from top to bottom). The inset shows the dependence of the generalized survival time scale $\tau_s(R)$ on the reference level value (up to $R = 5$). The continuous curve represents a fit to an exponential decay of $\tau_s(R)$ vs. R.

shown in the inset of Fig. 5.1, the dependence of $\tau_s(R)$ on R is exponential, but clearly more work is needed in order to understand this trend.

5.2 Scaling form of $S(t, R)$

In Fig. 5.2 we have used several lattice sizes, sampling times and reference levels in order to identify the scaling behavior of $S(t, R)$. In panel (a) we show the generalized survival with respect to level $R = 1$, measured using $\delta t = 1$, for two system sizes: $L = 100$ and $L = 200$. We observe that the underlying survival time scale increases rapidly with L. In fact, $\tau_s(R)$ for a fixed R is expected to grow proportionally to L^z [43]. However, we obtain that $\tau_s(R = 1) \simeq 103$ for $L = 100$, and $\tau_s(R = 1) \simeq 429$ for $L = 200$, so the measured generalized survival time exhibits a small deviation from the expected value of $103 \times 4 = 412$. We find that this small effect is due to the dependence of the generalized survival on sampling time δt. This is clearly seen in panel (b). It turns out that a system with a fixed size ($L = 200$) is characterized by different values of $\tau_s(R)$ if the sampling time of the measurement is adjusted. We observe that $\tau_s(R)$ increases weakly as the sampling time is increased. One might argue that this effect is very small and could be neglected, but we have found that the effect of the sampling time on the measured generalized survival probability has to be taken into account in order to find the complete scaling function of $S(t, R)$. In addition, this effect is even stronger for systems with slower dynamics (i.e. larger z) [43]. Interestingly enough, we note that fixing the reference height level in the generalized survival probability problem introduces an additional length scale, that

is related to the steady state value of the interface width, i.e. L^{α}. Indeed, in panel (c) we look at three different systems with $L = 200$, 400 and 900, respectively, and the generalized survival curves are calculated for $R = 1$, 2 and 3, respectively, i.e the level R is varied proportionally to L^{α}, with $\alpha = 1/2$ as appropriate for the EW equation. In addition, the sampling time for each of these three cases is also varied, $\delta t \propto L^{z}$ ($z = 2$), so we have considered $\delta t = 1$ for $L = 100$, $\delta t = 16$ for $L = 400$, and $\delta t = 81$ for $L = 900$, respectively. A perfect collapse of the curves $S(t, R)$ vs. t/L^{z} occurs when using $z = 2.03$, which agrees with the expected value $z = 2$, characteristic for the EW dynamics. This numerical analysis allows us to conclude that the scaling form of the generalized survival probability is

$$S(t, L, R, \delta t) = f(t/L^{z}, R/L^{\alpha}, \delta t/L^{z}), \tag{5.2}$$

where the function $f(x, y, z)$ decays exponentially for large values of x. The rate of this decay decreases rather rapidly as y is decreased and increases rather slowly as z is decreased. Note that for $y = 0$ we recover the scaling form of the usual survival probability with $R = 0$ [43] that has been analyzed in details in the previous chapter.

5.3 Conclusion

To conclude, we have shown that the generalized survival probability of equilibrium step fluctuations on vicinal surfaces with Edwards–Wilkinson dynamics decays exponentially at long times. We have investigated the associated generalized survival time scale that depends on the system size L, sampling time δt, and the choice of the reference level R. In particular, the dependence of $\tau_s(R)$ on R, which based on our

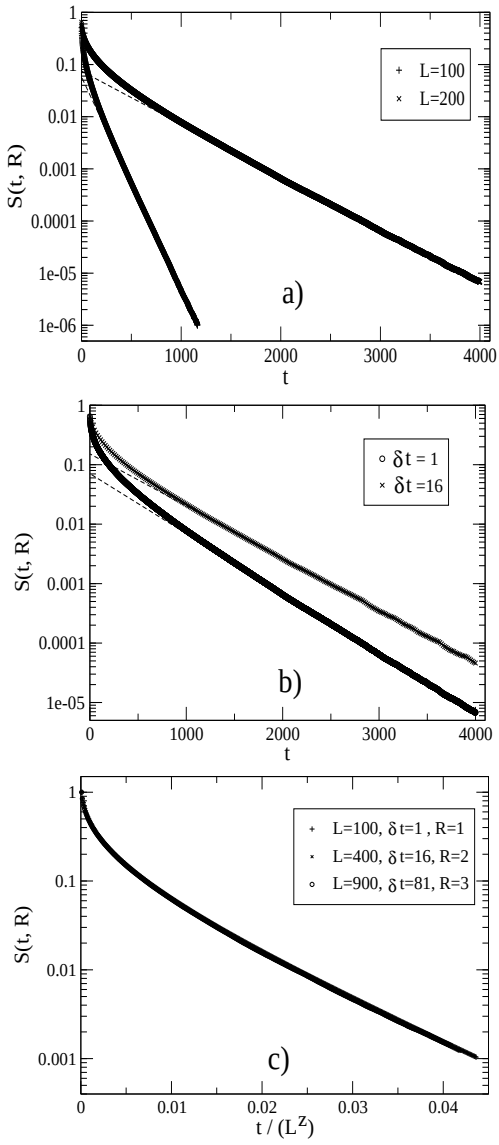

Figure 5.2: $S(t, R)$ for the Family model. The dashed lines are fits of the long–time data to an exponential form. (a): $L = 100$ (lower curve) and $L = 200$ (upper curve), using fixed sampling time $\delta t = 1$ and reference level $R = 1$. (b): $\delta t = 1$ (lower plot) and $\delta t = 16$ (upper plot) with fixed system size $L = 200$ and $R = 1$. (c): Scaling of $S(t, R)$ using different system sizes with δt and R varied such that $\delta t/L^z$ and R/L^α are kept constant (i.e. $\delta t/L^z = 1/10000$ and $R/L^\alpha = 1/\sqrt{100}$). A perfect collapse of the curves with L=100, 400 and 900, respectively, occurs when using $z = 2.03$.

preliminary investigations seems to have an exponential trend, should be useful in understanding the stability of thermally fluctuating interfaces. We have also shown that the generalized survival probability exhibits simple scaling as a function of L, δt, and R. Our numerical results on $S(t, R)$ can be easily extended to fluctuating interfaces characterized by different dynamical evolutions (such as low–temperature step edge diffusion limited kinetics) belonging to different universality classes. Our goal here, using the example of the step fluctuations process characterized by the EW universality class, is to establish the generalized survival probability as an important statistical concept in studying thermally fluctuating interfaces.

Finally, we mention that the generalized survival probability could be experimentally measured using dynamical STM step fluctuations data, opening the possibility for a direct approach to the crucial issue of interfacial stability. Our theoretical considerations for $S(t, R)$ should also be useful in understanding the dynamical evolution of other physical processes [34, 35, 36, 37, 74] where a first-passage statistics has proven to be an useful concept.

6. SPATIAL PERSISTENCE AND SURVIVAL PROBABILITIES FOR FLUCTUATING INTERFACES

6.1 Introduction

The concept of temporal persistence [19], which is closely related to first-passage statistics, has been used recently to study various non-Markovian stochastic processes both theoretically [23, 29, 30] and experimentally [34, 35, 36, 37, 38, 39, 74]. On the other hand, very little is known about the behavior of the *spatial persistence and/or survival probability*. As explained in Section 1.3.5 there are two exponents, θ_{SS} and θ_{FIC}, associated with $P(x_0, x_0 + x)$. The values of the exponents θ_{SS} and θ_{FIC} for interfaces with dynamics described by a class of linear Langevin equations have been determined in Ref. [45] using a mapping between the spatial statistical properties of the interface in the steady state and the temporal properties of stochastic processes described by a generalized random-walk equation. It turns out that for these systems, θ_{SS} is equal to either $3/2 - n$ for $1/2 < n < 3/2$ or 0 for $n > 3/2$, where $n = (z - d + 1)/2$, d is the spatial dimension, and z is the standard

dynamical exponent of the underlying Langevin equation. The FIC spatial persistence exponent is found to have the value $\theta_{FIC} = \theta(n)$, where $\theta(n)$ is a temporal persistence exponent for the generalized random walk problem to which the spatial statistics of the interface is mapped. Two exact results for $\theta(n)$ are available in the literature: $\theta(n = 1) = 1/2$, corresponding to the classical Brownian motion [57] and $\theta(n = 2) = 1/4$, corresponding to the random acceleration problem [58, 75].

Very recently, experimental measurements of the spatial persistence probability have been performed [74] for a system (combustion fronts in paper) that is believed to belong to the Kardar–Parisi–Zhang (KPZ) [13] universality class. However, the FIC spatial persistence probability is not investigated at all in this work. Instead, the authors analyze a "transient" spatial persistence (i.e., the probability is measured by sampling over all the sites of a transient interfacial profile obtained before the steady state is reached). This transient spatial persistence is completely different from the FIC spatial persistence which is measured in the steady-state regime by sampling a special class of initial sites. As a consequence, additional study is required in order to understand the experimental and numerical possibilities for measuring P_{FIC} and its associated nontrivial exponent θ_{FIC}.

In this chapter, we present the results of a detailed numerical study of spatial persistence in a class of one-dimensional models of fluctuating interfaces. Our interest in analyzing the spatial persistence of fluctuating interfaces is motivated to a large extent by their important (and far from completely understood) role in the rapidly developing field of nanotechnology where the desired stability of nanodevices requires understanding and controlling thermal interfacial fluctuations. In

this context, the study of first-passage statistics in general, or of the persistence probability (both spatial and temporal) [29, 30, 45] in particular, turns out to be a very useful approach. To address this problem we consider stochastic interfaces with dynamics governed by the Edwards–Wilkinson (EW) [12] and KPZ equations. For the EW equation, we consider both white noise (uncorrelated in both space and time) and "colored"noise that is correlated in space but uncorrelated in time. The effect of noise in spatially distributed systems is an interesting problem by itself and has been widely studied [76]. In this chapter, we investigate the effects of noise statistics on the spatial structure of fluctuating interfaces using the conceptual tool of spatial persistence probability. Using the isomorphic mapping procedure of Ref. [45], we derive exact analytical results for the spatial persistence exponents of $(d+1)$–dimensional EW interfaces driven by power-law correlated noise. We then compare our analytical results with those obtained from numerical integrations of the corresponding stochastic equations. The use of power-law correlated noise in the EW equation allows us to explore the situation where the two spatial persistence exponents θ_{SS} and θ_{FIC} are different.

Our numerical study also provides a characterization of the scaling behavior of spatial persistence probabilities as functions of the system size. Information about the system-size dependence of persistence probabilities is necessary for extracting the persistence exponents from experimental and numerical data. In studies of the scaling behavior of spatial persistence probabilities, one has to consider another important length scale that always appears in practical measurements: this is the *sampling distance* δx which represents the "nearest-neighbor"spacing of the uniform

grid of spatial points where the height variable $h(x, t_0)$ is measured at a fixed time t_0. The sampling distance δx is the spatial analog of the "sampling time" [43, 65] that represents the time-interval between two successive measurements of the height at a fixed position in experimental and computational studies of temporal persistence. Once the effect of a finite δx on the measured spatial persistence is understood, one can relate correctly the experimental and numerical results to the theoretical predictions. Our study shows that the spatial persistence probabilities (both SS and FIC) exhibit simple scaling behavior as functions of the system size and the sampling distance.

In addition to the temporal persistence probability, the temporal survival probability [38, 43, 44] has been shown recently to represent an alternative valuable statistical tool for investigations of first-passage properties of spatially extended systems with stochastic evolution. In the context of interface dynamics, the temporal survival probability is defined as the probability that the height of the interface at a fixed position does not cross its *time-averaged* value over time t. In contrast to the power-law behavior of the temporal persistence probability (which, we recall, measures the probability of not returning to the initial position), the temporal survival probability exhibits an exponential decay at long times, providing information about the underlying physical mechanisms and their associated time scales [43]. In this study, we make the first attempt to analyze the behavior of the *spatial survival probability*, $S(x_0, x_0 + x)$, defined as the probability of the interface height between points x_0 (which is an arbitrarily chosen initial position) and $x_0 + x$ not reaching the average level $\langle h \rangle$ (rather than the original value $h(x_0, t_0)$). We present numerical

results for $S(x_0, x_0 + x)$ that show that its spatial behavior in the SS regime is neither power-law, nor exponential, while in the FIC regime, it becomes very similar to the spatial persistence probability, $P_{FIC}(x_0, x_0 + x)$.

The chapter is organized as follows. In Sec. 6.2, we define the models studied in this work, review existing analytical results about their spatial persistence properties, and present new analytical expressions for the spatial persistence exponents for EW interfaces with colored noise in arbitrary spatial dimension. In Sec. 6.3, we describe the numerical methods used in our study and discuss how the spatial persistence and survival probabilities are measured in our numerical simulations. The results obtained in our (1+1)–dimensional numerical investigations are described in detail and discussed in Sec. 6.4, for both discrete stochastic solid-on-solid models (Sec. 6.4A) and the spatially discretized EW equation with colored noise (Sec. 6.4B). Sec. 6.5 contains a summary of the main results and a few concluding remarks.

6.2 Stochastic equations for fluctuating interfaces

We have performed a detailed numerical study of the spatial persistence of (1+1)–dimensional fluctuating interfaces where the dynamics is described by the well known EW equation

$$\frac{\partial h(x,t)}{\partial t} = \nabla^2 h(x,t) + \eta(x,t), \tag{6.1}$$

or alternatively by the KPZ equation

$$\frac{\partial h(x,t)}{\partial t} = \nabla^2 h(x,t) + (\nabla h(x,t))^2 + \eta(x,t), \tag{6.2}$$

where ∇ and ∇^2 refer to spatial derivatives with respect to x, and $\eta(x,t)$ with $\langle \eta(x,t)\eta(x',t') \rangle \propto \delta(x-x')\delta(t-t')$ is the usual uncorrelated random Gaussian noise. The dynamical exponent for Eq. (6.1) is $z = 2$, and since $d = 1$ in our study, the variable n defined in Sec. 6.1 is equal to 1. So, we expect both θ_{SS} and θ_{FIC} for this system to be equal to 1/2 [45]. Although the KPZ equation is nonlinear, characterized by $z = 3/2$, it is well-known that in the long time limit, the probability distribution of the stochastic height variable $h(x,t)$ in this equation is the same as that in the EW equation (i.e. $P(h) \sim \exp[\ -\int dx(\nabla h)^2\ ]$) in (1+1) dimensions. The static roughness exponent, α, is the same ($\alpha = 1/2$) for both cases. The 1+1–dimensional KPZ model differs from the EW model in the *transient* scaling regime where the interfacial roughness grows as a power-law in time, but this temporal regime is not involved in the calculation of the spatial persistence probabilities, as explained in Sec. 6.1. As a consequence, the steady-state spatial properties of (1+1)–dimensional interfaces governed by Eq. (6.2) can be mapped, as for Eq. (6.1), into a stochastic process with $n = 1$. So, the expected values of θ_{SS} and θ_{FIC} for the (1+1)–dimensional KPZ universality class are also equal to 1/2. Thus, studies of (1+1)–dimensional KPZ and EW interfaces do not bring out the interesting possibility of different values for the spatial persistence exponents θ_{SS} and θ_{FIC}.

To examine the theoretical prediction [45] of a possible difference between the values of θ_{SS} and θ_{FIC}, we consider the case when the interface dynamics is governed by a EW-type equation with long-range spatial correlations in the noise. Specifically,

we consider Eq. (6.1) with Gaussian colored noise [77] with variance given by

$$\langle \eta_c(x,t)\ \eta_c(x',t')\rangle = g_\rho(x-x')\delta(t-t'), \tag{6.3}$$

where $0 \leq \rho < 1/2$ is a parameter that characterizes the spatial correlation of the noise, and

$$g_\rho(x-x') = \begin{cases} |x-x'|^{2\rho-1} & \text{if} \quad |x-x'| \neq 0 \\ \\ g_\rho(0) & \text{if} \quad x = x' \end{cases} \tag{6.4}$$

We have chosen $g_\rho(0)$ as in Ref. [77] (i.e. $g_\rho(0) = 1/\rho(1/2)^{2\rho}$). As discussed below, the SS and FIC spatial persistence exponents for (1+1)–dimensional interfaces described by the EW equation with this kind of colored noise are expected to be different from one another. This system, thus, provides an opportunity to examine in detail the role of the choice of the initial points in determining the form of the decay of the spatial persistence probability.

By applying the isomorphic mapping recipe of Ref. [45] to the (d+1)–dimensional version of Eq. (6.1) with colored noise η_c whose statistics is defined by Eqs. (6.3) and (6.4), we obtain the result $n = (z-d+1)/2 + \rho$ with $z = 2$, implying the following analytical expressions for the spatial persistence exponents:

$$\theta_{SS} = \frac{d}{2} - \rho \tag{6.5}$$

and

$$\theta_{FIC} = \theta\left(\frac{3-d}{2} + \rho\right). \tag{6.6}$$

Thus, the value of θ_{SS} is completely determined by the noise correlation parameter ρ. However, based on the range of values for ρ, we can only infer that θ_{FIC} varies (presumably in a continuous manner) between $\theta(\frac{3-d}{2})$ and $\theta(\frac{4-d}{2})$ as the parameter

ρ is increased from 0 to 1/2. For $d = 1$, this implies a change from the value $\theta(1) = 1/2$ to $\theta(3/2)$, expected to lie between 1/2 and $\theta(2) = 1/4$, as ρ changes from 0 to 1/2. Since the value of θ_{SS} for $d = 1$ goes to 0 as ρ approaches the value 1/2, it is clear that the values of the two spatial persistence exponents must be different for a general value of ρ in the range [0,1/2). This difference would be small for ρ near zero (the two persistence exponents have the same value for $\rho = 0$), and maximum for ρ near 1/2. Therefore, the model with ρ substantially different from zero provides a numerically tractable situation where the interesting theoretical prediction of the existence of two different nontrivial spatial persistence exponents can be tested. We also mention that the usual dynamical scaling exponents take the following ρ-dependent values in the model with colored noise: $\alpha = (2 - d + 2\rho)/2$, $\beta = (2 - d + 2\rho)/4$. Thus, the general result [45], $\theta_{SS} = 1 - \alpha$, is satisfied for all d and ρ.

We have investigated these aspects in a detailed numerical study of models that belong in the universality classes of the Langevin equations of Eqs. (6.1) and (6.2). For Eq. (6.1) with uncorrelated white noise, we have used a discrete stochastic solid-on-solid model (the Family model [3]) which is rigorously known to belong to the same dynamical universality class. For Eq. (6.2) with uncorrelated white noise, we have also used a discrete solid-on-solid model (the Kim–Kosterlitz model [8]). Finally, for the EW equation with colored noise, the numerical results were obtained from a direct numerical integration of the spatially discretized stochastic differential equation.

6.3 Numerical methods

Simulations of the atomistic Family and Kim-Kosterlitz models are carried out using the standard Monte Carlo method for implementing the stochastic deposition rules of each model. Numerical integration of the EW equation with colored noise is performed using the simple Euler method [29, 78]. We solve the (1+1)–dimensional Eq. (6.1) with spatially long-range correlated noise for the real variable $h(x_j, t_n)$, where $t_n = n\Delta t$ $(n = 0, 1, \ldots)$ and $x_j = j\Delta x$ $(j = 0, 1, \ldots, L-1)$, with periodic boundary conditions. Here, Δt and Δx are the spatial and temporal grid spacings, respectively. Using the forward-time centered-space representation [78], Eq. (6.1) becomes:

$$h(x_j, t_{n+1}) - h(x_j, t_n) = \Delta t \left[\frac{h(x_{j+1}, t_n) - 2h(x_j, t_n) + h(x_{j-1}, t_n)}{(\Delta x)^2} \right] + \sqrt{\Delta t}\, \eta_c(x_j, t_n). \tag{6.7}$$

We have chosen $\Delta x = 1$ and Δt small enough (i.e. $\Delta t = 0.01$) in order to satisfy the stability criterion $2\Delta t/(\Delta x)^2 \leq 1$. The spatial correlation of the noise is given by

$$\langle \eta_c(x_j, t_n)\ \eta_c(x_k, t_m) \rangle = g_\rho(x_j - x_k)\delta_{n,m} \tag{6.8}$$

with

$$g_\rho(x_j - x_k) = \begin{cases} |x_j - x_k|^{2\rho-1} & \text{if} \quad 1 \leq |x_j - x_k| \leq \frac{L}{2} \\ (L - |x_j - x_k|)^{2\rho-1} & \text{if} \quad |x_j - x_k| > \frac{L}{2} \\ g_\rho(0) & \text{if} \quad x_j - x_k = 0 \end{cases} \tag{6.9}$$

where $g_\rho(0) = 1/\rho(1/2)^{2\rho}$. The colored noise is generated using the recipe from Ref. [77]. The Fast Fourier Transform operation that is used in the noise-generation

procedure constrains the system size to be an integral power of 2. Due to the use of periodic boundary conditions (which are also imposed on the noise correlation function, see Eq. (6.9)), the range of x over which spatial correlations and persistence properties are meaningfully measured is of the order of $L/2$.

The SS spatial persistence probability $P_{SS}(x_0, x_0 + x)$ is measured at a fixed time t_0 (which is much larger than the time $t_{sat} \sim L^z$ required for the interface roughness to saturate) as the probability that the interface height variable does not cross its value, $h(x_0, t_0)$, at the initial point x_0 as one moves along the interface from the point x_0 to the point $x_0 + x$. This probability is averaged over all the sites in a steady-state configuration and also over many independent realizations of the stochastic evolution. Thus,

$$P_{SS}(x_0, x_0 + x) \equiv \text{Prob } \{ \text{ sign } [h(x_0 + x') - h(x_0)] = \text{ constant }, \\ \forall\ 0 < x' \leq x\ ,\ \forall\ x_0 \in \mathcal{S}_{SS}\ \}\,, \qquad (6.10)$$

where sign $[y]$ represents the sign of the fluctuating quantity y, and $\mathcal{S}_{SS}$ is the ensemble containing all the lattice sites in a steady-state configuration. The FIC spatial persistence probability $P_{FIC}(x_0, x_0 + x)$ is obtained in a similar manner, except that the average is performed over a particular subensemble of the steady-state configuration sites, $\mathcal{S}_{FIC} \subset \mathcal{S}_{SS}$, characterized by *finite* values of the height variable and its spatial derivatives:

$$P_{FIC}(x_0, x_0 + x) \equiv \text{Prob } \{ \text{ sign } [h(x_0 + x') - h(x_0)] = \text{ constant }, \\ \forall\ 0 < x' \leq x\ ,\ \forall\ x_0 \in \mathcal{S}_{FIC}\ \}\,. \qquad (6.11)$$

Since the persistence probabilities are averaged over the choice of the initial point x_0, we omit writing x_0 explicitly in the arguments of P_{SS} and P_{FIC} from now on, while

stressing the important fact that the ensemble of initial sites used in the averaging process determines which one of the two persistence probabilities is obtained. We consider two different methods for measuring $P_{FIC}(x)$, depending on the type of the model (atomistic solid-on-solid model or spatially discretized Langevin equation) being studied. In the former case where the height variables are integers, the FIC spatial persistence probability measurement involves a sampling procedure from the subset of sites characterized by a fixed integer value of the height (measured from the average, $\langle h \rangle$, of the heights of all the sites at time t_0) which is substantially smaller than the typical value of the height fluctuations measured by the saturation width of the interface profile. In calculations using the direct numerical integration technique, the height variable can take any real value. Thus, the probability of finding a fixed value of the stochastic height variable is infinitesimally small. For this reason, fixing a reference level H and sampling over the sites with $h(x_0, t_0) = \langle h \rangle + H$ is useless. We, therefore, consider in this case a continuous interval of height values (symmetric with respect to the average height $\langle h \rangle$) with width w which is considerably smaller than the amplitude of the height fluctuations. The positions characterized by a height variable within this interval represent the subensemble of lattice positions involved in the sampling procedure necessary for measuring $P_{FIC}(x)$.

The spatial survival probabilities corresponding to the SS and FIC conditions are calculated similarly to the corresponding persistence probabilities, except that

the stochastic variable under consideration becomes $h(x_0 + x') - \langle h \rangle$. Thus,

$$S_{SS}(x_0, x_0 + x) \equiv \text{Prob } \{ \text{ sign } [h(x_0 + x') - \langle h \rangle] = \text{ constant }, \\ \forall\ 0 \leq x' \leq x\ ,\ \forall\ x_0 \in \mathcal{S}_{SS}\ \}\,, \tag{6.12}$$

and

$$S_{FIC}(x_0, x_0 + x) \equiv \text{Prob } \{ \text{ sign } [h(x_0 + x') - \langle h \rangle] = \text{ constant }, \\ \forall\ 0 \leq x' \leq x\ ,\ \forall\ x_0 \in \mathcal{S}_{FIC}\ \}\,. \tag{6.13}$$

6.4 Results and discussions

6.4.1 Solid-on-solid models

In the solid-on-solid Family and Kim–Kosterlitz models, the interface configuration is characterized by a set of integer height variables $\{h_i\}_{i=1,L}$ corresponding to the lattice sites $i = 1, \ldots, L$, with periodic boundary conditions. Since all the measurements of the spatial persistence and survival probabilities are done in the steady-state regime (i.e. in the regime where the interfacial roughness has reached a time-independent saturation value), we used relatively small systems with $L \sim 200 - 3000$ in order to be able to achieve the steady state within reasonable simulation times. The resulting steady-state interfacial profile, corresponding to a final time $t_0 >> L^z$, is used to compute the spatial persistence and survival probabilities. The calculation of $P_{SS}(x)$ is relatively simple: it involves measuring the fraction of initial lattice positions (all possible choices of the initial point are allowed) for which the interface height has not returned to the height of the initial point (for persistence probability) or to the average height level $\langle h \rangle$ (for survival probability) over a distance x,

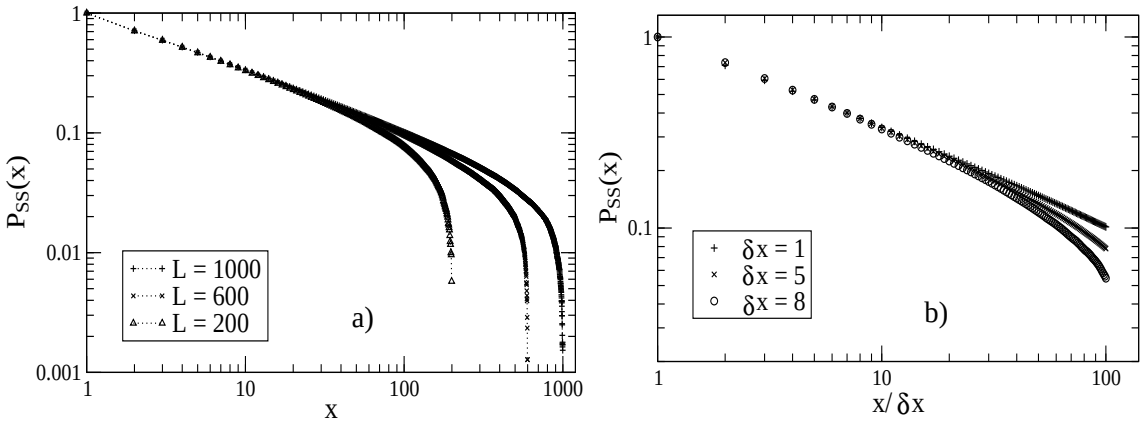

Figure 6.1: The steady state spatial persistence probability, $P_{SS}(x)$, for (1+1)–dimensional EW interfaces with white noise, obtained using the discrete Family model. Panel (a): Double-log plots of $P_{SS}(x)$ vs x for a fixed sampling distance $\delta x = 1$, using three different values of L, as indicated in the legend. Panel (b): Double-log plots of $P_{SS}(x)$ vs $x/\delta x$ for a fixed system size, $L = 1000$, and three different values of δx, as indicated in the legend.

averaged over many independent realizations ($\sim 10^3 - 10^4$) of the steady state configuration. Measurements of $P_{FIC}(x)$ or $S_{FIC}(x)$ involve, in addition to these steps, a preliminary selection of a subensemble of lattice sites which are characterized by a fixed and small value H of the height measured relative to the spatial average. Only the sites that belong to this subensemble (i.e. only the sites with $h_i = H + \langle h \rangle$) are used as initial points in the FIC measurements.

Two distinct length scales have to be taken into consideration in the interpretation of the numerical results for the spatial persistence probability: the size L of the sample used in the simulation, and the sampling distance δx which denotes the

spacing between two successive points where the height variables are measured in the calculation of the persistence probability. The minimum value of δx is obviously one lattice spacing, but one can use a larger integral value of δx in the calculation of persistence and survival probabilities. For example, a calculation of the persistence probability with $\delta x = m$ would correspond to checking the heights of only the sites with index $i_0 + jm$, where i_0 is the index of the initial site and $j = 1, 2, \ldots$. While the importance of L in the measurement of $P(x)$ is obvious (it sets the maximum distance for which $P(x)$ can be meaningfully measured), the effect of δx is rather intricate and has to be carefully investigated. In Fig. 6.1(a) we start to analyze these effects by looking at $P_{SS}(x)$ for EW-type interfaces. We note that when $P_{SS}(x)$ is measured in systems with different sizes, using the smallest possible value for δx (i.e. $\delta x = 1$), the exponent associated with the power-law decay of the persistence probability does not change, but there is an abrupt downward departure from a power-law behavior near $x = L/2$. It is not difficult to understand this behavior qualitatively: as discussed earlier, measurements of spatial correlations and persistence probabilities in a finite system of size L with periodic boundary conditions are meaningful only for distances smaller than $L/2$. In Fig. 6.1(b), we have shown the results for $P_{SS}(x)$ when L remains fixed and δx is varied. Since the the persistence probability is, by definition, equal to unity for $x = \delta x$ (see Eq. (1.3.7)), we have plotted P_{SS} as a function of $x/\delta x$ in this figure to ensure that the plots for different values of δx coincide for small values of the x-coordinate. The plots for different δx are found to splay away from each other at large values of $x/\delta x$, with the plots for larger δx exhibiting more pronounced downward bending. Again, the reason for

this behavior is qualitatively clear: since a double-log plot of $P_{SS}(x)$ vs x begins to deviate substantially from linearity as x approaches $L/2$ [see Fig. 6.1(a)], the downward bending of the plots in Fig. 6.1(b) (which are all for a fixed value of L) occurs at a smaller value of $x/\delta x$ for larger δx. A more detailed scaling analysis of the dependence of the persistence probabilities on x and δx is described below.

In Fig. 6.2 we show the results for spatial persistence and survival probabilities for the discrete Family model. It is obvious from the plots that the spatial persistence probabilities $P_{SS}(x)$ (panel (a)) and $P_{FIC}(x)$ (panel (c)) exhibit power-law decays over an extended range of x values. The abrupt decay to zero near $x = L/2$ is due, as discussed above, to finite size effects. The spatial persistence exponents are extracted from the power-law fits shown in the log-log plots as dashed straight lines. We find that $\theta_{SS} \simeq 0.51$, in good agreement with the expected value 1/2. However, it is clear that the steady state survival probability $S_{SS}(x)$, shown in Fig. 6.2(a), does not exhibit a power-law behavior. This is similar to the qualitative behavior of the *temporal* survival probability in the steady state of the Family model [43].

We now return to the dependence of the persistence probabilities on the sample size L and the sampling distance δx. Since L and δx are the only two length scales in the problem (the lattice parameter serves as the unit of length), it is reasonable to expect [43] that the persistence probabilities would be functions of the (dimensionless) scaling variables x/L and $\delta x/L$. If this is true, then plots of P vs. x/L for different sample sizes should show a scaling collapse if the ratio $\delta x/L$ is kept constant. A similar scaling behavior of the temporal survival probability as functions of L and the sampling time δt (in that case, the scaling variables are t/L^z

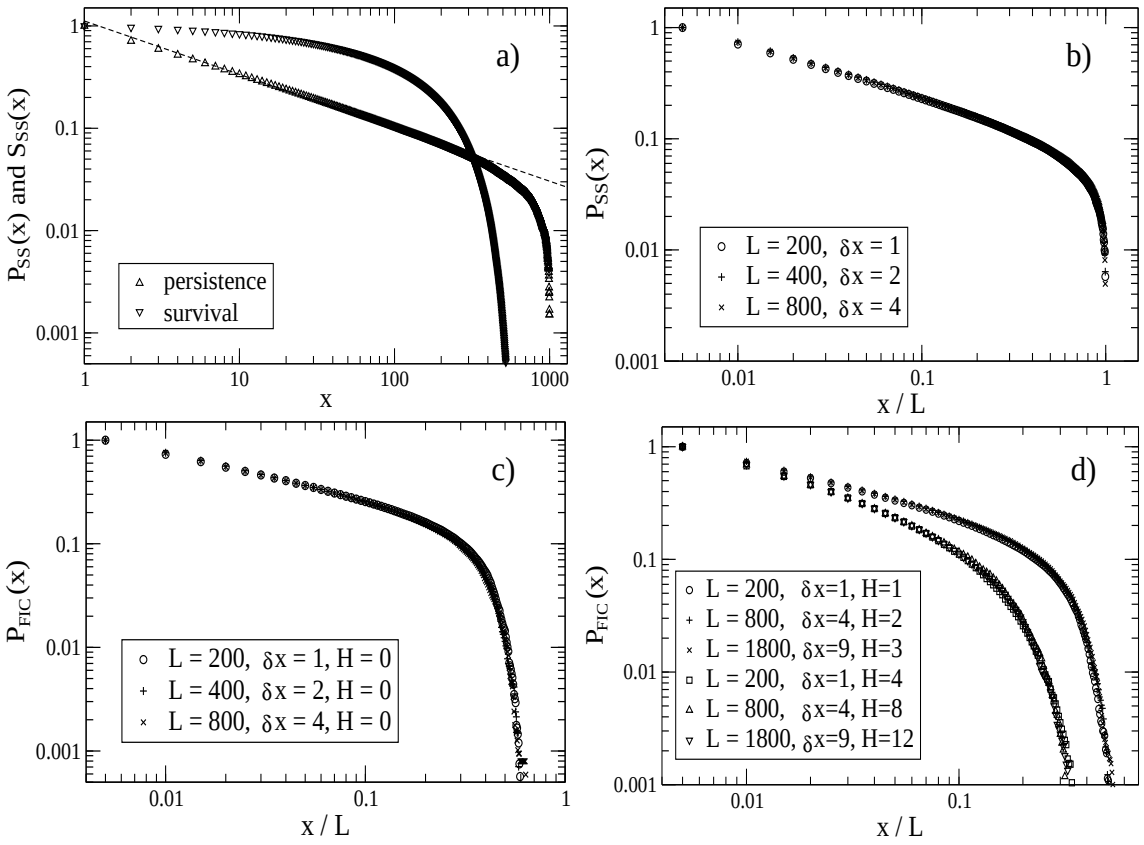

Figure 6.2: $P_{SS}(x)$, $P_{FIC}(x)$, and $S_{SS}(x)$, obtained from simulations of the Family model in (1+1) dimensions. In panels (a) and (b) we show the data for $P_{SS}(x)$ and $S_{SS}(x)$, while in panels (c) and (d) we display the data for $P_{FIC}(x)$. (a): $P_{SS}(x)$ and $S_{SS}(x)$ for $L = 1000$, $\delta x = 1$. The dashed line represents the best fit of the $P_{SS}(x)$ data to a power–law form. (b): Finite-size scaling of $P_{SS}(x, L, \delta x)$. Three probability curves are obtained for three different sample sizes with the same value for the ratio $\delta x/L = 1/200$. (c): Scaling of $P_{FIC}(x, L, \delta x, H)$ for the same values of L and δx as in panel (b). P_{FIC} is calculated by sampling over lattice sites with $H = 0$. (d): Scaling of $P_{FIC}(x, L, \delta x, H)$ for three different sample sizes with the same value for the ratio $\delta x/L$, sampling over two subsets of lattice sites with the same value of H/L^{α} ($\alpha = 0.5$): $1/\sqrt{200}$ (upper plot) and $4/\sqrt{200}$ (lower plot).

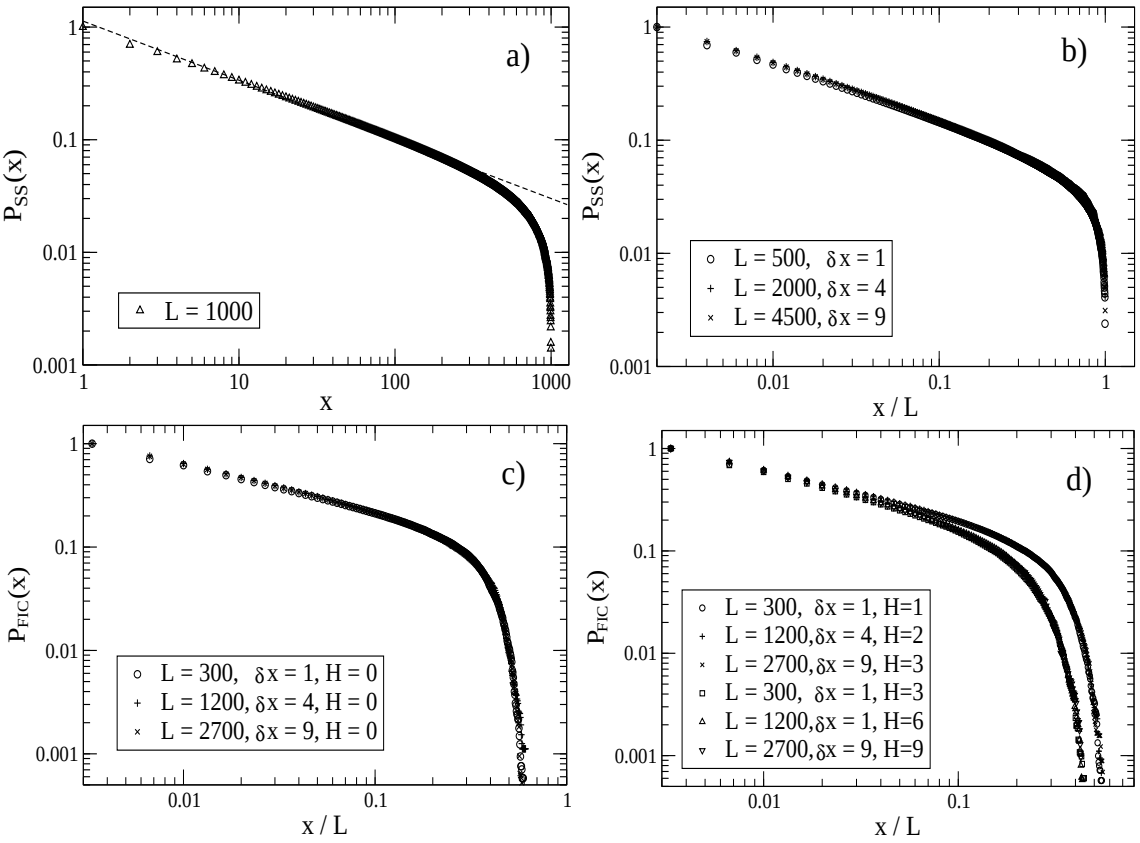

Figure 6.3: The spatial persistence probabilities, $P_{SS}(x)$ and $P_{FIC}(x)$, for the (1+1)-dimensional Kim-Kosterlitz model which is in the KPZ universality class. As in Fig. 6.2, in panels (a) and (b) we show the data for $P_{SS}(x)$. Panels (c) and (d) display the data for $P_{FIC}(x)$. (a): $P_{SS}(x)$ for $L = 1000$, $\delta x = 1$. (b): Finite-size scaling of $P_{SS}(x, L, \delta x)$. Three probability curves are obtained for three different sample sizes with the same value for the ratio $\delta x/L = 1/500$. (c): Scaling of $P_{FIC}(x, L, \delta x, H)$, obtained by sampling over the lattice sites with $H = 0$, for three different values (same as those in panel (b)) of L and δx. (d): Scaling of $P_{FIC}(x, L, \delta x, H)$ for three different sample sizes with the same value for the ratio $\delta x/L$, sampling over two subsets of lattice sites with the same value of H/L^{α} ($\alpha = 0.5$): $1/\sqrt{300}$ (upper plot) and $3/\sqrt{300}$ (lower plot).

and $\delta t/L^z$) was found in Ref. [43]. As indicated in panels(b-d) of Fig. 6.2, we have used various values for the sampling distance δx in the measurement of $P_{SS}(x)$ and $P_{FIC}(x)$. We observe that when the sampling distance is increased in proportion to the system size (so that $\delta x/L$ is held fixed), all the $P_{SS}(x)$ curves collapse when plotted vs. x/L (see panel (b)). This confirms that the scaling form of the steady state persistence probability is:

$$P_{SS}(x, L, \delta x) = f_1(x/L,\ \delta x/L), \tag{6.14}$$

where the function $f_1(x_1, x_2)$ shows a power-law decay with exponent θ_{SS} as a function of x_1 for small values of x_1 and $x_2 \ll 1$.

Let us turn our attention to $P_{FIC}(x)$. In the data shown in panel (c) of Fig. 6.2, we have chosen the subensemble $\mathcal{S}_{FIC}$ of sampling positions to contain only the lattice sites whose height h_i is equal to the average value $\langle h \rangle$ (i.e. $H = 0$). Obviously, in this case the definitions for persistence and survival probabilities become identical, since the probability that the height variable does not return to the original value (i.e. $h_i = \langle h \rangle$) is precisely the probability that the height variable does not reach the average level $\langle h \rangle$. We find that $\theta_{FIC} \simeq 0.48$ using a system with $L = 1000$ and $\delta x = 1$ and considering the subensemble of sites with $H = 0$. We note that a remarkable collapse of $P_{FIC}(x)$ vs. x/L curves for different values of L is again obtained when δx is adjusted to be proportional to the system size L, as shown in panel (c). More interestingly, we observe that fixing the level H to a nonzero value introduces a "height" scale in the problem that is related to the steady-state value of the interface width. Since this width is proportional to L^α, where α is the roughness

exponent, we expect the dependence of P_{FIC} on H for nonzero values of H to be described by the scaling variable H/L^{α}. We observe that if the level H is chosen to be proportional to L^{α}, then the calculated values of P_{FIC} for different sample sizes, obtained using values of δx such that the ratio $\delta x/L$ is also held constant, exhibit a perfect scaling collapse, as shown in panel (d) of Fig. 6.2. This observation leads us to the conclusion that the scaling form of the FIC persistence probability with nonzero values of the level H is:

$$P_{FIC}(x, L, \delta x, H) = f_2(x/L,\ \delta x/L,\ H/L^{\alpha}), \tag{6.15}$$

where $f_2(x_1, x_2, x_3)$ exhibits a power-law behavior with exponent θ_{FIC} as a function of x_1 for small x_1 if $x_2 \ll 1$ and $x_3 \to 0$. As the value of x_3 is increased, the range of x_1 values over which the power-law behavior is obtained decreases and a more rapid decay of the probability is noticed.

The predictions concerning the scaling behavior of the spatial persistence probabilities are confirmed by the results for the atomistic Kim–Kosterlitz model. The same discussion for Fig. 6.2 applies to Fig. 6.3 where we have shown the results for the Kim-Kosterlitz model. We find that $\theta_{SS} \simeq 0.52$ [see Fig. 6.3(a)], in good agreement with the expected value of 1/2, and also that $\theta_{FIC} \simeq 0.47$, using a rather small simulation with $L = 300$ and $\delta x = 1$ and sampling over the subensemble of sites with height at the average level [see Fig. 6.3(c)]. As shown in Fig. 6.3(b), the SS persistence probability obeys the scaling form of Eq. (6.14). In Fig. 6.3(d), we display the results for the measured P_{FIC} for systems with different sizes and sampling distances such that $\delta x/L$ remains constant and considering two different

subsets of sampling sites, each subset being characterized by a fixed value of H/L^{α}. These results are in perfect agreement with the scaling form of Eq. (6.15).

Equations (6.14) and (6.15) provide a complete scaling description of the SS and FIC persistence probabilities for (1+1)–dimensional fluctuating interfaces belonging to two different universality classes (i.e. EW and KPZ), modeled using discrete solid-on-solid models. The associated spatial persistence exponents θ_{SS} and θ_{FIC} are in good agreement with the theoretical values [45]. However, these studies do not illustrate the interesting possibility of a dependence of the persistence exponent on the sampling procedure used in the selection of the initial sites used in the calculation of the persistence probability: the two persistence exponents θ_{SS} and θ_{FIC} have the same value for (1+1)–dimensional EW and KPZ interfaces. We present and discuss below the results for a model where these two exponents have different values.

6.4.2 Edwards–Wilkinson equation with colored noise

In order to measure the spatial persistence and survival probabilities in this system, we have applied the steps described above on systems of sizes $\sim 2^8 - 2^{10}$, using 100–400 independent realizations for averages. While the calculation of $P_{SS}(x)$ and $S_{SS}(x)$ involves the same method as the one used in the case of the solid-on-solid models, for measuring $P_{FIC}(x)$ and $S_{FIC}(x)$ we have selected the subensemble of lattice sites whose heights $h(x_j, t_0)$ at time $t_0 \gg L^z$ satisfy the condition $\langle h \rangle - w/2 \leq h(x_j, t_0) \leq \langle h \rangle + w/2$, where $\langle h \rangle$ is the spatial average of the height at time t_0. The

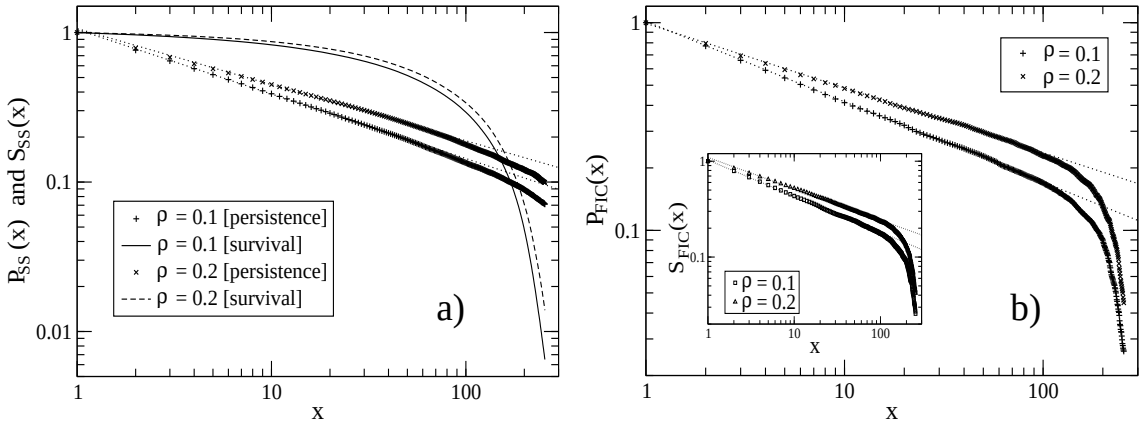

Figure 6.4: Spatial persistence and survival probabilities for the EW equation with spatially correlated noise. Panel a): $P_{SS}(x)$ and $S_{SS}(x)$ using a fixed system size $L = 2^9$, two values of the noise correlation parameter ($\rho = 0.1$ and 0.2) and sampling distance $\delta x = 1$. Panel b): $P_{FIC}(x)$ and $S_{FIC}(x)$ (inset), using the same parameters as in panel a), and sampling initial sites from a band of width $w = 0.10$ centered at the average height. The straight lines drawn through the data points in these double-log plots represent power-law fits.

width w of the sampling window has to be chosen to be much smaller than the amplitude of the interface fluctuations, but large enough to include a relatively large fraction of the total number of sites in order to ensure adequate statistics. Under these circumstances we have computed the fraction of these selected sites which do not reach the "original" height $h(x_j, t_0)$ (in the case of persistence probability) or the average height level $\langle h \rangle$ (in the case of survival probability) up to a distance x from the point x_j. The numerical results for these probabilities, along with a finite-size scaling analysis of their behavior, are shown in Figs. 6.4 and 6.5.

We find that both SS and FIC spatial persistence probabilities for (1+1)–dimensional interfaces described by the EW equation with colored noise exhibit the expected power-law behavior as a function of x, as shown in Fig. 6.4, while the SS survival probability shows a more complex x-dependence [see Fig. 6.4(a)]. Further work is needed in order to understand the behavior of $S_{SS}(x)$. When a relatively small system with size $L = 2^9$ is used, the numerical results for the spatial persistence exponents extracted from the power-law fits shown in Fig. 6.4 (for $\rho = 0.1$, we obtain $\theta_{SS} \simeq 0.43$ and $\theta_{FIC} \simeq 0.38$, while for $\rho = 0.2$, the exponent values are found to be $\theta_{SS} \simeq 0.37$ and $\theta_{FIC} \simeq 0.31$) appear to be affected by finite-size effects. Specifically, the values of θ_{SS} extracted from fits to the numerical data are systematically larger than the theoretically expected values, $\theta_{SS} = 0.4$ for $\rho = 0.1$ and 0.3 for $\rho = 0.2$ (see Eq. (6.5)). Similar deviations from the analytical results are also found for the usual dynamical scaling exponents α and β. We have checked that simulations of larger samples bring the measured values of the exponents closer to the expected values, but the convergence is rather slow. These finite-size effects become more pronounced as the noise correlation parameter ρ is increased. In Fig. 6.4 we show the results for $\rho = 0.1$ and $\rho = 0.2$, but we have verified from simulations with larger values of ρ that the difference between the expected and measured values of θ_{SS} increases as ρ is increased. This is expected because the spatial correlation of the noise falls off more slowly with distance as ρ is increased, thereby making finite-size effects more pronounced. Another possible source of the discrepancy between the numerical and exact results for the exponent θ_{SS} is the spatial discretization used in the numerical work. The effects of using a

finite discretization scale Δx on the observed scaling behavior of continuum growth equations in the steady state have been studied in Ref. [79] where it was found that the effective value of the roughness exponent α obtained from calculations of the local width using a finite Δx is smaller than its actual value. Since $\theta_{SS} = 1 - \alpha$, the values of θ_{SS} obtained from our calculations with $\Delta x = 1$ are expected to be larger than their exact values. Our results are consistent with this expectation. As shown in the inset of Fig. 6.4(b), the FIC survival probability $S_{FIC}(x)$ behaves similarly to $P_{FIC}(x)$ for both $\rho = 0.1$ and 0.2, exhibiting a power-law decay with an exponent (of 0.38 and 0.33 for $\rho = 0.1$ and 0.2, respectively) that is very close to θ_{FIC}. This is consistent with the expectation that the FIC persistence and survival probabilities should become identical as the width parameter w used in the selection of initial sites approaches zero (in this limit, both persistence and survival probabilities measure the probability of not crossing the average height). Finally, we point out that both SS and FIC exponents obtained from the numerical study exhibit the correct trend, increasing in magnitude as ρ decreases. Also, the measured FIC spatial persistence exponents satisfy the constraint $1/4 < \theta_{FIC} \leq 1/2$. Our numerical results also confirm the interesting theoretical prediction that the SS and FIC spatial persistence exponents are different for the EW equation with spatially correlated noise.

We have found that the scaling forms of Eqs. (6.14) and (6.15) also provide a correct description of the numerically obtained persistence and survival probabilities for the EW equation with spatially correlated noise. This is illustrated in Fig. 6.5. In Fig. 6.5(a), we show that the results for $P_{SS}(x, L, \delta x)$ obtained for different values of L and δx fall on the same scaling curve when plotted against x/L if the ratio

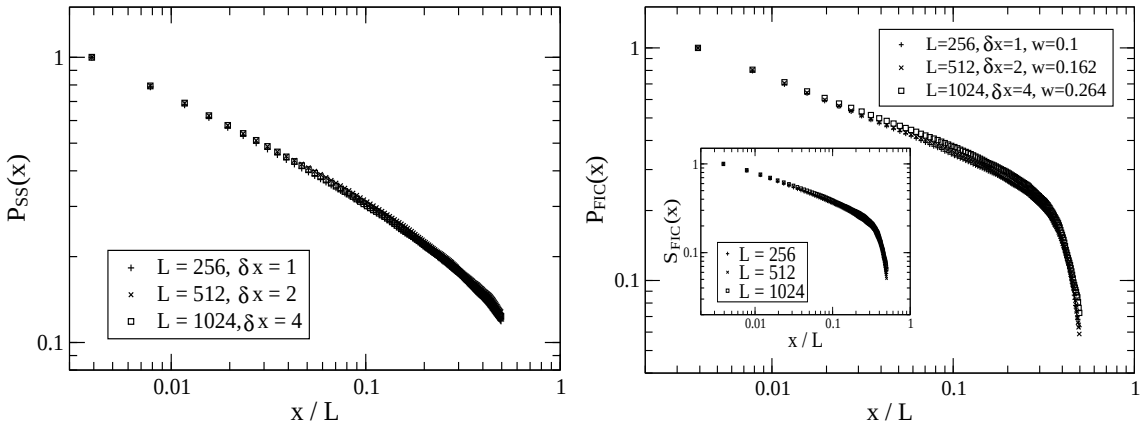

Figure 6.5: Finite-size scaling of the persistence probabilities, $P_{SS}(x)$ and $P_{FIC}(x)$, and the FIC survival probability $S_{FIC}(x)$ for the EW equation with spatially correlated noise. The noise correlation parameter is $\rho = 0.2$ and the sampling interval δx takes three different values. Panel a): The SS persistence probability $P_{SS}(x, L, \delta x)$ for three different sample sizes with a constant ratio $\delta x/L = 1/2^8$. Panel b): The FIC persistence probability $P_{FIC}(x, L, \delta x, w)$ with fixed values of the quantities $\delta x/L$ $(= 1/2^8)$ and w/L^α $(= 0.1/2^{5.6})$, where $\alpha = 0.7$. Inset: Same as in the main figure, but for the FIC survival probability.

$\delta x/L$ is held fixed. This is precisely the behavior predicted by Eq. (6.14). As shown in Fig. 6.5(b), the data for $P_{FIC}(x, L, \delta x, w)$ also exhibit good finite-size scaling collapse if δx is varied in proportion to L and the width w of the sampling band is increased in proportion to L^{α}. This is in perfect analogy with the scaling behavior of the FIC persistence probability for the discrete stochastic models discussed in Sec. 6.4.1, with the variable w playing the role of H in Eq. (6.15). This suggests that the scaling behavior of the FIC persistence probability in the continuum EW equation is of the form

$$P_{FIC}(x, L, \delta x, w) = f_3(x/L,\ \delta x/L,\ w/L^{\alpha}), \tag{6.16}$$

where the function f_3 has the same characteristics as f_2 in Eq. (6.15). A similar scaling description also applies to $S_{FIC}(x)$, as shown in the inset of Fig. 6.5(b). This scaling description should be useful in the analysis of experimental data on equilibrium step fluctuations [38, 39] because the images obtained in experiments provide the values of a real "height" variable (position of a step-edge) at discrete intervals of a finite sampling distance δx.

6.5 Summary and concluding remarks

In this chapter, we have analyzed the spatial first-passage statistics of fluctuating interfaces using the concepts of spatial persistence and survival probabilities. Specifically, we have presented the results of detailed numerical measurements of the SS and FIC spatial persistence probabilities for several models of interface fluctuations. Results for the spatial survival probabilities are also reported. These

results confirm that the concepts of persistence and survival are useful in analyzing the spatial structure of fluctuating interfaces. The exponents associated with the power-law decay of the spatial persistence probabilities as a function of distance x are valuable indicators of the universality class of the stochastic processes that describe the dynamics of surface fluctuations. Our results for these exponents for (1+1)-dimensional interfaces in the EW and KPZ universality classes are in good agreement with the corresponding analytic predictions. We have also obtained analytic results for the spatial persistence exponents in the (1+1)-dimensional EW equation with spatially correlated noise, and reported the results of a numerical calculation of the persistence and survival probabilities in this system. While the numerical results show strong finite-size effects, the qualitative trends predicted by the analytic treatment are confirmed in the numerical work. In particular, the numerical results show evidence for an interesting theoretically predicted difference between the persistence exponents obtained for two different ways of sampling the initial points used in the measurement of the spatial persistence probability. We also find that the steady-state survival probability has a complex spatial behavior that requires further investigations. In the past, there has been some confusion in the literature about the distinction between the persistence and survival probabilities [43]. Our study shows that these two quantities are very different in the SS situation, whereas the distinction between them essentially disappears in the FIC situation.

The numerical results reported here are for models that exhibit "normal" scaling behavior with the same local and global scaling properties of interface fluc-

tuations. There are other models of interface growth and fluctuations that exhibit "anomalous" scaling [7], for which the global and local scaling properties are different. In such models, the "global" roughness exponent α_g that describes the dependence of the interface width in the steady state on the sample size L ($W(t_0, L) \propto L^{\alpha_g}$ for $t_0 \gg L^z$) is different from the "local" exponent α_l that describes the x-dependence of the height-difference correlation function $g(x) \equiv \langle [h(x + x_0, t_0) - h(x_0, t_0)]^2 \rangle^{1/2}$ in the steady state ($t_0 \gg L^z$) for small x ($g(x) \propto x^{\alpha_l}$ for $x \ll L$). The exponent α_g is greater than unity (the steady-state interface is "super-rough") in such cases, whereas the local exponent α_l is always less than or equal to unity. It is interesting to enquire about the behavior of the spatial persistence probabilities in such models. The numerical results reported in the preceding sections show that the steady-state persistence probability $P_{SS}(x)$ exhibits a power-law decay in x only for values of x that are much smaller than the sample size L. Since the roughness of the steady-state interface of super-rough models at length scales much smaller than L is described by the local exponent α_l, we expect the steady-state spatial persistence probability in such models to exhibit a power-law decay with exponent $\theta_{SS} = 1 - \alpha_l$ for $x \ll L$. For example, the one-dimensional Mullins-Herring model [11] is super-rough with $\alpha_g = 3/2$ and $\alpha_l = 1$. For this model, the above argument suggests that the steady-state spatial persistence exponent θ_{SS} is equal to 0, which agrees with the exact result reported in Ref. [45].

An important feature of our investigation is the development of a scaling description of the effects of a finite system size and a finite sampling distance on the measured persistence probabilities. We have also shown that the dependence of the

FIC persistence and survival probabilities on the reference level H (in atomistic models) or the width w of the band (in continuum models) used in the selection of the subset of sampling sites is described by a scaling form. These scaling descriptions would be useful in the analysis of experimental and numerical data on fluctuations in spatially extended stochastic systems.

7. MAPPING SPATIAL PERSISTENT LARGE DEVIATIONS OF NONEQUILIBRIUM SURFACE GROWTH PROCESSES ONTO THE TEMPORAL PERSISTENT LARGE DEVIATIONS OF STOCHASTIC RANDOM WALK PROBLEM

Non-Markovian Gaussian stochastic processes are very widely encountered in a large variety of nonequilibrium physical problems [80]. As we have mentioned before, considerable theoretical [81] and experimental efforts have recently been devoted to understanding the first-passage statistics in such nonequilibrium systems. In this chapter, we consider the interfaces described by linear Langevin equations of the type

$$\partial h(x,t)/\partial t = -(-\nabla^2)^{z/2} h(x,t) + \xi(x,t), \tag{7.1}$$

where $h(x,t)$ is the step height fluctuation corresponding to the lateral step position x, at time t, $\xi(x,t)$ is a white uncorrelated Gaussian noise, and z is the dynamical exponent. We have seen in Chapter 3 that, in addition to the usual

persistence probability, more general information can be extracted from the natural generalization of the persistence through the probability of *temporal* persistent large deviations [32], $P_t(t,s)$, where $-1 \leq s \leq 1$. We have also seen in Chapter 6 that the dynamics of the spatially extended systems with fluctuations governed by stochastic differential equations can be further elucidated by looking at the spatial persistence probability [45, 82], $P_x(x)$, and its associated exponents. The aim of this chapter is to establish numerically the concept of *spatial* persistent large deviations probability, $P_x(x,s)$ with $-1 \leq s \leq 1$, as a natural generalization of the spatial persistence probability concept. We also show that $P_x(x,s)$ measured for growth processes in the well-studied Edwards-Wilkinson [12] universality class [described by Eq. (7.1) with $z = 2$] can be mapped isomorphically onto $P_t(t,s)$ of the simple random walk stochastic problem [83]. This mapping possibility is inspired by the work of Majumdar and Bray [45], who have shown in a recent Letter that the *spatial* persistence probability characteristics of growth processes involving the interfacial height stochastic variable $h(x,t)$ with the dynamics described by Eq. (7.1) can be mapped onto the *temporal* persistence characteristics of the "random walk" processes of the type $\mathrm{d}^n x/\mathrm{d}t^n = \eta(t)$, where $n = (z-d+1)/2$ and $\eta(t)$ is a white noise as well. The purpose of the current chapter is to show that this exact mapping, as expected, works for the generalized (large deviations) persistence probability and the corresponding continuous family of persistence exponents as well, and to numerically calculate $\theta_x(s)$ for the important class of processes controlled by the Edwards-Wilkinson equation.

7.1 Spatial persistent large deviations

We consider the average sign of the interfacial height stochastic variable measured at a fixed time t with respect to the original value corresponding to the initial position x_0,

$$S_{\rm av}(x) = \frac{1}{x}\int_0^x {\rm sgn}[h(x_0+x',t) - h(x_0,t)]\; dx'. \tag{7.2}$$

The spatial persistent large deviations probability is defined, in analogy with its temporal correspondent, as the probability that the average sign $S_{\rm av}$ remains persistently above a particular value s, with $-1 \leq s \leq 1$, up to a longer distance x measured from the initial position x_0,

$$P_x(x,s) \equiv {\rm Prob}\ \{\ S_{\rm av}(x') \geq s,\ \forall x' \leq x\ \}. \tag{7.3}$$

We provide numerical evidence showing that $P_x(x,s)$ has a power law behavior for $x < L$, where L is the typical length scale in the numerical simulations (i.e. system size), independent of the choice of the average sign parameter s,

$$P_x(x,s) \propto x^{-\theta_x(s)}, \tag{7.4}$$

where the spatial persistent large deviations exponent $\theta_x(s)$ depends continuously on the parameter s that appears in the definition of the probability. The importance of $P_x(x,s)$ lies in the fact that it provides an $infinite$ family of persistence exponents, instead of only one exponent as in the case of $P_x(x)$. Obviously, $P_x(x, s=1)$ and its associated exponent $\theta_x(s=1)$ are precisely the spatial persistence probability and the nontrivial persistence exponent (θ_{SS} or θ_{FIC}, depending on the sampling

procedure applied to x_0), respectively. The opposite limit $s \to -1$ is trivial in the sense that $P_x(x, s = -1) = 1$ independent of x and as a consequence $\theta_x(s = -1) = 0$.

The s dependence of the temporal persistent large deviations exponents is known exactly for the simple random walk case, which is one of the few analytically solved persistence problems [84],

$$\theta_t(s) = \frac{2\theta_t(1)}{\pi} \arctan \sqrt{\frac{1+s}{1-s}}. \tag{7.5}$$

The mapping [45] between the *temporal* properties of the random walker (RW) problem and the *spatial* properties of the Edwards-Wilkinson (EW) fluctuating interfaces implies that the expression of Eq. (7.5) also applies to the distribution of the *spatial* persistent large deviations exponent as a function of s. This conjecture is verified numerically in this study.

7.2 Numerical results

We have carried out the first application of the spatial persistent large deviations concept to the case of (1+1)-dimensional fluctuating interfaces characterized by the EW dynamical equation. Using the configuration of the interface corresponding to a fixed time of the order of the time required by the interface width to saturate (i.e., $t \sim L^z$), we have computed $P_x(x, s)$ as the fraction of lattice sites x_j (with $j = 1, 2, ..., L-1$) which maintained their stochastic variable $S_{\rm av}$ persistently above a fixed s value, up to a distance x_j+x. The initial measurement points, x_j, are sampled from the entire set of the steady-state interfacial profile. The numerical integration of the stochastic equation is performed using the simple forward-time centered-space

representation [78]. We have used numerical systems of size $L \sim 1000$, and we have averaged the results over many ($\sim$ 1000) independent runs to obtain convergent statistics.

In Fig. 7.1 we show the results for $P_x(x, s)$ as a function of x for (1+1)-dimensional EW interfaces simulated numerically. We display ten log-log spatial persistent large deviations curves versus the distance x for ten values of the average sign parameter s (i.e., $s = +1,\ +0.8,\ \ldots,\ -0.8$). We observe that $P_x(x, s) \sim x^{-\theta_x(s)}$ for $x < L/2$, while for larger values of x and $s \geq 0$ there is a downward deviation of the probability from the power law behavior due to finite-size limitations. Except for the curve corresponding to $s = 1$, which gives the usual spatial persistence exponent $\theta_{SS} \simeq 0.50$, in agreement with Refs. [45, 82], all the other curves with $s < 1$ provide new information concerning spatial behavior of the interface fluctuations.

The temporal persistent large deviations probability of the random walk model is shown in Fig. 7.2. We have used similar s values, as in the case of $P_x(x, s)$ described above. $P_t(t, s)$ shows a clear power law behavior versus t. We find that $P_t(t, s = 1)$ is characterized by an exponent of 0.50, in agreement with the theoretical value $\theta_t = 1/2$. Individual temporal persistent large deviations exponents $\theta_t(s)$ are extracted from the linear regions of the log-log plots of $P_t(t, s)$ versus t, and they are compared in Fig. 7.3 to the corresponding spatial set of exponents $\theta_x(s)$ for the EW interfaces.

The level of agreement between $P_x(x, s)$ corresponding to the EW dynamical equation and $P_t(t, s)$ of the RW case can be seen in Fig. 7.3. To generate this figure we have used an increment of the average sign parameter (s) of 0.1. We observe that the two sets of exponents, $\theta_t(s)$ and $\theta_x(s)$, overlap very well within the errors of our

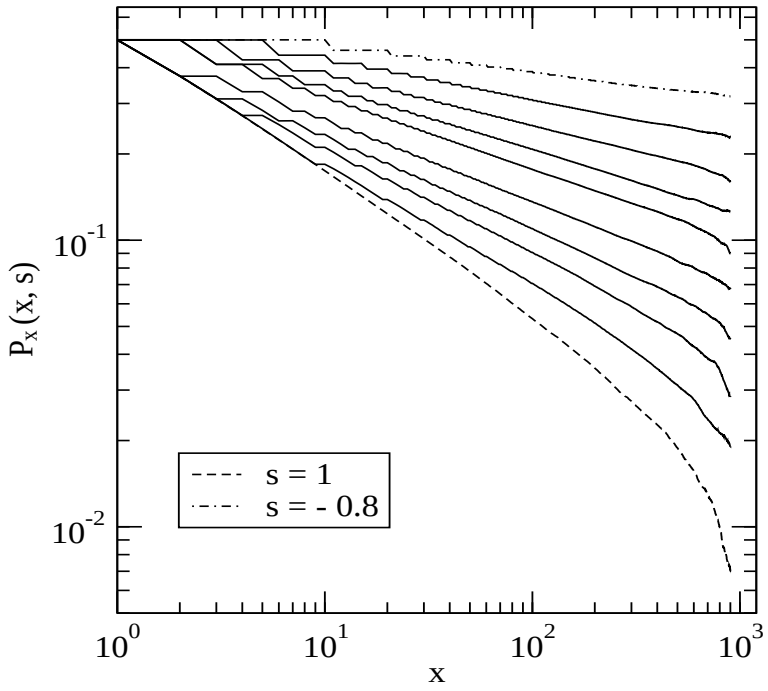

Figure 7.1: Log-log plot of $P(x, s)$ versus x for the EW equation based on the direct numerical integration of Eq. (7.1) with $z = 2$, using a system of size $L = 1000$. The average sign parameter takes ten different values decreasing from $s = 1$ (bottom curve) to $s = -0.8$ (top curve) with an average sign difference $\Delta s = 0.2$. All spatial persistent large deviations probabilities show power law decay vs distance for $x < L/2$. Finite-size effects are responsible for the deviations of the probabilities from the power law trend at large values of x.

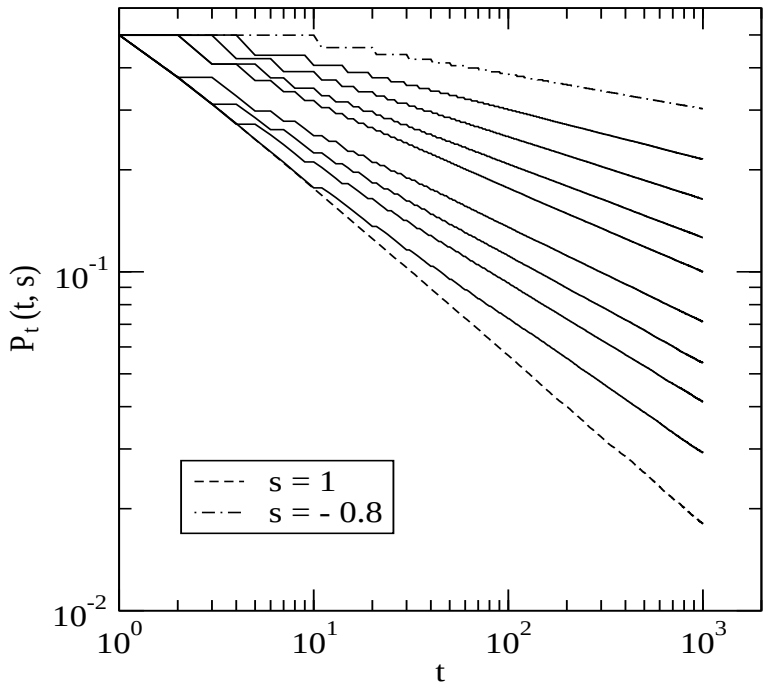

Figure 7.2: Log-log plot of simulated $P_t(t,s)$ vs t for the RW problem. The system size is $L = 500$ and the average sign parameter takes ten different values decreasing from $s = 1$ (bottom curve) to $s = -0.8$ (top curve) with $\Delta s = 0.2$ between successive probability curves. All temporal persistent large deviations probabilities show power law behavior vs time.

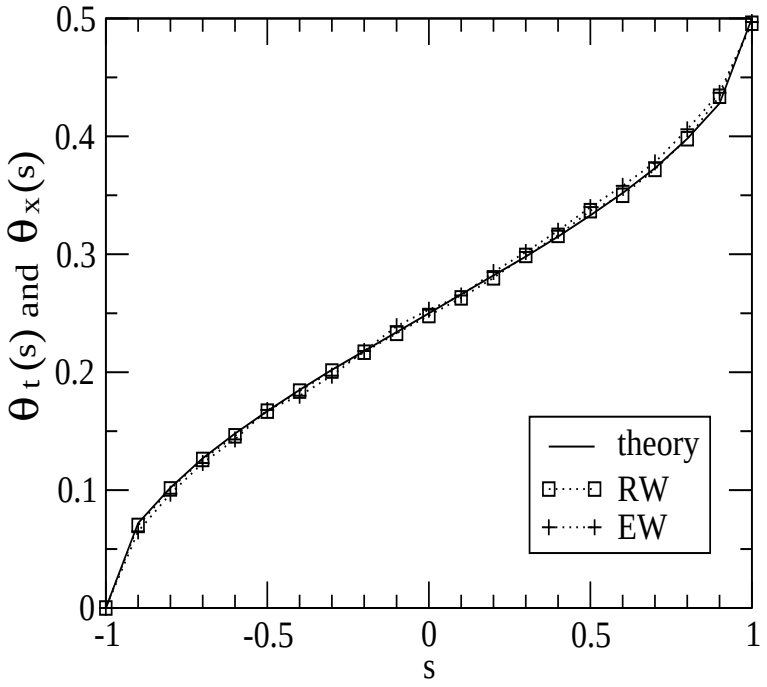

Figure 7.3: $\theta_t(s)$ and $\theta_x(s)$ vs s as extracted from the power-law decay of $P(t,s)$ (for the RW problem) and $P(x,s)$ (for the EW fluctuating interfaces), respectively. The increment of the average sign parameter is $\Delta s = 0.1$. The continuous curve represents the theoretical prediction of Eq. (7.5).

simulations, showing that the mapping procedure involved in this study is perfectly applicable. Both cases are in agreement with the theoretical prediction of Eq. (7.5). We have also simulated a discrete stochastic growth model, the so-called Family model, which is theoretically known to belong exactly to the EW universality class [67]. The Family model results (not shown here) for $P_x(x,s)$ and $\theta_x(s)$ are very similar to those shown in Fig. 7.1 since they have identical stochastic dynamics.

Despite the downward deviation of the probability $P_x(x,s)$ from the power law behavior due to finite-size limitations, we have checked that larger system sizes

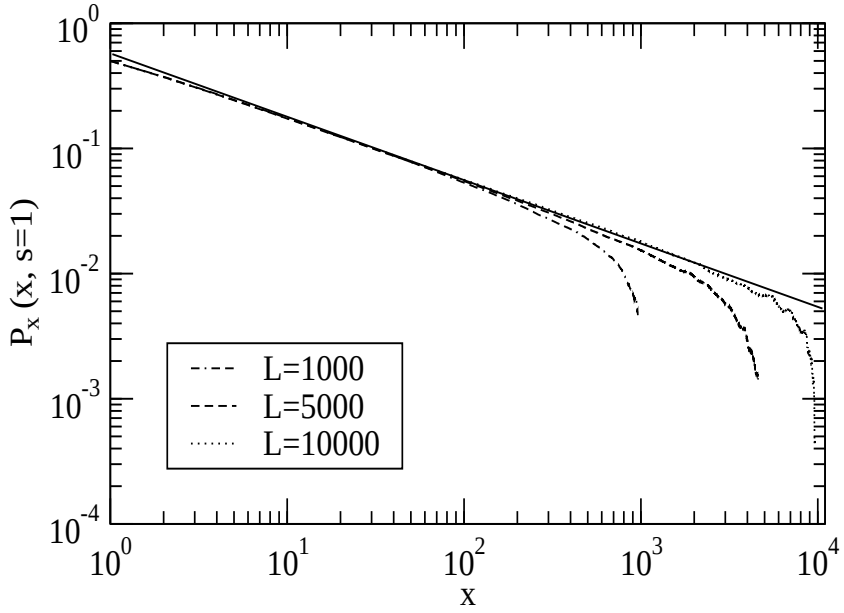

Figure 7.4: Log-log plot of $P_x(x, s)$ for $s = 1$ corresponding to the EW equation based on the direct numerical integration of Eq. (7.1) with $z = 2$, using three system sizes, as shown in the legend. The straight line represents the fit for $L = 10^4$ simulation, providing an exponent equal to 1/2.

would provide a wider range of distances over which the spatial persistence large deviations exponent can be extracted with a better precision. This can be seen in Fig. 7.4.

Another case of interest for epitaxial surface dynamics is growth under surface diffusion minimizing the local curvature, which belongs asymptotically to the Mullins-Herring (MH) [11] universality class [i.e. Eq. (7.1) with $z = 4$]. The exact mapping prediction by Majumdar and Bray [45] suggests that the spatial persistence properties of the *continuum* version of the growth models belonging to this universality class could be mapped onto the temporal persistence characteristics

of the random acceleration problem described by the stochastic random equation $\mathrm{d}^2x/\mathrm{d}t^2 = \eta(t)$ with an analytically known exponent of $\theta_t = 1/4$ [75]. One expects to obtain $\theta_{SS} = 0$ and $\theta_{FIC} = 1/4$ [45] when measuring the steady-state and finite initial conditions regimes of $P_x(x)$, respectively, for the Mullins-Herring surface growth dynamics. An example of this case is the (1+1)-dimensional model introduced by Kim and Das Sarma [6]. This discrete solid-on-solid atomistic model, the so-called larger curvature (LC) model [6] is known to belong asymptotically to the MH universality class. As a consequence, we focus on the measurement of $P_{FIC}(x)$ for the discrete LC model [6], since $P_{SS}(x)$ is trivially described by a null exponent. The definition of $P_{FIC}(x)$ involves the selection of the subset of sites characterized by *finite* height and height derivatives. One possibility would be to sample over the subset of sites placed on the average level. However, it turns out that a system with $L = 200$, which is the typical system size in our simulations, usually has only a couple of discrete positions on the average level. For this reason, we have sampled over all the lattice sites x_j with the height variable (measured with respect to the average level) within a band of values characterized by a width w [i.e., $-w/2 \leq h(x_j) \leq w/2$], where w is taken to be smaller than the maximum magnitude of interface fluctuations. This selection ensured the possibility of sampling over a reasonable number of lattice sites presumably sufficient for good statistical results of $P_{FIC}(x)$.

In Fig. 7.5 we show the x dependence of $P_{FIC}(x)$ corresponding to the LC discrete model for three values of w: 30, 70 and 110, respectively. The steady-state probability is shown for comparison. We note that $P_{FIC}(x)$ does not display the

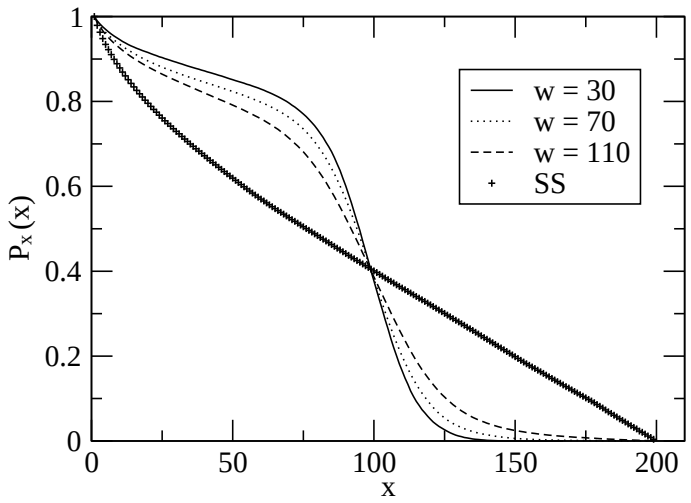

Figure 7.5: Numerical results of $P_{FIC}(x)$ and $P_{SS}(x)$ for the LC discrete model with system size $L = 200$. The measurements are performed from steady-state configurations. $P_{FIC}(x)$ probabilities have been obtained by using three different band widths, as shown in the legend. $P_{FIC}(x)$ does not display a power-law behavior as a function of x over the entire range of system size.

expected power-law behavior as a function of x. As the bandwidth w increases, more and more lattice sites are included in the sampling subset, and $P_{FIC}(x)$ tends to reach the behavior displayed by $P_{SS}(x)$. In addition, we observe that when using a numerical system with $L = 200$, $P_{SS}(x)$ has a rather linear dependence on x, for $50 < x < 200$. The impossibility to recover the theoretically predicted behavior of $P_{FIC}(x)$ may be due to the reduced system size used in our simulations. This limitation is imposed by the requirement of measuring the probability $P_{FIC}(x)$ using an ensemble of steady-state configurations that can be achieved only by using an extensive computational time $\sim L^4$. We note that reducing or increasing the system size by a factor of 2 did not produce any qualitative change in the overall behavior of $P_{FIC}(x)$ or $P_{SS}(x)$. In addition, we have checked that the direct numerical integration of Eq. (7.1) with $z = 4$ provides results consistent with the discrete LC model. Also, it turns out that similar probability curves are obtained for solid-on-solid models belonging asymptotically to the molecular beam epitaxy universality class (such as the (1+1)-dimensional DT model [4]). We believe that our problem with the spatial persistence $P_x(x)$ for the LC model belonging to the MH universality class [6] arises most likely from the severe finite-size problems in simulating systems with large values ($z = 4$) of the dynamical exponent. The large dynamical exponent implies very slow lateral correlations, which considerably complicates studying steady-state behavior in the MH universality problem. In fact, this issue is very well known in traditional studies of dynamical scaling involving surface phenomena characterized by a large value of the dynamical exponent [52, 85]. A large variety of stochastic discrete models show long-time transients, and they cross

over very slowly to their corresponding asymptotic behavior. Only extensive simulations of stochastic discrete models in the MH universality class can provide the asymptotic dynamical scaling associated with the continuous limit of the Eq. (7.1) with $z = 4$. This forbids us from pursuing further measurements of $P_x(x, s)$ for the MH universality class and checking the validity of the mapping procedure, which remains an interesting open problem.

7.3 Conclusions

To conclude, we have shown numerically that the spatial persistent large deviations probability represents a possible generalization of the spatial persistence probability, providing a useful family of spatial exponents for the surface growth phenomena. We have mapped these exponents into the family of temporal persistent large deviations exponents obtained from the evolution of a simple stochastic "random walk" process. We have established the validity of this generalization for the case of fluctuating interfaces described by the Edwards-Wilkinson evolution equation. However, the similar problem involving the Mullins-Herring universality class remains open since the corresponding discrete LC model [6] simulation shows severe finite-size problems.

8. CONCLUSIONS AND OPEN QUESTIONS

As Watson wrote [86] in a recent Science paper, "persistence pays off in defining history of diffusion", since one of the most simple problems in physics, the classical problem of diffusion, has been characterized by a new exponent [23], the persistence exponent, and this fact has opened a new and exciting field of research. We would like to add that, as we have seen in this study, persistence and survival "pay off" in characterizing surface growth and fluctuations [41, 43, 44, 67, 82, 83] as well. Since fluctuating interfaces are of crucial importance at very small scales (i.e. nanoscales) [87] involved in the fabrication of current electronic devices, it is of particular importance to look for new methods to analyze and understand surface fluctuations. In addition to the traditional way of analyzing various aspects of growth processes based on the dynamical scaling behavior of the interface width and temporal and spatial correlation functions [1, 47], we have shown that the persistence and survival probabilities, along with their generalizations, can alternatively be used to attack this problem. The nontrivial persistence exponents associated with the power–law decay of the positive/negative persistence probabilities have been shown in Chapter

2 to have the potential for identifying the underlying universality class of the dynamical process [29] and the presence of the nonlinearities [67] associated with the dynamical evolution.

Recent experimental studies have shown that the concept of persistence can be applied to analyze the dynamics of fluctuating steps on Al/Si(111), Ag(111) and Pb(111) surfaces [38, 39, 40, 70] recorded using STM methods. We believe that in view of the importance of thermal and shot–noise fluctuations in the dynamics of growing and fluctuating interfaces, theoretical and experimental studies of persistence would play an important role in the analysis of the dynamics of nonequilibrium surface growth.

Once the persistence probability behavior is found, one can immediately calculate the asymptotic behavior of the first-passage probability [22], $F(t)$, which represents the distribution of the time when the stochastic variable under consideration *first* reaches a fixed reference value: $F(t) = -dP_t(t)/dt$. In addition, one can also obtain the mean first-passage time which provides the representative time scale characterizing the stability of the dynamical process. Such a time scale might be of interest for the study of the evolution of fluctuating interfaces or for understanding the behavior of a collection of stochastic spin variables. Although the problem of calculating the mean first–passage time looks simple and solvable, we have already seen in this study that dealing with the persistence aspects of stochastic processes is not an easy task; therefore, this interesting open question has to be addressed with caution.

The persistence probability concept can be generalized, as seen in Chapter 3,

using the persistent large deviations probability, which represents a valuable tool because it provides a continuous family of exponents. One interesting problem for the future would be the analytical calculation of the s–dependence of θ_l for growth models or fluctuating interfaces belonging to different universality classes. Some progress in this direction would make the information provided by $P(t, s)$ extremely valuable in assigning the universality class of a particular surface growth model or fluctuating process.

The sampling time effect on the persistence and survival probabilities presented in this work are of particular importance since any experimental or numerical technique involves the discretization of the time and/or space scales. Our work exposed in Chapter 4 about the sampling effects on the survival aspects of step fluctuations has motivated additional studies on the influence of this quantity on other variables relevant in surface dynamics studies, such as the correlation functions [70]. We have found that the temporal sampling procedure produces an apparent correlation length L_{eff}, governed by the longest wavelength of step fluctuations than can be sampled in the measurement time interval, which is substantially smaller than the real spatial limitations of the physical system. In addition, Dougherty and collaborators [40] have analyzed systematically the sampling time effect for persistence and survival in step structural fluctuations. Although $P(t)$ scales simply with $t/\delta t$, the survival probability scales with either system size or sampling time only when the ratio $\delta t/L^z$ is kept constant. Since L (which represents the system size in numerical simulations or the effective length of the step set by the longest wavelength fluctuation) is proportional with $t_m^{1/z}$ [70], it is clear that the survival probability

shows scaling with $t/\delta t$ only when the ratio $\delta t/t_m$ remains constant. Similar scaling applies to the generalized survival probability, as seen in Chapter 5, except that the scaling function of $S(t, R)$ also depends on R/L^{α} because choosing different reference levels imposes a new length scale (i.e., L^{α}) in the problem.

Some of the numerical results reported in Chapter 6 (such as the behavior of the steady state spatial survival probability and the forms of the scaling functions that describe the dependence of the spatial persistence probabilities on the parameters L, δx and H or w) should be amenable to analytic treatment, especially for the EW equation with white noise, whose spatial properties can be mapped [45] to the temporal properties of the well-known random walk problem. Further work along these lines would be very interesting. The spatial persistence and survival probabilities considered here should be measurable in imaging experiments on step fluctuations [38, 39, 40, 70]. Such experimental investigations would be most welcome.

Finally, we show schematically in Table 8.1 all the statistical quantities measured in this study related to the first–passage statistics of fluctuating interfaces and stochastic growth processes and the possible mappings between some of them. We also indicate the relationship between the steady state (SS) temporal and spatial persistence exponents and the universal exponents provided by the traditional dynamical scaling analysis. However, as pointed out above, several open questions are still remaining (and they are indicated by question marks), making this research field active and interesting.

Variable	Statistical quantity	Important relations
$h_x(t)_x$	$P_t(t,s) \sim t^{-\theta_t(s)} \xrightarrow[s\to 1]{} P(t) \sim t^{-\theta_t}$	$\theta_S = 1 - \beta$
	(T/S regimes)	
	$S(t,R) \sim \exp[-t/\tau_s(R)] \xrightarrow[R\to 0]{} S(t) \sim \exp(-t/\tau_s)$	
$h_t(x)_t$	$P_x(x,s) \sim x^{-\theta_x(s)} \xrightarrow[s\to 1]{} P(x) \sim x^{-\theta_x}$	$\theta_{SS} = 1 - \alpha_l$
	(FIC/SS regimes)	
	$S(x,R)$?	
	$S_{SS}(x)$? (no power–law)	
	$S_{FIC}(x) \sim x^{-\theta_{FIC}}$	
	$[\theta_x(s)]_{EW} \Longleftrightarrow [\theta_t(s)]_{RW}$	
	?	
	$[\theta_x(s)]_{MH} \Longleftrightarrow [\theta_t(s)]_{RA}$	

Table 8.1: Summary of the temporal and spatial first–passage probabilities measured in this study, along with their behavior at large time/space scales. $h_x(t)$ denotes a temporal stochastic variable, while $h_t(x)$ denotes a spatial stochastic variable. RW stands for random walker and RA stands for random acceleration problem. The existing open questions are marked with "?".

A. AUTOCORRELATION FUNCTIONS FOR SURFACE GROWTH PROCESSES

The temporal autocorrelation function $a_h(t_1, t_2)$ of the stochastic variable $h(\mathbf{r}, t)$, representing in our study the height of an interface growing on a d-dimensional substrate, measured at a fixed position $\mathbf{r}$ and arbitrary times t_1 and t_2 is defined in the following way:

$$a_h(t_1, t_2) \equiv \langle h(\mathbf{r}, t_1) h(\mathbf{r}, t_2) \rangle, \tag{A.1}$$

where $\langle \cdots \rangle$ denotes the expectation value over all spatial positions $\mathbf{r}$ and all realizations of the stochastic process. We first want to show that $a_h(t_1, t_2)$ for *linear* Gaussian stochastic equations, such as the ones involved in the description of fluctuating interfaces with up-down ($h \to -h$) symmetry, has the form:

$$a_h(t_1, t_2) = K[(t_1 + t_2)^{2\beta} - |t_2 - t_1|^{2\beta}], \tag{A.2}$$

where K is a constant and β, as we have seen in Section 1.1, is the universal growth exponent related to the rate of interface roughness growth in the transient regime. This result has tremendous importance in understanding the first–passage statistics

of fluctuating interfaces, and for this reason we start by presenting its derivation. Let us consider a general linear stochastic evolution equation for (d+1)-dimensional Gaussian interfaces of the type

$$\frac{\partial h(\mathbf{r},t)}{\partial t} = -(-\nabla^2)^{z/2} h(\mathbf{r},t) + \eta(\mathbf{r},t), \tag{A.3}$$

where ∇^2 refers to the spatial derivatives and $\eta(\mathbf{r},t)$ denotes the noise term which can be characterized by spatial correlations, as we consider below. We mention that when no specific information is given about the noise we tacitly assume that the noise is the usual uncorrelated random Gaussian noise [i.e., $\langle \eta(\mathbf{r},t)\eta(\mathbf{r}^{'},t^{'})\rangle = \delta^d(\mathbf{r}-\mathbf{r}^{'})\delta(t-t^{'})$]. In Eq. (A.3) above z is the universal dynamical exponent related to the relaxation mechanism of the stochastic process under consideration. We address again the case $z = 2$ or the Edwards–Wilkinson universality (where the fluctuations of steps are driven by high–temperature attachment-detachment (AD) of the atoms at the step edge), and also the case $z = 4$ with a conserved noise characterized by the correlator $\langle \eta(\mathbf{r},t)\eta(\mathbf{r}^{'},t^{'})\rangle = -\nabla^2\delta^d(\mathbf{r}-\mathbf{r}^{'})\delta(t-t^{'})$. The latter situation corresponds to the low–temperature step-edge diffusion (SED) limited kinetics (i.e., the step fluctuations are driven by the atoms diffusing along the step edge). We mention that the absence of the incoming particle flux in Eq. (A.3) shows that the interfacial height variable is measured with respect to the spatial average height value (i.e. in the interfacial comoving reference frame), $\langle h\rangle = 1/V \int \mathrm{d}^d\mathbf{r}\ h(\mathbf{r},t)$. The stochastic process $h(\mathbf{r},t)$ in Eq. (A.3) for a fixed $\mathbf{r}$, as a function of time t, is Gaussian albeit *non-Markovian*. The non-Markovian property arises due to the Laplacian term that generates interaction between heights at two different space points.

The traditional method to obtain the temporal autocorrelation function is to Fourier transform Eq. (A.3) above,

$$\frac{\partial h(\mathbf{k},t)}{\partial t} = -\alpha(k)\ h(\mathbf{k},t) + \eta(\mathbf{k},t), \tag{A.4}$$

where $\alpha(k) = |\mathbf{k}|^z$. The Fourier transform of the noise term for the two cases considered above is described in a compact fashion by the correlator $\langle \eta(\mathbf{k},t)\eta(\mathbf{k}',t')\rangle = (2\pi)^d k^{z-2}\delta(\mathbf{k}+\mathbf{k}')\delta(t-t')$. In Eq. (A.4) we have used that

$$h(\mathbf{k},t) = \int d^d\mathbf{r}\ e^{i\mathbf{k}\cdot\mathbf{r}}\ h(\mathbf{r},t). \tag{A.5}$$

It is straightforward to show that the solution of Eq. (A.4) is

$$h(\mathbf{k},t) = e^{-\alpha(k)t}h(\mathbf{k},0) + e^{-\alpha(k)t}\int_0^t dt_1\ e^{\alpha(k)t_1}\eta(\mathbf{k},t_1). \tag{A.6}$$

Let $C_k(t_1,t_2) \equiv \langle k(\mathbf{k},t_1)h(-\mathbf{k},t_2)\rangle$, then the temporal autocorrelation function is given by

$$\langle h(\mathbf{r},t_1)h(\mathbf{r},t_2)\rangle = \int \frac{d^d\mathbf{k}}{(2\pi)^d}\ C_k(t_1,t_2)\ e^{-a^2\alpha(k)}, \tag{A.7}$$

where $C_k(t_1,t_2)$ is

$$\begin{aligned} C_k(t_1,t_2) &= e^{-\alpha(k)(t_1+t_2)}\langle h(\mathbf{k},0)h(-\mathbf{k},0)\rangle \\ &+ e^{-\alpha(k)(t_1+t_2)}\int_0^{t_1} dt' \int_0^{t_2} dt'' e^{\alpha(k)(t'+t'')}\langle \eta(\mathbf{k},t')\eta(-\mathbf{k},t'')\rangle, \end{aligned}$$

and a is a ultraviolet cutoff that has to be introduced to ensure finite values of $\langle h^2\rangle$ in the limit $t \longrightarrow \infty$. However, for $d < 2$ the cutoff plays no role since the interface width roughens with time, therefore we can simply consider $a \equiv 0$ in that case.

After some algebra, $C_k(t_1, t_2)$ becomes

$$\begin{aligned} C_k(t_1, t_2) &= e^{-\alpha(k)(t_1+t_2)}\Delta(\mathbf{k}) \\ &+ \frac{(2\pi)^d k^{z-2}}{2\alpha(k)}\left[e^{-\alpha(k)|t_2-t_1|} - e^{-\alpha(k)(t_2+t_1)}\right], \end{aligned} \tag{A.8}$$

where $\Delta(\mathbf{k}) \equiv \langle h(\mathbf{k}, 0)h(-\mathbf{k}, 0)\rangle$. Assuming that the initial interface is flat, i.e. $h(\mathbf{r}, 0) = 0$, and performing the integration over the $\mathbf{k}-$space, Eq. (A.7) becomes:

$$\langle h(\mathbf{r}, t_1)h(\mathbf{r}, t_2)\rangle = K\left[|a^2 + t_2 + t_1|^{2\beta} - (a^2 + |t_2 - t_1|)^{2\beta}\right], \tag{A.9}$$

where

$$2\beta = (2 - d)/z, \tag{A.10}$$

and K is a constant. For $d < 2$, we can simply take $a \equiv 0$ and we obtain the result shown previously in Eq. (A.2). In addition, if $t_1 = t_2$ the interface width is described by a power-law growth, i.e., $\langle h^2(\mathbf{r}, t)\rangle \sim t^{2\beta}$ as $t \longrightarrow \infty$. However, for $d > 2$ the interface width saturates, i.e., $\langle h^2(\mathbf{r}, t)\rangle \sim (a^2)^{-(d-2)/z}$ as $t \longrightarrow \infty$.

With this result for the autocorrelation function $a_h(t_1, t_2)$ in mind, we introduce two different new stochastic variables: $H(\mathbf{r}, t) = h(\mathbf{r}, t_0 + t) - h(\mathbf{r}, t_0)$ and $G(\mathbf{r}, t) = h(\mathbf{r}, t_0 + t) - \langle h\rangle$, with $\langle h\rangle$ being the spatial average height. When $H(\mathbf{r}, t)$ vanishes the variable $h(\mathbf{r}, t_0 + t)$ reaches its *initial* value corresponding to the initial time t_0. On the other hand, the zeros of $G(\mathbf{r}, t)$ are associated with the discrete times when $h(\mathbf{r}, t_0 + t)$ reaches its equilibrium *average* value. The evolution of these two variables is closely related to the persistence and survival behavior of surface fluctuations, respectively. It turns out that by looking at the autocorrelation functions a_H and a_G of the variables $H(\mathbf{r}, t)$ and $G(\mathbf{r}, t)$, respectively, one can in fact

obtain information about the *persistence* probability, $P(t)$ (i.e. the probability of *not* crossing the *original* configuration up to time t) and the *survival* probability, $S(t)$ (i.e., the probability of *not* crossing the *average* value up to time t), respectively. The relationship between a_G and $S(t)$ has been explained in Chapter 4. We now focus on the relationship between a_H and $P(t)$.

Let us first calculate the *steady state* value of $a_H(t_1, t_2)$. This is achieved by considering very large time scales, i.e.,

$$\begin{aligned} a_H^S(t_1,t_2) &= \lim_{t_0\to\infty} \langle\ H(\mathbf{r},t_0+t_1)H(\mathbf{r},t_0+t_2)\ \rangle \\ &= \lim_{t_0\to\infty} (\ \langle\ h(\mathbf{r},t_0+t_1)h(\mathbf{r},t_0+t_2\ )\ \rangle\ -\ \langle\ h(\mathbf{r},t_0+t_1)h(\mathbf{r},t_0)\ \rangle \\ &- \ \langle\ h(\mathbf{r},t_0)h(\mathbf{r},t_0+t_2)\ \rangle\ +\ \langle\ h(\mathbf{r},t_0)^2\ \rangle\ ) \\ &= \lim_{t_0\to\infty} [\ a_h(t_0+t_1,t_0+t_2)\ -\ a_h(t_0+t_1,t_0) \\ &- \ a_h(t_0,t_0+t_2)\ +\ a_h(t_0,t_0)]. \end{aligned} \tag{A.11}$$

Using Eq. (A.2) (i.e., for simplicity we consider that $d < 2$), the steady state autocorrelation function of the variable $H(\mathbf{r}, t)$ becomes:

$$a_H^S(t_1,t_2) = K\ [t_2^{2\beta} + t_1^{2\beta} - |t_2 - t_1|^{2\beta}]. \tag{A.12}$$

It is interesting to point out that Eq. (A.12) is precisely the autocorrelation function of the *fractional Brownian motion* (fBm) with $\beta = H$ being the well–known Hurst exponent, $0 < H < 1$. The ordinary Brownian motion is characterized by $H = 1/2$. Several analytical and numerical results are available in the literature for the persistence probability of a fBm (see Section A.1), allowing us to understand the steady state regime of interface fluctuations, as we will show later on in Section A.2.

The second case of interest is the *transient* value of the autocorrelation function obtained using very small values of t_0. Without loss of generality, one can assume that $h(\mathbf{r}, t_0) = 0$ (i.e., flat initial interface). By considering the limit $t_0 \to 0$, $a_H^T(t_1, t_2)$ is nothing but $a_h(t_1, t_2)$, i.e.,

$$a_H^T(t_1, t_2) = K[(t_2 + t_1)^{2\beta} - |t_2 - t_1|^{2\beta}]. \tag{A.13}$$

We observe that both the transient and the steady state values of $a_H(t_1, t_2)$ do not depend exclusively on the time difference $|t_2 - t_1|$, so the underlying dynamics (although Gaussian) is not a stationary process. However, it turns out that the following relatively simple change of variables

$$\begin{cases} X &= \frac{h(\mathbf{r},t)}{\sqrt{\langle h(\mathbf{r},t)^2\rangle}} \\ T &= \ln t \end{cases} \tag{A.14}$$

transforms the process into a stationary one. Indeed, the new normalized expressions of the temporal autocorrelation functions in the transient and steady state regimes read:

$$\begin{aligned} A^T(T_1, T_2) &\equiv \frac{\langle h(\mathbf{r}, t_1) h(\mathbf{r}, t_2)\rangle}{\sqrt{\langle h(\mathbf{r}, t_1)^2\rangle \langle h(\mathbf{r}, t_1)^2\rangle}} \\ &= \left[\cosh\left(\frac{T_2 - T_1}{2}\right)\right]^{2\beta} - \left|\sinh\left(\frac{T_2 - T_1}{2}\right)\right|^{2\beta}, \end{aligned} \tag{A.15}$$

and

$$\begin{aligned} A^S(T_1, T_2) &\equiv \frac{\langle H(\mathbf{r}, t_1) H(\mathbf{r}, t_2)\rangle}{\sqrt{\langle H(\mathbf{r}, t_1)^2\rangle \langle H(\mathbf{r}, t_1)^2\rangle}} \\ &= \cosh\left[\beta(T_2 - T_1)\right] - \frac{1}{2}\left|2\sinh\left(\frac{T_2 - T_1}{2}\right)\right|^{2\beta}. \end{aligned} \tag{A.16}$$

We notice that both the transient and the steady state autocorrelation functions have the same type of short–time singularity, but their behavior at large time is

different if $\beta < 1/2$, i.e.,

$$A^T(T) = \begin{cases} 1 - O(T^{2\beta}) & \text{for} \quad T \longrightarrow 0 \\ \mathrm{e}^{-(1-\beta)T} & \text{for} \quad T \longrightarrow \infty \end{cases} \tag{A.17}$$

and

$$A^S(T) = \begin{cases} 1 - O(T^{2\beta}) & \text{for} \quad T \longrightarrow 0 \\ \mathrm{e}^{-\min(\beta,1-\beta)T} & \text{for} \quad T \longrightarrow \infty. \end{cases} \tag{A.18}$$

As discussed in Ref. [29], it has been shown a long time ago that the calculation of the persistence exponent θ for processes with a general autocorrelation function $A(T)$ is very difficult [31]. Approximate analytical results can be derived for certain cases characterized, for example, by $A^T(T) = 1 - O(T^2)$ for $T \longrightarrow 0$ (as in the case of the diffusion equation) [23]. Also, if $A^T(T) = 1 - O(|T|)$ one can calculate perturbatively the value of θ [88]. However, when $\beta < 1/2$, which is the case of the dynamical interfaces and growth processes considered in this work, the density of zero crossings is infinite [31], prohibiting the analytical calculation of θ. Therefore, the only investigation tools we are left with are the numerical ones. This explains why the main results presented in this thesis are based on numerical methods.

A.1 The Persistence Exponent of Fractional Brownian Motion

Before proceeding further, we summarize the definition and the known first–passage property of a fBm. A stochastic process $\xi(t)$ (with zero mean $\langle \xi(t) \rangle = 0$) is called a fBm if its two–time incremental correlation function $C(t_1, t_2) = \langle [\xi(t_1) - \xi(t_2)]^2 \rangle$ is (i) *stationary*, i.e., depends only on the time difference $|t_2 - t_1|$ and (ii) grows

asymptotically as a power law [61]

$$C(t_1, t_2) \sim |t_2 - t_1|^{2H}, \qquad |t_2 - t_1| >> 1. \tag{A.19}$$

The parameter H $(0 < H < 1)$ is called the Hurst exponent that characterizes the fBm and $\langle \cdots \rangle$ denotes the expectation value over all realizations of the process $\xi(t)$. For the sake of completeness we also mention that, alternatively, a zero mean stochastic process $\xi(t)$ is called a fBm if its autocorrelation function has the following expression:

$$a_\xi(t_1, t_2) = \langle \xi(t_1)\xi(t_2) \rangle \sim t_1^{2H} + t_2^{2H} - |t_2 - t_1|^{2H}. \tag{A.20}$$

The zero crossing properties of a fBm have been studied extensively in the past [89, 90, 91]. In particular, we are interested in the probability $P(t)$ that a fBm does *not* cross zero upto time t. It turns out that $P(t)$ decays as a power–law at large times, $P(t) \sim t^{-\theta_S}$ with the steady state persistence exponent θ_S obeying the relation [91]

$$\theta_S = 1 - H. \tag{A.21}$$

We note that this relation holds for any zero mean process (not necessarily Gaussian [90, 92]) that satisfies the requirements (i) and (ii) above. Both analytic arguments as well as numerical simulations supporting the relation (A.21) have been presented previously in the literature, as well as throughout this thesis. We present below a simple derivation of the Eq. (A.21) along the lines of Ref. [29].

Let $P(\xi, \tau)$ denote the probability distribution that the process has the value ξ at time τ, given that it starts from 0 at $\tau = 0$. This probability obeys a very

simple scaling relation

$$P(\xi,\tau) = \frac{1}{\sigma(\tau)} f\left(\frac{\xi}{\sigma(\tau)}\right), \tag{A.22}$$

where $\sigma(\tau) = \langle(\xi(\tau))^2\rangle^{1/2} \sim \tau^H$ for large τ and the scaling function $f(y)$ is a constant at $y = 0$. The density of zero crossings in the interval $[\tau, \tau + d\tau]$ is given by

$$\rho(\tau) = P(0,\tau) \sim \frac{1}{\sigma(\tau)} \sim \tau^{-H}. \tag{A.23}$$

In other words, $\rho(\tau)$ denotes the probability that the process ξ returns to zero at time τ, not necessarily for the first time. Thus, the total number of zeros up to a total time T is

$$N(T) = \int_0^T d\tau \rho(\tau) \sim T^{1-H}, \qquad T \gg 1. \tag{A.24}$$

Next, the strategy is to relate the persistence probability $P(\tau)$ to the number of zero crossings. $P(\tau)$ is the probability that the process ξ never returns to zero up to time τ. By definition, $P(\tau) \sim \tau^{-\theta_S}$ for large τ. Then $Q(\tau) = -\mathrm{d}P/\mathrm{d}\tau \sim \tau^{-(1+\theta_S)}$ denotes the probability that the process will cross zero next time between τ and $\tau + d\tau$. $Q(\tau)$ is in fact the probability distribution of time intervals between zero crossings. Next, let us consider a large time interval T. Let $N(T)$ denote the total number of intervals in this period of time and $n(\tau, T)$ the number of intervals of length τ within the period T. $n(\tau, T)$ is proportional to $Q(\tau)$,

$$n(\tau,T) = N(T)Q(\tau) \sim N(T)\tau^{-(1+\theta_S)}, \qquad 1 \ll \tau \ll T. \tag{A.25}$$

The length conservation constraint for the interval T reads

$$T = \int_0^T d\tau\ \tau\ n(\tau,T) \sim \int_0^T N(T)\tau^{-\theta_S} \sim N(T)T^{1-\theta_S}. \tag{A.26}$$

This gives $N(T) \sim T^{\theta_S}$ and by comparison with Eq. (A.24) we obtain the desired relation $\theta_S = 1 - H$.

A.2 Hints on How to Compute the Persistence Exponents for Fluctuating Interfaces

It is well known that the analytical calculation of the persistence exponent is very hard for a non-Markovian process even if the process is Gaussian [19] and obviously additional complications appear if the process is non-Gaussian. One escape from this problem is found when it is possible to map the underlying stochastic process into a fBm. When this is the case, one can use known results of first–passage statistical properties of fBm such as Eq. (A.21) shown above to calculate the persistence exponent analytically. This strategy has been applied successfully to several systems [19, 29, 30, 42, 93].

Indeed, from Eq. (A.12) we see that a fluctuating interface in the limit $t_0 \longrightarrow \infty$ and for $d < 2$ is a fBm with a Hurst exponent $H = (2-d)/2z$. This implies that the steady state persistence probability has a power–law behavior at large times, $P(t) \sim t^{-\theta_S}$, where

$$\theta_S = 1 - H = \frac{2z + d - 2}{2z}. \tag{A.27}$$

In particular, the 1–dimensional nonconserved noise AD case is described by $\theta_S = 3/4$, while for the conserved noise SED case the steady state persistence exponent is $7/8$. These exact results have been confirmed both experimentally and numerically [38, 39, 41].

However, for $d > 2$ the steady state persistence probability behaves differently [93]. In this case the interface width saturates to a constant as $t \longrightarrow \infty$ and the evolution of the stochastic height variable cannot be mapped into a fBm anymore. Further progress can be made by looking at the Eq. (A.9) in the limit of large t_1 and t_2, such that $|t_2 - t_1|$ is kept fixed (and denoted by τ),

$$a_h(\tau) \sim \frac{1}{(a^2 + \tau)^{(d-2)/z}} \quad . \tag{A.28}$$

Under these approximations $h(\mathbf{r}, t)$ becomes a Gaussian *stationary* process with an algebraically decaying autocorrelator, $a_h(\tau) \sim \tau^{-\alpha}$, with $\alpha = (d-2)/z$. Newell and Rosenblatt have studied such processes a long time ago [71] and provided a set of bonds on the associated persistence probability. These conditions read:

$$\begin{aligned} P(t) &\sim \exp[-K_1 t], \qquad \alpha > 1 \\ \exp[-K_2 t^\alpha \ln t] \;\leq\; P(t) \;&\leq\; \exp[-K_3 t^\alpha], \qquad 0 < \alpha < 1. \end{aligned} \tag{A.29}$$

As a consequence, the persistence probability of interfaces with dimensionality higher than $d = 2$ has a stretched exponential behavior for $2 < d < z + 2$ and an exponential behavior for $d > z + 2$. Obviously, these behaviors are different from the power–law decay $P(t) \sim t^{-\theta_s}$ for $d < 2$.

BIBLIOGRAPHY

[1] A. -L. Barabasi and H. E. Stanley, *Fractal Concepts in Surface Growth* (Cambridge University, Cambridge, 1995).

[2] A. McKane, M. Droz, J. Vannimenus, and D. Wolf, *Scale Invariance, Interfaces, and Non–Equilibrium Dynamics* (New York and London, 1995).

[3] F. Family, J. Phys. A: Gen. **19**, L441 (1986).

[4] S. Das Sarma and P. Tamborenea, Phys. Rev. Lett. **66**, 325 (1991); P. Tamborenea and S. Das Sarma, Phys. Rev. E **48**, 2575 (1993).

[5] D. Wolf and J. Villain, Europhys. Lett. **13**, 389 (1990).

[6] J. M. Kim and S. Das Sarma, Phys. Rev. Lett. **72**, 2903 (1994); J. Krug, Phys. Rev. Lett. **72**, 2907 (1994).

[7] S. Das Sarma, S. V. Ghaisas, and J. M. Kim, Phys. Rev. E **49**, 122 (1994).

[8] J. M. Kim and J. M. Kosterlitz, Phys. Rev. Lett. **62**, 2289 (1989).

[9] J. M. Kim, J. M. Kosterlitz, and T. Ala-Nissala, J. Phys. A **24**, 5569 (1991).

[10] Y. Kim, D. K. Park, and J. M. Kim, J. Phys. A **27**, L533 (1994).

[11] W. W. Mullins, J. Appl. Phys. **28**, 333 (1957); C. Herring, J. Appl. Phys. **21**, 301 (1950).

[12] S. F. Edwards and D. R. Wilkinson, Proc. R. Socs. London, Ser.A **381**, 17 (1982).

[13] M. Kardar, G. Parisi, and Y. -C. Zhang, Phys. Rev. Lett. **56**, 889 (1986).

[14] Z. -W. Lai and S. Das Sarma, Phys. Rev. Lett. **66**, 2348 (1991).

[15] J. Villain, J. Phys. I (France) **1**, 19 (1991).

[16] C. Dasgupta, S. Das Sarma, and J. M. Kim, Phys. Rev. E **54**, R4552 (1996); C. Dasgupta, J. M. Kim, M. Dutta, and S. Das Sarma, Phys. Rev. E **55**, 2235 (1997).

[17] J. Krug, Adv. Phys. **46**, 139 (1997).

[18] J. Krim and G. Palasantzas, Int. J. Mod. Phys. **B9**, 599 (1997).

[19] S. N. Majumdar, Curr. Sci. **77**, 370 (1999).

[20] A. J. F. Siegert, Phys. Rev. **81**, 617 (1951).

[21] S. O. Rice, Bell Sys. Tech. J. **38**, 581 (1958).

[22] S. Redner, *A guide to first-passage processes* Cambridge (Cambridge University Press, 2001).

[23] S. N. Majumdar, C. Sire, A. J. Bray, and S. J. Cornell, Phys. Rev. Lett. **77**, 2867 (1996); B. Derrida, V. Hakim, and R. Zeitak, Phys. Rev. Lett. **77**, 2871 (1996).

[24] S. Redner, Phys. Rev. E **56**, 4967 (1997).

[25] B. Derrida, A. J. Bray, and C. Godreche, J. Phys. A **27**, L357 (1994).

[26] B. Derrida, V. Hakim, and V. Pasquier, Phys. Rev. Lett. **75**, 751 (1995).

[27] S. N. Majumdar and C. Sire, Phys. Rev. Lett. **77**, 1420 (1996).

[28] S. Cueille and C. Sire, Eur. Phys. J. B **7**, 111 (1999).

[29] J. Krug, S. N. Majumdar, S. J. Cornell, A. J. Bray, and C. Sire, Phys. Rev. E **56**, 2702 (1997).

[30] H. Kallabis and J. Krug, Europhys. Lett **45**, 20 (1999).

[31] D. Slepian, Bell Syst. Tech. J. **41**, 463 (1962).

[32] I. Dornic and C. Godreche, J. Phys. A **31**, 5413 (1998).

[33] T. J. Newman and Z. Toroczkai, Phys. Rev. E **58**, R2685 (1998); Z. Toroczkai, T. J. Newman, and S. Das Sarma, Phys. Rev. E **60**, R1115 (1998).

[34] M. Marcos-Martin, D. Beysens, J. P. Bouchaud, C. Godreche, and I. Yekutieli, Physica A **214**, 396 (1995).

[35] W. Y. Tam, R. Zeitak, K. Y. Szeto, and J. Stavans, Phys. Rev. Lett. **78**, 1588 (1997); W. Y. Tam and K. Y. Szeto, Phys. Rev. E. **65**, 042601 (2002).

[36] B. Yurke, A. N. Pargellis, S. N. Majumdar, and C. Sire, Phys. Rev. E **56**, R40 (1997).

[37] G. P. Wong, R. W. Mair, and R. L. Walsworth, Phys. Rev. Lett **86**, 4156 (2001).

[38] D. B. Dougherty, I. L. Lyubinetsky, E. D. Williams, M. Constantin, C. Dasgupta, and S. Das Sarma, Phys. Rev. Lett **89**, 136102 (2002).

[39] D. B. Dougherty, O. Bondarchuk, M. Degawa, and E. D. Williams, Surf. Sci. **527** L213 (2003).

[40] D. B. Dougherty, C. Tao, O. Bondarchuk, W. G. Cullen, E. D. Williams, M. Constantin, C. Dasgupta, and S. Das Sarma, Phys. Rev. E **71**, 021602 (2005).

[41] M. Constantin, S. Das Sarma, C. Dasgupta, O. Bondarchuk, D. B. Dougherty, and E. D. Williams, Phys. Rev. Lett. **91**, 086103 (2003).

[42] S. N. Majumdar and D. Das, Phys. Rev. E **71**, 036129 (2005).

[43] C. Dasgupta, M. Constantin, S. Das Sarma, and S. N. Majumdar, Phys. Rev. E **69**, 022101 (2004).

[44] M. Constantin and S. Das Sarma, Phys. Rev. E **69**, 052601 (2004).

[45] S. N. Majumdar and A. J. Bray, Phys. Rev. Lett. **86**, 3700 (2001).

[46] F. Family and T. Vicsek, J. Phys. A **18**, L75 (1985); F. Family, Physica **168A**, 561 (1990).

[47] H. Jeong and E. D. Williams, Surf. Sci. Reports **34**, 171 (1999).

[48] S. Das Sarma, C. J. Lanczycki, R. Kotlyar, and S. V. Ghaisas, Phys. Rev. E **53**, 359 (1996).

[49] S. Das Sarma and P. Punyindu, Phys. Rev. E **55**, 5361 (1997).

[50] D. E. Wolf and J. Kertesz, Europhys. Lett. **4**, 651 (1987); J. Kertesz and D. E. Wolf, J. Phys. A **21**, 747 (1988).

[51] P. Devillard and H. E. Stanley, Phys. Rev. A **38**, 6451 (1988).

[52] P. Punyindu and S. Das Sarma, Phys. Rev. E **57**, R4863 (1998).

[53] P. Punyindu Chatraphorn and S. Das Sarma, Phys. Rev. E **66**, 041601 (2002).

[54] P. Smilauer and M. Kotrla, Phys. Rev. B **49**, 5769 (1994).

[55] S. Das Sarma, P. Punyindu Chatraphorn, and Z. Toroczkai, Phys. Rev. E **65**, 036144 (2002).

[56] Z. Racz, M. Siegert, D. Liu, and M. Pliscke, Phys. Rev. A **43**, 5275 (1991).

[57] W. Feller, *Introduction to Probability Theory and its Applications*, 3rd ed. Vol. 1 (Wiley, New York, 1968).

[58] Y. G. Sinai, Theor. Math. Phys. **90**, 219 (1992).

[59] S. N. Majumdar and A. J. Bray, Phys. Rev. Lett. **81**, 2626 (1998).

[60] J. Krug, P. Meakin, and T. Halpin-Healy, Phys. Rev. A **45**, 638 (1992).

[61] B. B. Mandelbrot and J. W. van Ness, SIAM Rev. **10**, 422 (1968).

[62] S. N. Majumdar, Phys. Rev. E **68**, 050101(R) (2003).

[63] J. Krug, Physica A **340**, 647 (2004).

[64] A. Kundagrami and C. Dasgupta, Physica A **270**, 135 (1999).

[65] S. N. Majumdar, A. J. Bray and G. C. M. A. Ehrhardt, Phys. Rev. E **64**, 015101 (2001).

[66] G. C. M. A. Ehrhardt, A. J. Bray, and Satya N. Majumdar, Phys. Rev. E **65**, 041102 (2002).

[67] M. Constantin, C. Dasgupta, P. Punyindu Chatraphorn, S. N. Majumdar, and S. Das Sarma, Phys. Rev. E **69**, 061608 (2004).

[68] I. L. Lyubinetsky, D. B. Dougherty, T. L. Einstein, and E. D. Williams Phys. Rev. B **66**, 085327 (2002).

[69] N. C. Bartelt, J. L. Goldberg, T. L. Einstein, and Ellen D. Williams, Surf. Sci. **273**, 252 (1992).

[70] O. Bondarchuk, D. B. Dougherty, M. Degawa, E. D. Williams, M. Constantin, C. Dasgupta, and S. Das Sarma, Phys. Rev. B **71**, 045426 (2005).

[71] G. F. Newell and M. Roseblatt, Ann. Math. Stat. **33**, 1306 (1962).

[72] G. Manoj and P. Ray, Phys. Rev. E **62**, 07755 (2000).

[73] I. Lyubinetsky, D. B. Dougherty, H. L. Richards, T. L. Einstein, and E. D. Williams, Surf. Sci. **492**, L671 (2001).

[74] J. Merikoski, J. Maunuksela, M. Myllys, J. Timonen, and M. J. Alava , Phys. Rev. Lett. **90** 024501 (2003).

[75] T. W. Burkhardt, J. Phys. A **26**, L1157 (1993).

[76] J. Garcia-Ojalvo and J. M. Sancho, *Noise in spatially extended systems* Springer, Berlin, 1999.

[77] N.-N. Pang, Y.-K. Yu, and T. Halpin-Healy, Phys. Rev. E. **52**, 889 (1995).

[78] W. H. Press *et al.*, *Numerical Recipes* (Cambridge University Press, Cambridge, 1989).

[79] J. Buceta, J. Pastor, M. A. Rubio, and F. J. de la Rubia, Phys. Rev. E **61**, 6015 (2000).

[80] C. W. Gardiner, *Handbook of Stochastic Methods for Physics, Chemistry and the Natural Sciences* (Springer-Verlag, Berlin, 1983).

[81] J. Grasman, *Asymptotic Methods for the Fokker-Planck Equation and the Exit Problem in Applications* (Springer-Verlag, Berlin, 1999).

[82] M. Constantin, S. Das Sarma, and C. Dasgupta, Phys. Rev. E **69**, 051603 (2004).

[83] M. Constantin and S. Das Sarma, Phys. Rev. E **70**, 041602 (2004).

[84] A. Baldassarri, J. P. Bouchaud, I. Dornic, and C. Godreche, Phys. Rev. E **59**, R20 (1999).

[85] S. Das Sarma, C. J. Lanczycki, R. Kotlyar, and S. V. Ghaisas, Phys. Rev. E **53**, 359 (1996).

[86] A. Watson, Science **274**, 919 (1996).

[87] Z. Toroczkai and E. D. Williams, Physics Today, December, 24 (1999).

[88] S. N. Majumdar and C. Sire, Phys. Rev. Lett. **77**, 1420 (1996).

[89] S. M. Berman, Ann. Math. Stat. **41**, 1260 (1970).

[90] A. Hansen, T. Engøy, and K.J. Måløy, Fractals **2**, 527 (1994).

[91] M. Ding and W. Yang, Phys. Rev. E **52**, 207 (1995).

[92] S. Maslov, M. Paczuski, and P. Bak, Phys. Rev. Lett. **73**, 2162 (1994).

[93] S. N. Majumdar and Alan J. Bray, Phys. Rev. Lett. **91**, 030602 (2003).